TURKGEO

TURKISH JOURNAL OF GEOSCIENCES

e-ISSN 2717-7696

OPEN ACCESS

dergipark.org.tr/tr/pub/turkgeo
turkgeosciences@gmail.com

TURKGEO, December/2020
Volume: 1 - Issue: 2

About The Journal

Turkish Journal of Geosciences is a multi-disciplinary open-access journal aimed to publish peer-reviewed original research and review articles covering all aspects of geosciences. The journal includes a wide scope of information on scientific and technical advances in all areas related to geosciences and indexed in international indices and databases that publish studies on earth sciences.

Aim and Scope

TURKGEO Journal has the following aim and scopes;

Aim of TURKGEO

- TURKGEO aims to promote the theory and practice from the integration of instruments, methodologies, and technologies and their respective uses in the environmental and other natural sciences.
- TURKGEO aims to provide a widely accessible discussion environment that will strengthen and accelerate the exchange of knowledge and experience among scientists, researchers, engineers and other implementers involved in the subject directly or indirectly.

Scope of TURKGEO

- Earth and Environmental Sciences Applications
- Geographic Information Systems
- Remote Sensing
- Photogrammetry
- Geostatistics
- GPS/GNSS
- RADAR/SAR/LIDAR and Laser Scanning
- Spatial Data Infrastructure
- Spatial Decision Support Systems
- Climate Change
- Geology
- Geomorphology
- Hydrogeology
- Geophysics
- Hydrology and Water Resources
- Oceanography

Publishing Frequency 2 issues per year (June-December)

ISSN 2717-7696

WEB https://dergipark.org.tr/tr/pub/turkgeo

Contact sefa.bilgilioglu@gmail.com / osmanorhan44@gmail.com

Turkish Journal of Geosciences

Volume 1
Issue 2 *December, 2020*

Contents

Research Articles;

TURKGEO
TURKISH JOURNAL OF GEOSCIENCES

ISSN: *2717-7696*
Research Article
Vol; 1, Issue; 2, pp. 35-52, 2020
DOI:
Journal homepage:
https://dergipark.org.tr/en/pub/turkgeo

Organic Geochemical Evidence of the Working Petroleum System in Beypazarı Neogene Basin and Potential Traps (Northwest Central Anatolia, Turkey)

Adil Ozdemir*[1], Yildiray Palabiyik[2], Atilla Karataş [3], Alperen Sahinoglu [4]

[1]*Adil Ozdemir Consulting, Ankara, Turkey*
[2]*Istanbul Technical University, Department of Petroleum and Natural Gas Engineering, Istanbul, Turkey*
[3]*Marmara University, Department of Geography, Istanbul, Turkey*
[4]*Istanbul Esenyurt University, Institute of Science and Technology, Istanbul, Turkey*

Keywords
Beypazarı Neogene basin,
Reservoir-targeted
Petroleum exploration,
TPH in water analysis,
Hydrocarbon-rich water,
Oil shale and coal

ABSTRACT

The Miocene units of the Beypazarı Neogene Basin extensively outcrop and prevalently include oil shale and coal. In the previous studies, it has been determined that the total organic carbon (TOC) values of bituminous shales in the basin are concentrated between 4-8% and algal organic matter (Type I-II kerogen) are dominant. It has also been determined that the bituminous shales have pyrolyzable hydrocarbon content of 83% and a potential source rock feature that can produce oil in a large quantity if exposed to high temperatures. Beypazarı Neogene Basin consists of volcano-sedimentary units. Therefore, as a result of the idea that the immature source rocks can be matured by young volcanic that exhibit widespread outcrops, it has been aimed to investigate the oil and gas potential especially in the northeastern part of the basin by TPH (Total Petroleum Hydrocarbons) analysis performed on the samples taken from the natural cold water resources located in the related part of the basin. As a consequence of the analyses conducted, hydrocarbons have been detected in all the water samples. The organic geochemical methods have been used to determine the source of hydrocarbons detected in the water resources. The detected n-alkane hydrocarbons are the mature petroleum hydrocarbons derived from peat/coal type organic matter (Type III kerogen, gas-prone). The presence of these mature petroleum hydrocarbons is regarded as evidence for the existence of a working petroleum system in the study area. Due to the presence of waters containing mature petroleum hydrocarbons, the anticlines in the depth of approximately 110 m in fault-propagation folds identified in the investigation area by gravity and magnetic data have a very high potential to become gas reservoirs.

1. INTRODUCTION

The Beypazarı Neogene Basin, which commonly contains oil shale and coal, is located in the northwest of Ankara province (Figure 1). Regarding both interesting geology and economical value, lignite, gypsum, bituminous shale, clay, and trona deposits in the study area have been the subject of numerous geology targeted scientific studies in the literature until today. Coals and oil shales in the basin have been distinguished in many studies, and their formation environments, organic matter contents, and economic properties have been studied (Zieglar, 1939; Stchepinsky, 1941; Göktunalı, 1963; Aziz, 1976; Akkuş et al., 1982; Siyako, 1983; Yağmurlu et al., 1988a, b; Şener and Şengüler, 1991; Kavuşan, 1993; Şener et al., 1995; Özçelik, 2002; Özçelik and Altunsoy, 2005; Gülbay and Korkmaz, 2005, 2008; Şener, 2007; Toprak, 2010; Pehlivanlı, 2011; Vardaloğlu, 2016).

There are lignite seams in two stratigraphic levels in the Beypazarı Neogene Basin. The lower lignite seam is located at the lower levels of Çoraklar Formation while the upper lignite operated in Çayırhan Lignite Operation exists at the top levels of Çoraklar Formation (Figure 1). These units differ from the Hırka Formation with a characteristic contact. In the Koyunağılı lignite field, there is only the upper lignite seam (Figure 1). Lower lignite seams of Çoraklar formation present discontinuity in the lateral orientation. It was formed in the river environment and is completely different from the

* **Corresponding Author**

*(adilozdemir2000@yahoo.com) ORCID ID 0000-0002-3975-2846
(palabiyiky@itu.edu.tr) ORCID ID 0000-0002-6452-2858
(atilla.karatas@marmara.edu.tr) ORCID ID 0000-0001-9159-6804
(alperensahinoglu@esenyurt.edu.tr) ORCID ID 0000-0002-1930-6574

Received: 02/06/2020; Accepted: 28/06/2020

Cite this article

Ozdemir, A., Palabiyik, Y., Karataş, A., Sahinoglu A. (2020). Organic Geochemical Evidence of the Working Petroleum System in Beypazarı Neogene Basin and Potential Traps (Northwest Central Anatolia, Turkey). Turkish Journal of Geosciences, 1(2), 35-52.

upper lignite seam. The coals that make up the lower lignite level are generally characterized by blackish, locally banded, and matte colored soft lignites. The detectable thickness of the lower lignite level reaches up to 9 m. These coals, which are named as soft brown coal according to their physical properties, have a low calorific value (1700 kcal/kg). The upper lignite seam is laterally continuous and was formed in the mud plain facies of the playa-lake environment. The coals belonging to the upper lignite level are generally in dark brown and blackish, irregular bands, semi-gloss, and moderately hard. The total thickness of the upper lignite varies from 3.40 to 5.50 m and usually consists of two separate seams whereas the thickness of the coal seams of the upper lignite level varies from 1.40 to 2.10 according to the drilling and surface data. The calorific value of the upper lignite seam in the Çayırhan field was determined in the range from 3724 to 4602 kcal/kg while the calorific value of the lignite seam in the Koyunağılı field was measured as 2535 kcal/kg. The lignites in both fields are in uniform quality (Yağmurlu et al., 1988a). In the basin, 390 million tons of lignite reserves have been determined and Çayırhan Thermal Power Plant with a capacity of 620 MW power has been established in this area. Lignite seams outcropping in different thicknesses formed in the swampy environments of the lake basins in the Hırka Formation in different parts of the Beypazarı Neogene Basin have been identified. These lignites are called the plain basin type in terms of formation type (Toprak, 2010). The lignites of the Hırka formation exhibit different thicknesses. In the north and northwest of Beypazarı (Kabalar, Bahçeköy, Killikdere, Aşağıçay Dere, Sekili, and Hırkatepe), the thickness of the lignite veins ranges from 0.10 to 1.20 m (Özçelik, 2002; Toprak, 2010). In the Beypazarı Neogene basin, the coals in the Çayırhan region are named as Sector 1, and the coals between Çayırhan's coals in the Sector 1 and trona field are called Sector 2 (Figure 1) (Tarvirdi, 2013).

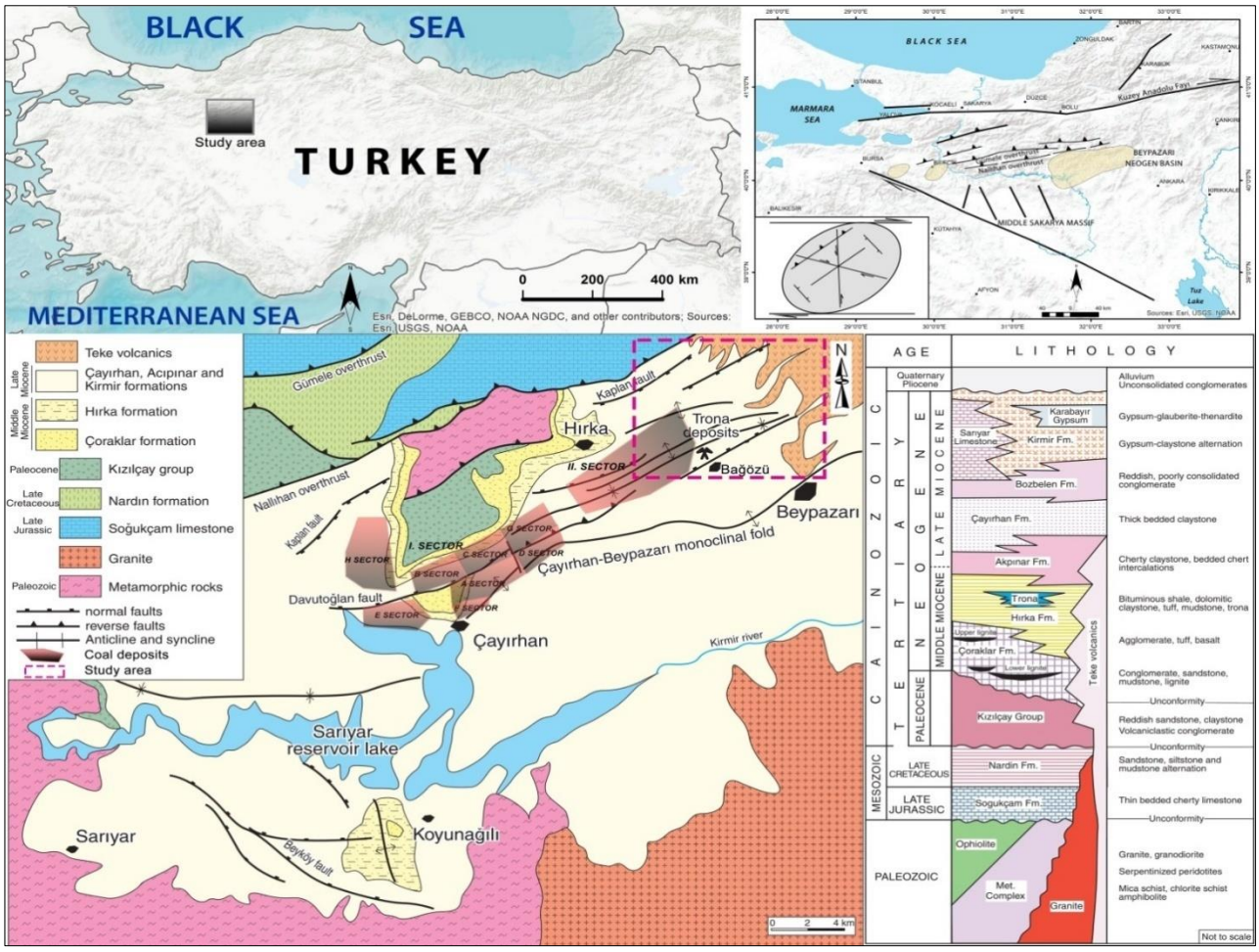

Figure 1. Geology and tectonic maps of the study area (modified from Yağmurlu et al., 1988a; Tarvirdi, 2013; Helvacı, 2018)

Oil shales in the Beypazarı Neogene Basin were formed within the Hırka Formation during the Miocene. Hırka Formation is a volcano-sedimentary sequence, reflecting the lacustrine environment conditions whose water level varies continuously (Yağmurlu et al., 1988c). Oil shales are in the form of small pockets (Ziegler, 1939). They are quite common in the basin and the thickness of the levels containing bituminous shale varies from 57 to 111 m (Gülbay, 2004; Vardaloğlu, 2016). Total organic

carbon (TOC) values change in each location and average TOC values are concentrated between 4% and 8% (Gülbay, 2004). Algal organic matter (kerogen) is dominant and featured by Type I-II. According to vitrinite reflection values and T_{max} values, the organic matter has not reached a sufficient maturity and not yet entered the oil window (Özçelik, 2002; Gülbay, 2004; Özçelik and Altunsoy, 2005; Vardaloğlu, 2016). Bituminous shales have 83% pyrolysable hydrocarbon content. They are appropriate for oil generation and a potential source that can produce oil on a large scale if exposed to higher temperatures (Gülbay, 2004). It can be interpreted that it reflects a lacustrine environment with high anoxicity, a possibly salty and mostly algal, and very little amount of terrestrial organic matter input (Gülbay and Korkmaz, 2005). Trona deposits, which constitute the other significant economic potential of the region, are located in the lowest part of the Hırka Formation and an alternating structure with bituminous shales (Yağmurlu et al., 1988a).

The bituminous shales of Beypazarı Neogene Basin have the potential source rock characteristics that can produce oil on a large scale if they are exposed to high temperatures. Beypazarı Neogene Basin consists of volcano-sedimentary units. Therefore, in this study, based on the idea that the immature source rocks can be matured by young volcanics that present widespread outcrops, especially in the northeastern part of the basin, it has been aimed to investigate the oil and gas potential of the basin by TPH (Total Petroleum Hydrocarbons) analysis performed on the samples taken from the natural cold water resources located in the northeastern of the basin. As a result of the analyses conducted, hydrocarbons have been detected in all the water samples. The determined n-alkane hydrocarbons are the mature petroleum hydrocarbons derived from peat/coal type organic mater (Type III kerogen, gas-prone) and these mature petroleum hydrocarbons are evidence for the presence of a working petroleum system in the research area.

2. GEOLOGICAL SETTING

Neogene sediments of Beypazarı Neogene basin are Middle-Upper Miocene aged and their total thickness is around 1200 meters. Paleozoic and Eocene basement rocks are unconformably covered by these Miocene aged sediments which filled the basin (Figure 1). These units are deposited in alluvial and lacustrine environments and locally contain volcanoclastic intercalations. The Miocene units in the Beypazarı Neogene Basin are separated from each other by time-exceeding boundaries that can be laterally and vertically inclined, depending on the changing lithofacies conditions from west to east. Most of the Miocene units are covered by Teke volcanics towards the northeast of the basin. Çoraklar Formation consists of a fluvial origin and cross-layered conglomerate, sandstone, siltstone, mudstone, terrestrial limestone intercalations, and two lignite levels. The thickness of Çoraklar Formation, which unconformably overlays the older units, varies from 80 to 237 m. The Hırka Formation composes of thin laminated mudstone, claystone, oil shale, calcareous shale, dolomitic limestone, tuff, trona, and locally intraformational breccia. The Hırka Formation, which reaches a thickness of 300 m in the basin, has been deposited in a playa-type lacustrine environment according to the composition and lithological characteristics it reflects (Yağmurlu et al., 1988a; İnci, 1991; Helvacı, 2018) whereas Cenozoic formations reflect a very shallow and active environment in Paleocene-Lower Eocene and Oligocene. The environmental conditions, which became quite shallow from the beginning of Paleocene-Eocene to the end of Oligocene, have acquired a terrestrial character in Miocene. In the Lower Miocene, terrestrial flow and rash volcanics developed from time to time. Volcanic units, which are highly effective on the sedimentation of coal and other sedimentary rocks and outcropped with extensional tectonics as a result of the movement of the North Anatolian Fault (NAF) in Miocene, present a rather complex relationship with Neogene basin sediments laterally and vertically. Paleotopographic basement uplifts controlled by developed block faults in Miocene indicates the presence of a lacustrine environment that deepens from south to north, where the uplifts of the basement are common in the southern parts. The outcrops, which usually characterize the coastal and near-shore parts, indicate the presence of a lake deepening under the volcanic cover. It is believed that suitable conditions for organic rock deposition occur in these lake(s) where the volcanic ash debris changes with the wind directions and the pH of the environment is controlled in paleoclimatological and paleogeographic parameters (Toprak, 2010).

There are thrust faults, high-angle reverse faults, and normal faults in the Beypazarı Neogene Basin. These faults are generally E-NE trending and approximately parallel to each other. The strike-slip faults transversely cut these fault systems. The normal faults were generally developed as step faults approximately parallel to each other in the south and north of the basin. These faults behaved as growth faults during the collapse. In later periods, normal and/or growth faults transformed to reverse faults. The formation of normal and strike-slip faults, which transversely or obliquely cut normal and reverse faults, also occurred during this compression period (Figure 2). The products of this compressional tectonics, probably occurring at the end of Miocene, outcropped in the north of the basin. Therefore, the basement rocks are visible on the surface. The breccia conglomerates in the Hırka Formation indicate concurrent tectonism along with precipitation. In particular, the structural development of the northern part of the basin has been largely completed by extensional tectonics.

Asymmetric fold systems, monoclinal structures, and reverse fault systems indicate that the compressional tectonics gradually took the place of the extensional tectonics in the basin towards the end of Miocene. The structural features in the Beypazarı Miocene Basin are controlled by the North Anatolian and Eskişehir Faults. The opposite movement of the North Anatolian Fault to the Eskişehir Fault and the geostationary block of Central Sakarya Massive may have caused a one-way compressional regime that runs from north to south in the region (Yağmurlu et al., 1988b; İnci, 1991). This one-way compressional regime in the Miocene and pre-Miocene units in the study area has created numerous structures such as anticlines, synclines, recumbent folds, and fractured systems (i.e., Zaviye Fault, Koçali River Anticline, Beypazarı Monocline/Flexure) (Figure 1).

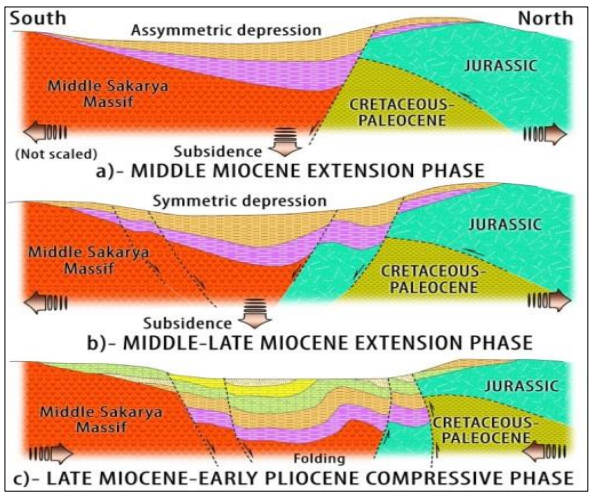

Figure 2. Tectonic development of Beypazarı Neogene basin (modified from Yağmurlu et al., 1988b; Helvacı, 2018)

3. MATERIAL AND METHOD

Eymold et al. (2018) have determined that shallow groundwaters above the basin formations containing shale gas are enriched in hydrocarbons. They have also expressed that the hydrocarbons in these hydrocarbon-rich waters migrated from deep source rocks to shallow aquifers. Moreover, Kreuzer et al. (2018) have mentioned that the faults in petroliferous basins make the transportation of hydrocarbon-rich brines to aquifer formations above source rocks easy by influencing the geochemistry of shallow groundwaters and cause a hydrocarbon enrichment in these waters. On the other hand, in recent times, TPH in water analysis has started to be utilized in petroleum exploration, which allows the determination of hydrocarbon-rich waters and organic geochemical properties in basins/regions where source rocks are not exposed at the surface as outcrops (covered basins) or has been exhausted (depleted or spent) (Ozdemir, 2019a-c; Karataş et al., 2019; Palabiyik et al., 2019, 2020; Palabiyik and Ozdemir, 2020; Ozdemir et al., 2020). Furthermore, in recent studies, it has been come into existnce that all organic geochemical analyses conducted on source rock and gas samples can also be applied to hydrocarbon-rich surface and subsurface waters determined by TPH in water analysis and that the same analysis and interpretation results for the same basins/regions have been reached (Figure 3) (Ozdemir, 2018; Liu et al., 2018). According to these studies, if an oil and/or gas reservoir exists in a region, the surface and subsurface waters in the study area should be rich in mature petroleum hydrocarbons (Figure 4). Therefore, it can be inferred that the technique of TPH analysis in water will significantly contribute to reservoir-targeted oil and gas exploration activities.

TPH value provides information on hydrocarbon contamination of water resources. Gas chromatography (GC) analyses are performed to detect the TPH concentrations of the water contaminated by hydrocarbons. In the determination of TPH content, the standard test method "the Determination of Hydrocarbons: Solvent extraction and gas chromatography method (ISO 9377-2)" is used (other methods: EPA Method 1664 and ASTM D7678-11). In this technique, aromatic hydrocarbons are separated, and the total amount of petroleum hydrocarbons is determined in the samples taken from the surface, subsurface, and distribution waters. These samples are stored by an acidification process to prevent the issues, which may affect the number of hydrocarbons, such as evaporation or biodegradation in the samples. Samples are analyzed within 14 days if acidified, or they are performed within 7 days if not done, and stored at 5°C ± 3°C before the analysis.

In the comprehension of this research, totally 25 samples have been taken by the scaled polyethylene bottles of 1 liter from the natural flowing waters (cold water fountains) in the region (Figures 5 and 6). The water samples are taken from the untreated water resources that are not related to tap water (running water). Since the water samples collected from the study area have been analyzed a few days after the sampling, no acidification process has not applied to the samples. They were collected and preserved according to the standard procedures (ISO 5667-3) and analyzed in the laboratory for TPH in water employing the standard methods (ISO 9377-2). In the samples, the TPH analyses have been conducted by a gas chromatography device in the laboratory to generate data for organic geochemical evaluations. Thus, direct TPH concentrations of the water samples (in mg/l) have been determined depending on the analyses and the required geochemical parameters (CPI, NAR, etc.) to be discussed in detail in the next section of the paper have been calculated by making use of gas chromatograms. In the geochemical evaluations, the TPH concentrations and the calculated parameters are utilized.

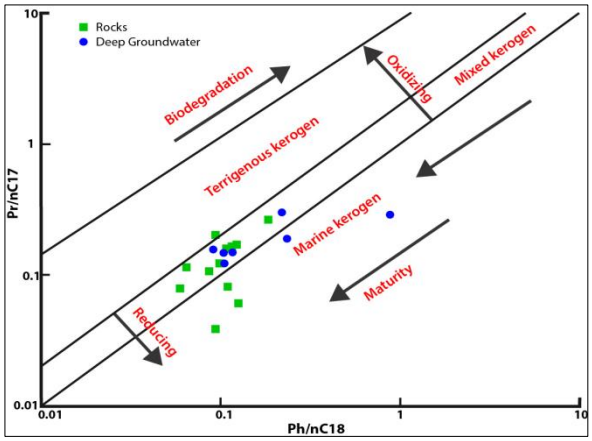

Figure 3. Ph/nC18 vs Pr/nC17 ratios of deep groundwater and rock samples taken from the same region (Liu et al., 2018) (Pr: Pristane and Ph: Phytane isoprenoid hydrocarbons, nC17 and nC18: n-alkane hydrocarbons)

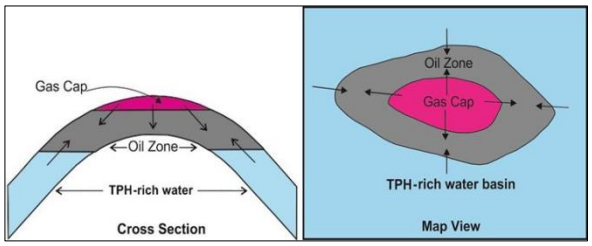

Figure 4. Components of an anticlinal type of petroleum reservoir that can be produced by primary methods (Ozdemir, 2018)

4. FINDINGS AND DISCUSSION

Based on the TPH analysis results regarding the water samples taken from the study area, concentrations, biodegradation conditions, source, maturity, and redox conditions of the depositional environment of the hydrocarbons in the waters are investigated in a geochemical point of view. Moreover, the aeromagnetic and gravity maps prepared for the study area are interpreted in terms of geological and tectonic aspects, and the construction of the conceptual occurrence, migration, and accumulation model of the hydrocarbons is targeted.

4.1. Contents, Source, and Biodegradation of Hydrocarbons in Waters

Liu et al. (2018) have defined groundwater of which hydrocarbon concentration exceeds 0.05 mg/l as original hydrocarbon-rich groundwater. The TPH limit values recommended for surface and subsurface waters are given in Table 1. Surface and subsurface waters exceeding the TPH values in Table 1 are defined as hydrocarbon-rich waters. The n-alkane hydrocarbons have been found in all the water samples in the study area. The hydrocarbon content of the water samples is much higher than the limit values suggested for the waters (Tables 1 and 2). Hence, it can be mentioned that water-rock-hydrocarbon interactions have created this hydrocarbon enrichment in waters.

Source, maturity, migration, and biodegradation are the main elements responsible for the compositional changes in hydrocarbons. Ph/n-C18 value less than 1 indicates non-biodegraded hydrocarbons (Hunt, 1995). Ph/n-C18 values of all the water samples are less than 1 and according to these values, the hydrocarbons in the water samples are in a non-biodegraded character.

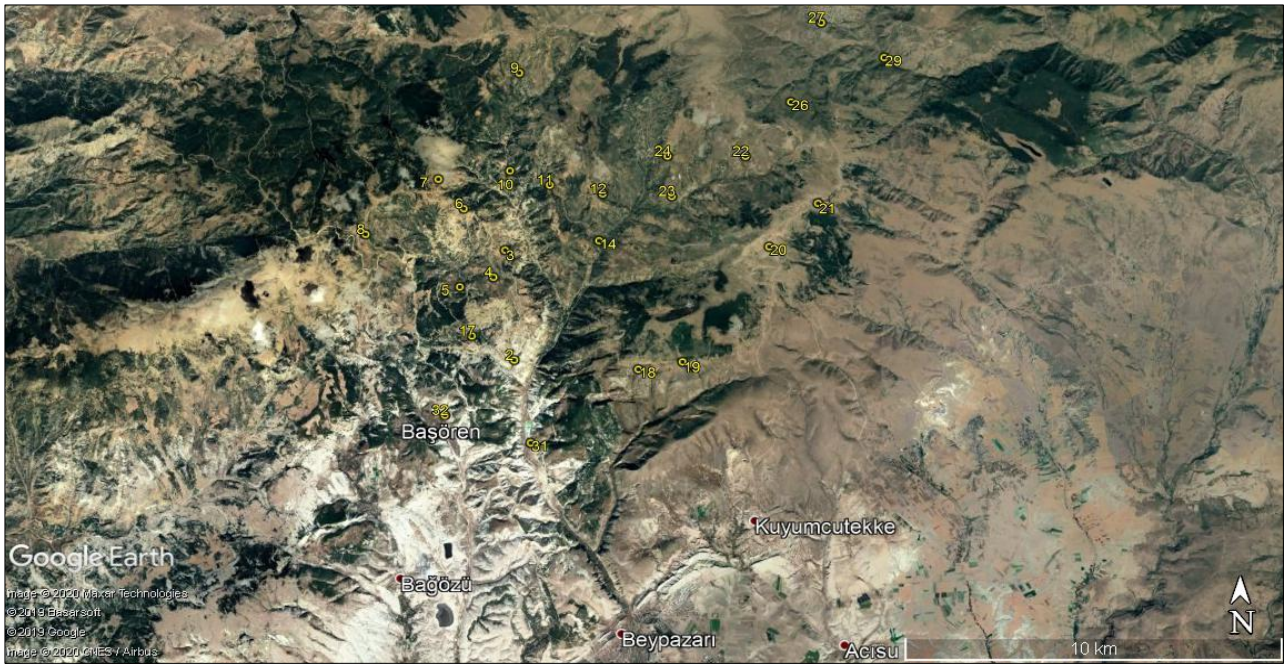

Figure 5. Location map of the taken water samples (yellow circles: the water samples)

Figure 6. A view of water sampling procedure from cold water fountains (pure and clean natural flowing waters) in the study area by using scaled polyethylene bottles

By making use of gas chromatography analysis outcomes, the Carbon Preference Index (CPI), Pr/Ph ratio, isoprenoid/n-alkane ratio (Pr/nC17 and Ph/nC18) have been computed, and the n-alkane distributions have been evaluated. In this study, Pr/Ph ratio (Didyk et al., 1978; Tissot and Welte, 1984; Banga et al., 2011), Carbon Preference Index (CPI) (Bray and Evans, 1961, 1965; Tissot and Welte, 1984), Pr/Ph versus CPI (Onojake et al., 2013; Hakimi et al., 2018), and Pr/n-C17 versus Pr/Ph (Syaifudin et al., 2015; Larasati et al., 2016; Devi et al., 2018) plots are utilized to assess the water samples. Organic geochemical parameters of bituminous shales in Beypazarı basin have been determined in some studies (Özçelik, 2002; Gülbay and Kormaz, 2005; Vardaloğlu, 2016). The results obtained from these studies are similar. Therefore, in this study, only the data in Vardaloğlu (2016)'s study are included in the plots.

Table 1. The TP limit values recommended for surface and subsurface waters

TPH (mg/l)	Reference
< 0.05	Liu et al. (2018)
< 0.1	Zemo and Foote (2003)
< 0.5	Ozdemir (2018)
< 0.2	Ministry of Agriculture and Forestry of Turkey (2004a), Surface Water Quality Regulation of Turkey (Appendix 5, Table 2: Oil and Grease)
< 0.02	Ministry of Agriculture and Forestry of Turkey (2004b), Water Pollution Control Regulation of Turkey (Appendices Table 1: Oil and Grease)

CPI is an indicator for the source of n-alkanes. The CPI, a ratio between the amounts of n-alkanes with odd and even carbon number, is calculated by measuring the heights of the peaks in gas chromatograms. The dominant peaks in these chromatograms are represented by n-alkanes. In the computation of the CPI, various equations have been proposed by numerous researchers. This index can be applied to any range of the carbon sequence. It is utilized to assess the kind of organic matter, the depositional environment, and thermal maturity. It is remarkably greater than 1 (odd n-alkane preferential) or lower than 1 (even n-alkane preferential), indicating thermally immature oil or bitumen samples (Tissot and Welte, 1984; Peters and Moldowan, 1993). A high value of CPI in the immature or low-maturity sample means the input of organic matter derived from higher terrestrial plants (Tran and Philippe, 1993). According to the CPI values (Table 2), the source of n-alkanes in the water samples remarks the petrogenic hydrocarbons and old organic-rich sediments (Table 3).

The term petrogenic sources describe unburned fossil resources like crude oil and coal. These types of sources were formed very slowly at moderate temperatures (between 100°C and 300°C) millions of years ago (Beyer et al., 2010). The parameter NAR (Natural n-alkane Ratio) has been suggested to interpret the source of hydrocarbons in the environment (natural or petroleum n-alkane). This ratio is zero or approximately zero for natural petroleum hydrocarbons and crude oil. In other hydrocarbon sources, those ratios are greater. According to the parameter NAR (Table 2), all the n-alkanes in the water samples indicate natural petroleum (petrogenic) hydrocarbons.

The parameter TAR (Terrestrial/aquatic hydrocarbon ratio) shows the ratio of n-alkanes derived from terrestrial organic matter to n-alkanes derived from aquatic algae (Cranwell et al., 1987; Goossens et al., 1989; Meyers and Ishiwatari, 1993; Bourbonniere and Meyers, 1996). High values of TAR (greater than 1) sign terrestrial plant source and its low values (less than 1) mean marine algae source (Kroon, 2011). The TAR values have been calculated as quite high for the inspected water samples (greater than 1) (Table 2). These values show that the n-alkanes having high carbon numbers indicating terrestrial organic matter are dominant in the water samples in the examined area.

Waxiness index can be utilized to determine the amount of terrestrial organic matter. This index depends on the assumption that regional terrestrial organic matter contributes to extracts with the n-alkane components with high molecular weight (Peters et al., 2005). It is observed that the water samples in the investigation area have high Waxiness values indicating high amounts of biomarkers derived from terrestrial plant (Table 2). This finding is also supported by the fact that the analyzed samples show high TAR values.

The n-C17/n-C31 ratio indicates the source of the hydrocarbons derived from the organic matter in the environment. High values (higher than 2) correspond to marine algae while low values (lower than 2) sign land plant sources (Forster et al., 2004). The ratio of n-C17/n-C31 of the water samples ranges from 0.11 to 0.26 by indicating the terrestrial organic matter. This consequence is consistent with TAR and Waxiness index values.

By calculating P_{aq} and P_{wax} parameters, some interpretations can be made about the plant species that make up the organic matter and the paleoclimate conditions of the environment (Zheng et al., 2007). These parameters are used only for coals. If P_{aq} value is less than 0.1, it will mean terrestrial plants; if it is between 0.1 and 0.4, it will refer to aquatic plants (floated in the swamp environment), and if it is between 0.4 and 1.0, it will mean that environments exist the presence of plants floated in the water (Ficken et al., 2000). According to P_{aq} values (Table 2), the types of plants that constitute the organic matter-deriving hydrocarbons in the water samples are predominantly aquatic plants (floated in the swampy environment). If the P_{wax} value is lower than 0.7, it means dry climate conditions whereas if it is less than 0.7, it will mean the existence of humid climate conditions (Zheng et al., 2007). According to the P_{wax} values (Table 2), the organic matter-deriving hydrocarbons in the water samples was formed in dry climate conditions.

Table 2. TPH analysis results of the water samples and the calculated parameters

Sample No.	Water Resource	Coordinates		TPH (mg/l)	CPI	TAR	NAR	n-C17/n-C31	P_{aq}	P_{wax}	Waxiness Index	Pr/Ph	Pr/n-C17	Ph/n-C18
		X	Y											
2	Natural flowing water	4454774	405296	0.62	1.61	11.78	0.06	0.12	0.07	0.93	2.58	6.87	0.31	0.11
3	Natural flowing water	4457891	405075	0.59	1.60	7.85	-	0.19	-	-	5.37	9.56	0.25	0.08
4	Natural flowing water	4457124	404758	0.46	1.59	7.10	0.03	0.26	0.18	0.82	3.43	7.93	0.25	0.09
5	Natural flowing water	4456858	403857	1.00	1.61	7.92	0.09	0.17	0.06	0.94	2.17	6.29	0.25	0.12
6	Natural flowing water	4459077	403980	0.47	1.52	9.63	0.11	0.16	0.06	0.94	2.72	12.18	0.29	0.06
7	Natural flowing water	4459918	403305	0.71	1.57	8.69	-	0.14	-	-	2.27	7.40	0.30	0.09
8	Natural flowing water	4458370	401349	0.68	1.62	8.26	0.02	0.17	0.11	0.89	2.64	8.91	0.28	0.09
9	Natural flowing water	4462912	405492	0.59	1.62	8.22	-	0.14	-	-	2.28	10.77	0.28	0.07
10	Natural flowing water	4460140	405221	0.52	1.62	7.98	-	0.15	-	-	2.28	17.17	0.30	0.06
11	Natural flowing water	4459726	406279	0.65	1.60	7.58	0.10	0.18	0.10	0.90	3.83	8.44	0.24	0.08
12	Natural flowing water	4459462	407693	0.53	1.61	7.56	-	0.19	-	-	4.26	13.04	0.29	0.06
14	Natural flowing water	4458137	407582	0.57	1.67	7.55	0.11	0.17	0.08	0.92	3.71	5.14	0.06	0.04
17	Natural flowing water	4455466	404170	0.58	1.57	-	0.10	0.11	0.17	0.83	-	6.40	0.33	0.11
18	Natural flowing water	4454486	408601	0.57	1.59	-	0.18	0.13	0.17	0.83	-	7.22	0.36	0.12
19	Natural flowing water	4454688	409785	0.47	1.61	7.61	0.20	0.19	0.17	0.83	6.12	9.45	0.27	0.08
20	Natural flowing water	4457929	412115	0.55	1.65	-	0.27	0.16	0.24	0.76	-	7.62	0.26	0.09
21	Natural flowing water	4459147	413428	0.64	1.67	-	0.27	0.15	0.20	0.80	-	7.87	0.31	0.11
22	Natural flowing water	4460495	411507	0.66	1.67	6.61	0.27	0.20	0.17	0.83	5.02	7.37	0.25	0.12
23	Natural flowing water	4459378	409534	0.60	1.64	6.67	0.32	0.19	0.20	0.80	5.13	6.78	0.25	0.14
24	Natural flowing water	4460520	409429	0.75	1.67	6.28	0.25	0.20	0.10	0.90	4.57	6.95	0.21	0.10
26	Natural flowing water	4462023	412729	0.43	1.63	8.17	0.24	0.17	0.16	0.84	6.13	7.00	0.32	0.13
27	Natural flowing water	4464265	413558	0.56	1.67	7.35	0.18	0.19	0.11	0.89	5.58	9.49	0.27	0.08
29	Natural flowing water	4463259	415222	0.57	1.60	8.72	0.05	0.13	0.09	0.91	2.21	14.38	0.27	0.05
31	Mineral water	4452425	405715	0.69	1.71	6.94	0.23	0.18	0.10	0.90	5.00	10.51	0.23	0.07
32	Natural flowing water	4453224	403432	0.63	1.61	6.54	0.23	0.20	0.14	0.86	4.68	11.69	0.23	0.07

CPI = {[(C23+C25+C27) + (C25+C27+C29)] / [2 *(C24+C26+C28)]} (Bray and Evans, 1961), TAR = (C27+C29+C31)/(C15+C17+C19) (Bourbonniere and Meyers, 1996), NAR = [Σn-alk (C_{19-32}) - 2Σ even n-alk (C_{20-32})] / Σ n-alk (C_{19-32}) (Mille et al., 2007), Waxiness Index:∑ (n-C21-n-C31)/∑ (n-C15-n-C20) (Peters et al., 2005), P_{aq} = (C23+C25)/(C23+C25+C27+C29+C31) (Ficken et al., 2000), P_{wax} = (C27+C29+C31)/(C23+C25+C27+C29+C31) (Zheng et al., 2007), - : Could not be calculated.

Table 3. Source of n-alkanes in water according to CPI value (Ozdemir, 2018)

CPI	Source
> 2.3	Young terrestrial sediments (biogenic hydrocarbons)
1.2 - 2.3	Old organic matter-rich sediments (marine shales, limestones, etc.)
≤ 1.2	Petrogenic hydrocarbons (values < 1 biodegraded oils)

4.2. Maturity of Hydrocarbons in Waters and Redox Conditions of Sedimentation Environment

CPI value of mature hydrocarbons is equal to 1 or close to 1 (Waples, 1985). The CPI values of oil and bitumen related to very salty carbonate or evaporitic environments are lower than 1 (Tissot and Welte, 1984; Peters and Moldowan, 1993). The maturity level of hydrocarbons is classified based on their CPI

values (Table 4) (Onojake et al., 2013), and depending on this classification, all the hydrocarbons in the water samples (Table 2) can be classified as mature (more oxidizing) level.

Table 4. The maturity level of hydrocarbons according to CPI value (from Onojake et al., 2013) (see Figure 7)

CPI	Maturity
>1	Mature (oxidizing-reducing)
0.8 - 1	Mature
< 0.8	Immature

The n-alkanes, which are the closest to isoprenoids in gas chromatograms, are utilized for isoprenoid/n-alkane ratios. The Pr/Ph ratio is an appropriate correlation parameter. Even though pristane (Pr) and phytane (Ph) define other sources, they are derived from phytyl, which is the side chain of chlorophyll, particularly in phototropic organisms. Under anoxic conditions, the side chain of phytyl breaks down to form the phytol, while phytol is also reduced to pristane under oxic conditions (Peters and Moldowan, 1993). Hence, the Pr/Ph ratio shows the redox potential of the depositional environment. Pr/Ph values lower than 1 reflect anoxic conditions while the values higher than 1 remark oxic conditions (Didyk et al., 1978; Hunt, 1995). The water samples in the study area exhibit a high Pr/Ph ratio varying from 5.14 to 17.17 (Table 2). Therefore, the water samples contain the hydrocarbons derived from sediments deposited in an oxic environment (Pr/Ph > 1). The Pr/Ph ratio also provides information about paleoenvironment and maturity (Volkman and Maxwell, 1986) level. In the Pr/Ph versus CPI relationship, it can be observed that the hydrocarbons in the water samples are located in the more oxidizing zone and have similar maturity levels (Figure 7).

Pr/n-C17 and Ph/nC18 ratios are commonly made use of in petroleum correlation studies. Samples containing high Pr reflect an oxidizing source, and high Ph content indicates a reducing source. Thus, the plot of Pr/n-C17 versus Ph/n-C18 is utilized to distinguish petroleum or bitumen in different groups (Hunt, 1995). Although the Pr/Ph ratio above 1.5 shows settling conditions in an oxygenated environment based on a standard geochemical interpretation, it is well-known that it may be lower than 1 for an anoxic depositional environment. Lower values may indicate less suitable oxic conditions than the other parts of the same sequence (Hartkopf-Fröder et al., 2007). The ratio of isoprenoid/n-alkane decreases with increasing maturity as more amounts of n-alkanes release from kerogen affected by a breaking down process (Tissot and Welte, 1984; Hunt, 1995) and is used as a degree of maturity for biodegradable oil and bitumen samples. It increases with the biodegradation (Hunt, 1995) and is also affected by organic matter input and secondary phenomena. Depending on their positions in the Pr/nC17 versus Ph/nC18 plot of the water samples, it is observed that the source rocks which generated the hydrocarbons in the water samples are deposited in oxic terrestrial (Type III kerogen, gas-prone) environment and exhibit a high maturity (Figures 7-11 and Table 5). Even though oxic paleo-environment conditions is generally probable for Çoraklar ve Hırka Formations, it has been concluded that anoxic and suboxic paleo-environment conditions is also possible (Sönmez, 2016). To sum up, it is revealed that the results obtained from this study are compatible with those of Sönmez (2016)'s study.

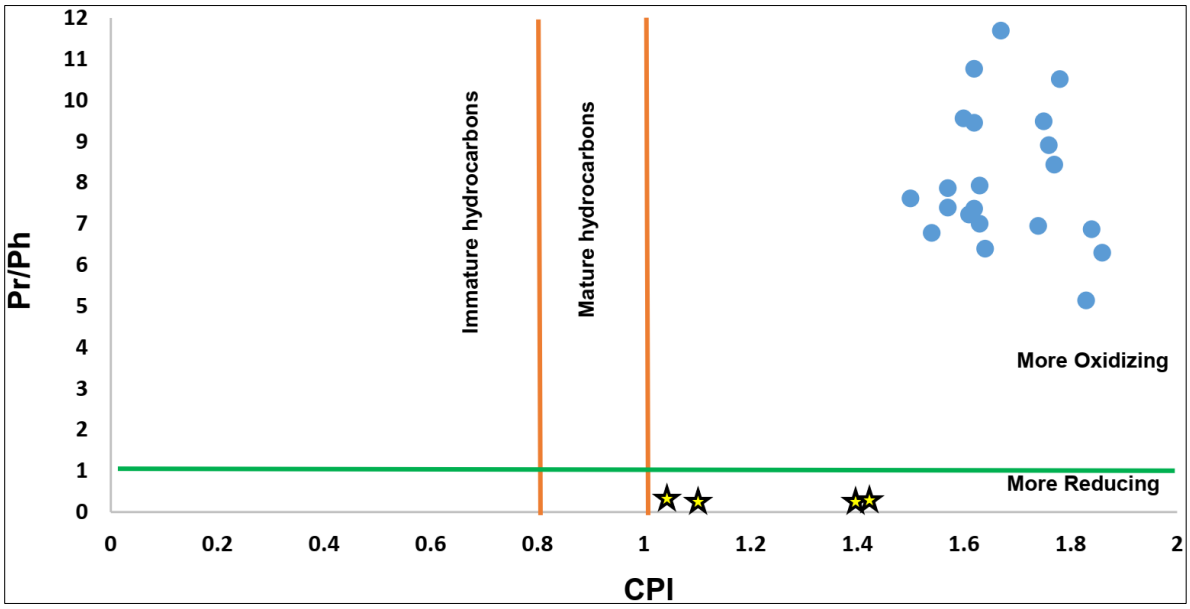

Figure 7. Pr/n-C17 vs Ph/n-C18 plot (the plot: from Peters et al., 1999). Blue circles: the water samples (this study), yellow stars: the samples of Beypazarı bituminous shale (the data: Vardaloğlu, 2016)

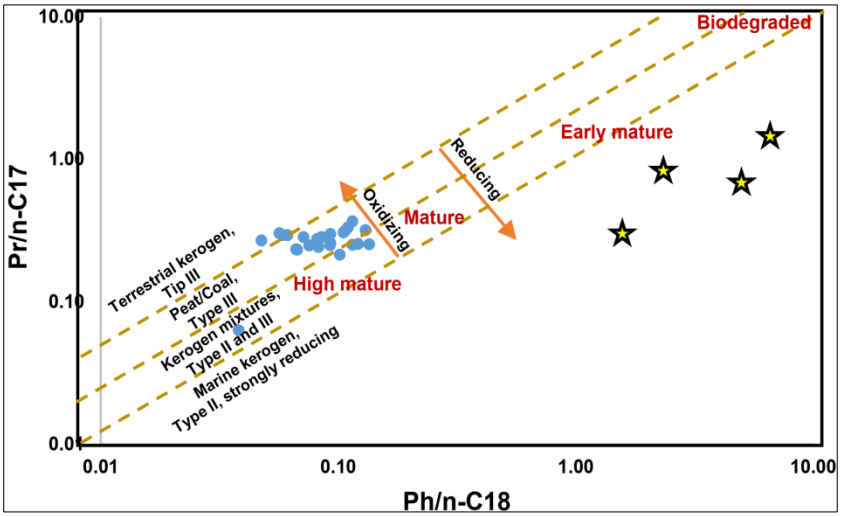

Figure 8. Pr/n-C17 vs Ph/n-C18 plot of the water samples (the plot: from Peters et al., 1999). Blue circles: the water samples (this study), yellow stars: the samples of Beypazarı bituminous shale (the data: Vardaloğlu, 2016)

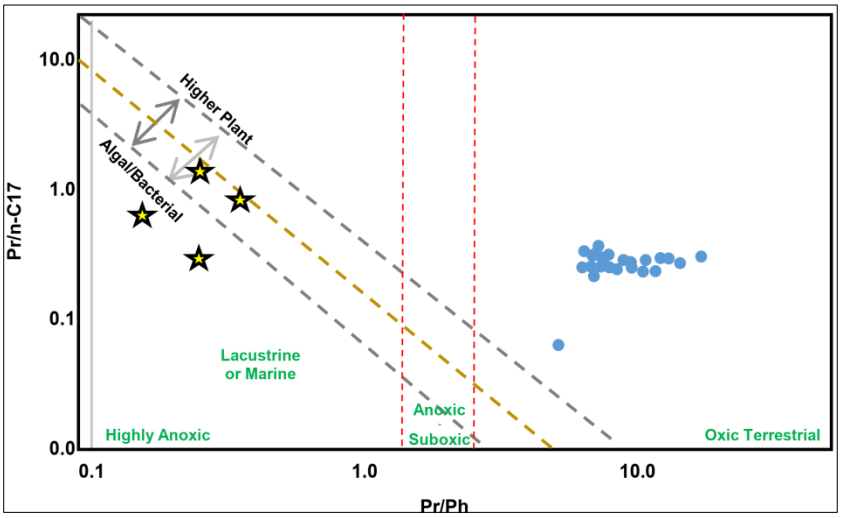

Figure 9. Pr/n-C17 vs Pr/Ph plot of the water samples (the plot: from Devi et al., 2018; Larasati et al., 2016; Syaifudin et al., 2015). Blue circles: the water samples (this study), yellow stars: the samples of Beypazarı bituminous shale (the data: Vardaloğlu, 2016)

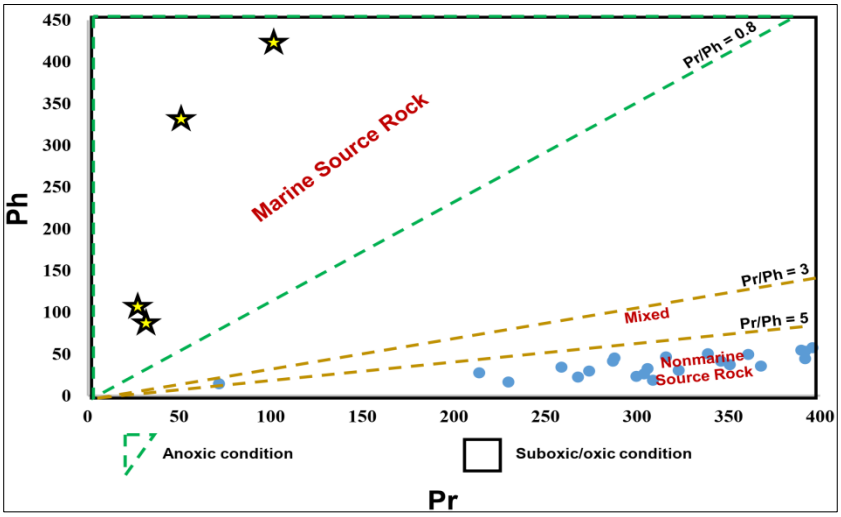

Figure 10. Ph vs Pr plot of the water samples (the plot: from Banga et al., 2011). Blue circles: the water samples (this study), yellow stars: the samples of Beypazarı bituminous shale (the data: Vardaloğlu, 2016)

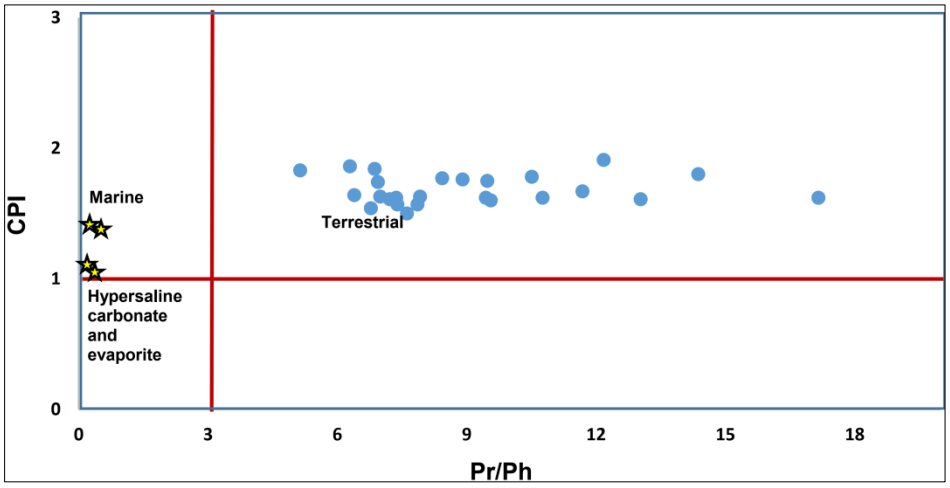

Figure 11. Pr/Ph vs CPI plot of the water samples (the plot: from Hakimi et al., 2018). Blue circles: the water samples (this study), yellow stars: the samples of Beypazarı bituminous shale (the data: Vardaloğlu, 2016)

Table 5. Source rock and depositional environment of hydrocarbons according to Pr/Ph value (from Banga et al., 2011) (see Figure 10)

Pr/Ph	Source rock	Pr/Ph	Environment
< 3	Marine	< 0.8	Anoxic
3 - 5	Marine - Terrestrial	> 0.8	Suboxic-Oxic
> 5	Terrestrial		

4.3. Aeromagnetic and Gravity Maps of the Study Area and Geological Interpretations

There are a lot of studies regarding the methods and field applications of gravity and aeromagnetic data for use in oil and gas exploration (Griffin, 1949; Nettleton, 1976; Geist et al., 1987; Lyatsky et al., 1992; Gadirov, 1994; Piskarev and Tchernyshev, 1997; Pašteka, 2000; Aydın, 1997, 2004; Gadirov and Eppelbaum, 2012; Ivakhnenko et al., 2015; Satyana, 2015; Eke and Okeke, 2016; Stephen and Iduma, 2018; Gadirov et al., 2018; Ozdemir, 2019a-c; Ozdemir et al., 2020). Analysis of gravity and magnetic anomalies has been a permanent component of hydrocarbon exploration and discovery in West Siberia for half a century (Piskarev and Tchernyshev, 1997). In the regions where the existence of mature petroleum hydrocarbons is proved by the determination of hydrocarbon-rich waters in this research, particularly seismic surveys are crucial to determine the locations of oil and gas reservoir(s)/trap(s). Unfortunately, no seismic lines/measurements are available in the investigated area. The contour maps specifically prepared for the study area from regional gravity and aeromagnetic data measured by the General Directorate of Mineral Research and Exploration of Turkey (MTA) have been utilized to evaluate subsurface geology of the area.

The gravity map prepared for the study area (Figure 12) contains young sediments composed of lower-density sedimentary origin rocks (siltstone, mudstone, claystone, conglomerate, shale, etc.) and metamorphic (slate, phyllite, etc.) rocks represented by dark blue, light blue, and green colors. In the areas featured by orange, red, and yellow colors, an anomaly is characterized by the rocks having relatively higher densities (crystallized limestone, marble, quartzite, schist, etc.).

The prepared aeromagnetic map for the study area (Figure 12) demonstrates the anomalies that originated from fully non-magnetic sedimentary (sandstone, limestone, siltstone, mudstone, claystone, conglomerate, shale, etc.) and metamorphic (crystallized limestone, marble, quartzite, schist, etc.) rocks represented by blue, green, and light green colors. In the areas represented by yellow, red, and white tones, there are the rocks with magnetic properties (pebbly volcanic sandstones, ophiolites, dikes, etc.). Hydrocarbon reservoirs are located mostly at the slopes of both positive gravity and magnetic anomalies (in areas where both gravity and magnetic anomaly are high) in Northwestern Siberia. All known oil and gas deposits are in regions characterized by relatively high gravity anomalies (Piskarev and Tchernyshev, 1997). In the magnetic and gravity maps of the study area, the structures located in the areas where both gravity and magnetic anomalies are positive together are potential gas reservoirs. Tectonic structures in and around the study area were investigated by İnci (1991) and Seyitoğlu et al. (2017). Seyitoğlu et al. (2017) stated that there are many blind thrust faults in the study area. According to the gravity map, the potential gas traps are located between these blind thrust zones (Figure 12).

In the study, the interpretation method proposed by Svancara (1983) and Töpfer (1977) is used to convert the 2D (two-dimensional) residual gravity anomalies into the depth values for the estimation of the basin and structure depths. In this method, if the density contrast is known, the depth of the sedimentary basin or structure can be determined by simple relations established between

gravity anomaly and parameters. The first stage of the interpretation gives the characteristic parameters of the anomaly (Figure 13). The relevant equations can be expressed as follows:

$$A = \frac{g_{mak}}{W_a \sigma} \quad (1)$$

Where

g_{mak}: Maximum amplitude of the gravity anomaly,

W_a: Distance corresponding to the half amplitude ($g_{mak}/2$) value of the gravity anomaly,

σ: Density contrast.

$$\frac{W_b}{W_a} = (-0.056A) + 1.827 \quad (2)$$

$$D_o = 23.866 \frac{g_{mak}}{\sigma} \quad (3)$$

For the condition 0 < A < 9 (Töpfer 1977):

$$\frac{D}{D_o} = 0.072A + 1.00 \quad (4)$$

For the condition 9 < A < 13 (Töpfer 1977):

$$\frac{D}{D_o} = 0.12A + 0.57 \quad (5)$$

where

W_b: Full width of the gravity anomaly,

D_i: Depth corresponding to the gravity anomaly value,

D_o: Depth obtained from the flat-plate formula,

D: Maximum depth.

An A-B profile is obtained from the residual gravity anomaly map of the study area (Figure 12). According to the anomalies of residual gravity map of the study area, the maximum depth of the structure (D) has been calculated as 110 m (Figure 14). The depth of the computed potential traps well-matches with the data of Seyitoğlu et al. (2017).

The mature hydrocarbons-rich waters are evidence for a working petroleum system in the study area. Possible gas reservoirs in the study area are the blind thrust anticlines which is determined by the gravity and magnetic maps (Figures 11 and 13). The fact that to be between two thrust zones of the structures, reinforces the possibility of having accumulated of hydrocarbons in these structures. Hydrocarbons-rich waters that migrate from the source rocks and/or oil reservoirs in the subsurface cause definable changes in the hydrocarbon concentration of surface and subsurface waters (Özdemir, 2018). Hydrocarbons in the water samples are enriched as a result of the water-rock-hydrocarbon interaction with the hydrocarbon-rich geological units in the subsurface and/or mixed with shallow groundwaters migrated from the potential reservoirs determined by gravity and magnetic maps (Figure 12).

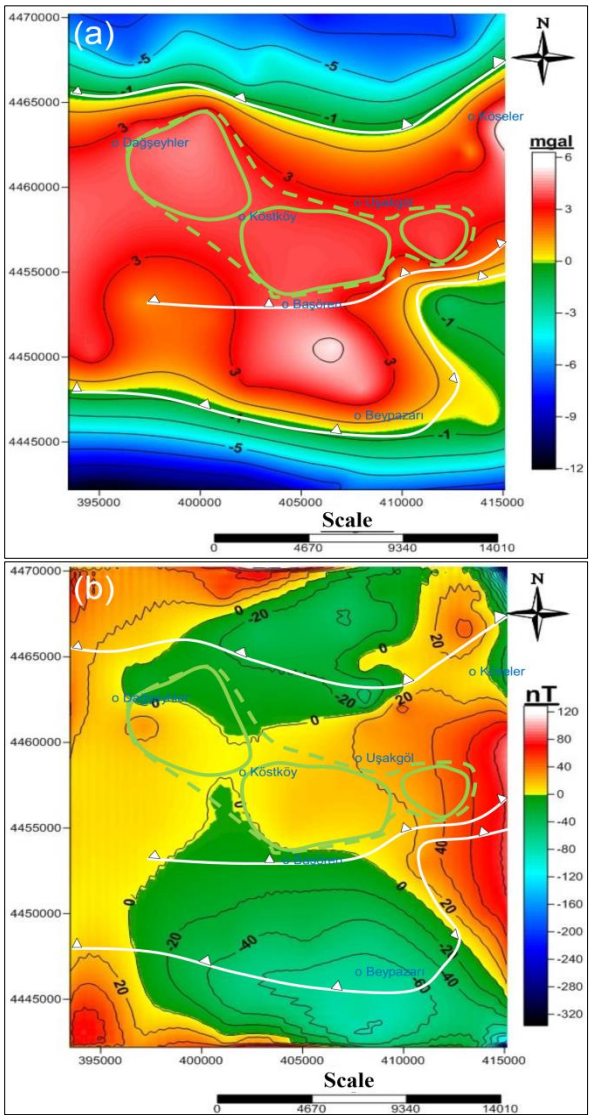

Figure 12. The colored contour maps and geological interpretations of the regional gravity (a) and aeromagnetic (b) anomalies of the study area. Green polygons: possible gas traps:, white lines: blind thrust faults (teeth show the overthrust unit)

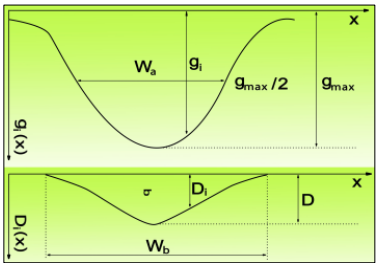

Figure 13. Ideal gravity anomaly of a basin and characteristic parameters (Svancara, 1983)

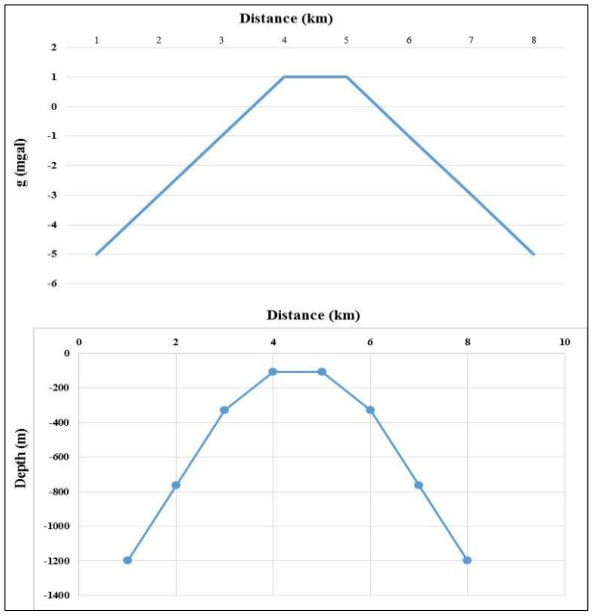

Figure 14. The depths of potential gas reservoirs in the study area

4.4. Conceptual Occurrence, Migration, and Trapping Model of Hydrocarbons in the Investigation Area

Ozdemir (2019a, b), Ozdemir and Palabiyik (2019a, b) and Ozdemir et al (2020) have mentioned that petroleum source rocks are formed in the mid-ocean ridges and the continental rifts (spreading centers). Hence, the source rocks which generated the hydrocarbons in the water samples should have formed in the geological periods that involved in the rifting process in the investigation area. In the area, the volcanism accompanying the expansion regime in the Early-Upper Miocene period should have brought about the occurrence of source rock in the region (Figures 2 and 15). Senger et al. (2017) have studied the impacts of magmatic intrusions on petroleum systems. The main elements of a petroleum system; (1) conditions leading to the hydrocarbon generation, (2) the ways in which hydrocarbons migrated from the source rock can migrate, (3) a porous and permeable rock acting as a reservoir for hydrocarbons, (4) low-permeable peripheral rock units, and (5) a covered structure (trap). Magmatic intrusions can affect anyone or several of these five major elements of a petroleum system. Jointed and permeable magmatic intrusions can create new migration paths, or act as a fluid barrier when they are crystallized and impermeable (Senger et al., 2017). Hydrocarbon-rich waters can be transported from the hydrocarbon reservoirs to the surface and mixing with different origin waters (meteoric or sea waters, etc.) with the effect of these magmatic activities,. In the maturation process of the hydrocarbons in the water samples, it is considered that the emplacement of Beypazarı granite and intense volcanic activities are effective (Figure 1).

In the Late Miocene-Early Pliocene period (Fig. 2), many blind thrusts (Seyitoğlu et al., 2017) and fault-progression folds (Yağmurlu et al., 1988b; Helvacı, 2018) was formed in the basin due to the compression tectonics. Fault-propagation folds between blind thrusts are potential gas reservoirs (Figure 16). There are two different dolomite levels in the Hırka Formation, in the trona levels, and above and below trona levels (Özpeker et al., 1991). Consequently, the dolomites of Hırka formation and carbonate rocks in younger units in the identified structures are possible reservoir rocks.

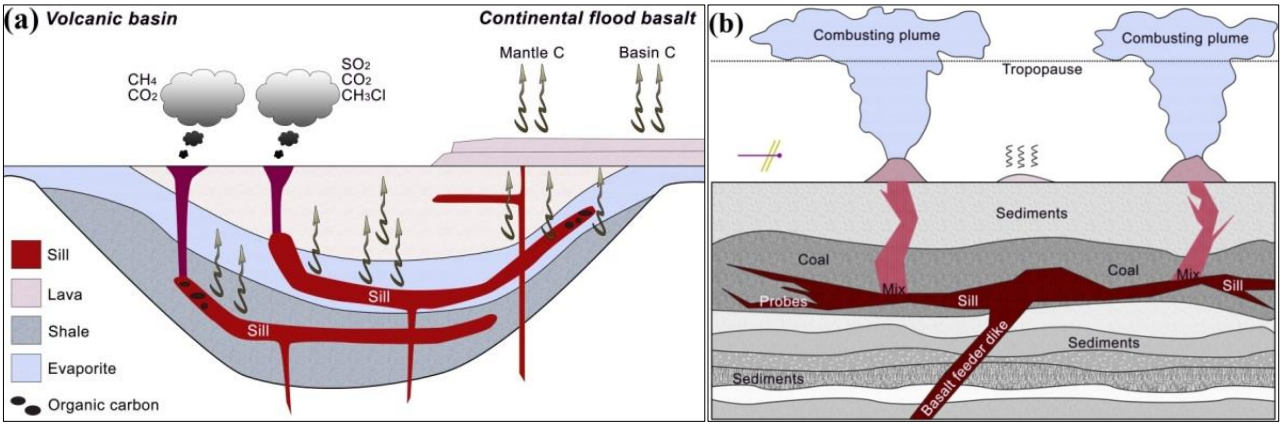

Figure 15. Schematic cross-section showing sil and dykes across a volcanic basin. The chemical composition of sedimentary rocks heated by igneous intrusions has a significant effect on the composition of the metamorphic fluid. For example, organic-rich shale produces CH_4 during contact metamorphism, while coal produces CO_2-derived fluids and also water. Many sedimentary basins with sil settlement may contain hydrogen-rich kerogen and oil and gas deposits, and fluids such as methane (CH_4) and ethane (C_2H_6) can be enriched in the basin (Svensen et al., 2015). (a: Svensen et al., 2015; b: Ogden and Sleep, 2011)

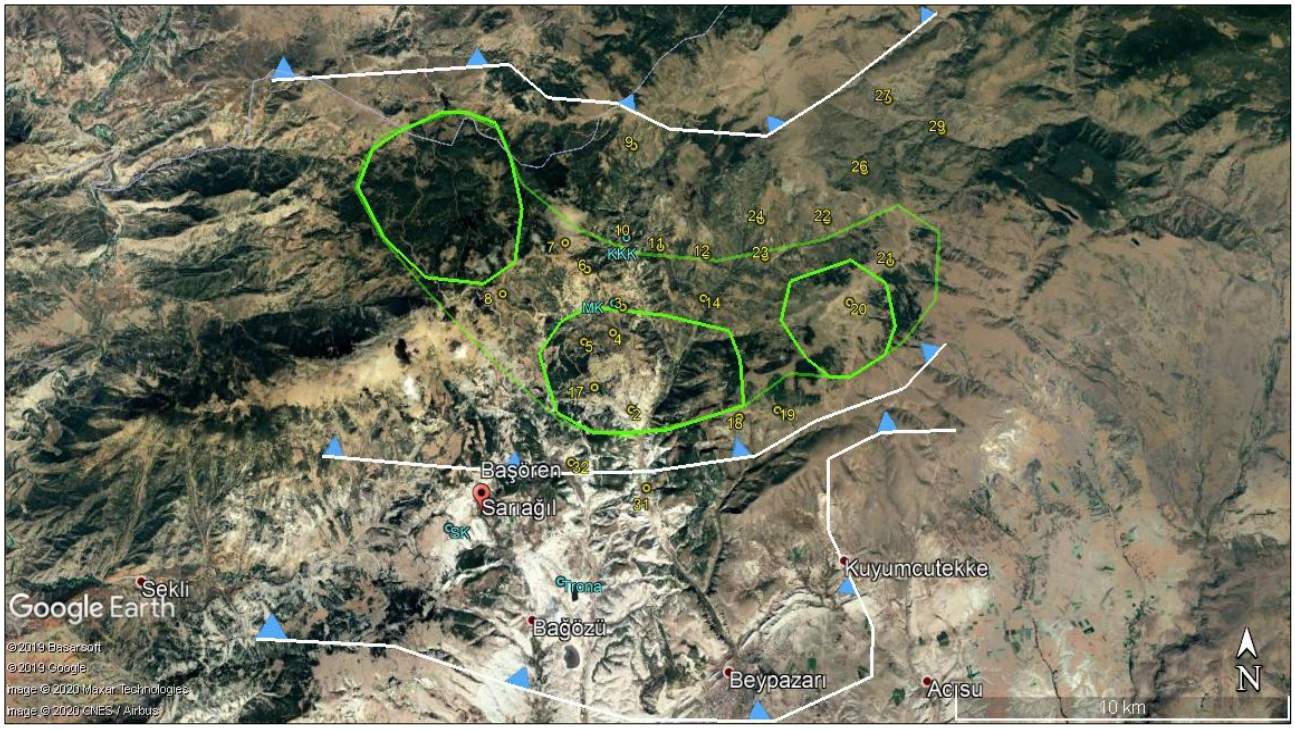

Figure 16. Possible gas traps in the study area (green polygons). Yellow circles: the water samples containing petroleum hydrocarbons, SK: Sarıağıl coal sector (Tarvirdi, 2013), KKK: Kabalar coal outcrop (Toprak, 2010), MK: Mençeler coal outcrop (Toprak, 2010), white lines: blind thrust faults (teethes are above the overthrust unit)

5. CONCLUSION

In this study, which is aimed to investigate the oil and gas potential of Beypazarı Neogene Basin using TPH analysis performed on the samples taken from water resources, the hydrocarbons have been determined in all the water samples based on the TPH analysis results. The TPH values are remarkably greater than the hydrocarbon limit values suggested for surface and subsurface waters. The source of n-alkanes in the water samples are petrogenic hydrocarbons and organic-rich sediments. Water-rock-hydrocarbon interactions have created a hydrocarbon enrichment in the waters in the examined area, and the hydrocarbons in the water samples are in a non-biodegraded character. It is come into existence that the source rocks which generated the hydrocarbons in the water samples were deposited in the oxic terrestrial environment (Type III kerogen, gas-prone) as well as corresponding to the mature-overmature level. In the magnetic and gravity maps of the investigation area, the anticlines in the fault-progression folds in the areas where both gravity and magnetic anomalies are positive are considered as potential gas reservoirs.

ACKNOWLEDGEMENT

We would like to thank Mr. Serkan Çelebi as well as the experts of SGS Supervise Gözetme Etüd Kontrol Servisleri A.S. for their precious performances to perform the required analyses to complete this research study.

REFERENCES

Akkuş, İ., Sümer, A., Şengüler, İ., Taka, M., Pekatan, R., & Işık, A. (1982). Geology and bituminous shale possibilities of Beypazarı Çayırhan region. *Mineral Research and Exploration (MTA)*, Report No: 7837 (in Turkish).

Aydın, A. (1997). Evaluation of gravity data in terms of hydrocarbon by normalized full gradient, variation and statistic methods, model studies and application in Hasankale-Horasan basin (Erzurum) (PhD thesis). Karadeniz Teknik University, Trabzon, Turkey (in Turkish).

Aydın, A. (2004). Evaluation of gravity anomalies by direct interpretation techniques: An application from Hasankale-Horasan region. *Pamukkale University Journal of Engineering Sciences*, 11(1), 95-102 (in Turkish with English abstract).

Aziz, A. (1976). Geology of the area between New Çayırhan and Karaköy and bituminous shale possibility. *Mineral Research and Exploration (MTA)*, Report No. 5732 (in Turkish).

Banga, T., Capuano, R.M. & Bissada, K.K. (2011). Petroleum generation in the southeast Texas basin: Implications for hydrocarbon occurrence

at the South Liberty salt dome. *AAPG Bulletin*, 95(7), 1257-1291.

Beyer, J., Jonsson, G., Porte, C., Krahn, M.M. & Ariese, F. (2010). Analytical methods for determining metabolites of polycyclic aromatic hydrocarbon (PAH) pollutants in fish bile: A review. *Environmental Toxicology and Pharmacology*, 30(3), 224-244.

Bourbonniere, R.A., Meyers, P.A. (1996). Sedimentary geolipid records of historical changes in the watersheds and productivities of lakes Ontario and Erie. *Limnology and Oceanography*, 41, 352-359.

Bray, E.E., Evans, E.D. (1961). Distribution of n-paraffins as a clue to the recognition of source rocks. *Geochimica et Cosmochimica Acta*, 22, 2-15.

Bray, E.E., Evans, E.D. (1965). Hydrocarbons in non-reservoir-rock source beds: Part 1. *AAPG Bulletin*, 49, 248-257.

Cranwell, P.A., Eglinton G. & Robinson, N. (1987). Lipids of aquatic organisms as potential contributors to lacustrine sediments-2. *Organic Geochemistry*, 11, 513-527.

Devi, E.A., Rachman, F., Satyana, A.H., Fahrudin & Setyawan, R. (2018). Geochemistry of Mudi and Sukowati oils, East Java basin and their correlative source rocks: Biomarkers and isotopic characterisation. *Procedings, Indonesian Petroleum Association, Forty-Second Annual Convention & Exhibition*, May 2018.

Didyk, B.M., Simoneit, B.R.T., Brassel, S.C. & Englington, G. (1978). Organic geochemical indicators of paleoenvironmental conditions of sedimentation. *Nature*, 272, 216-222.

Eke, P.O., Okeke, F.N. (2016). Identification of hydrocarbon regions in Southern Niger Delta Basin of Nigeria from potential field data. *International Journal of Scientific and Technology Research*, 5(11), 96-99.

Eymold, W.K., Swana, K., Moore, M.T., Whyte, C.J., Harkness, J.S., Talma, S., Murray, R., Moortgat, J.B., Miller, J., Vengosh, A. & Darrah, T.H. (2018). Hydrocarbon-rich groundwater above shale-gas formations: A Karoo basin case study. *Groundwater*, 56(2), 204-224.

Ficken, K.J., Li, B., Swain, D.L. & Eglinton, G. (2000). An n-alkane proxy for the sedimentary inputs of submerged/floating freshwater aquatic macrophytes. *Organic Geochemistry*, 31, 745-749.

Forster, A., Sturt, H. & Meyers, P.A. (2004). Molecular biogeochemistry of Cretaceous black shales from the Demerara Rise: Preliminary shipboard results from sites 1257 and 1258, Leg 207. In: Erbacher, J.,Mosher, D.C., Malone, M.J., et al., *Proceedings of the Ocean Drilling Program*, Initial Reports: 207, 1-22.

Gadirov, V.G., Eppelbaum, L.V., Kuderavets, R.S., Menshov, O.I. & Gadirov, K.V. (2018). Indicative features of local magnetic anomalies from hydrocarbon deposits: examples from Azerbaijan and Ukraine. *Acta Geophysica*, 66(6), 1463-1483.

Gadirov, V.G., Eppelbaum, L.V. (2012). Detailed gravity, magnetics successful in exploring Azerbaijan onshore areas. *Oil and Gas Journal*, 5, 60-73.

Gadirov, V.G. (1994). The physical-geological principles of application of gravity and magnetic prospecting in searching oil and gas deposits. *Proceed. of 10th Petroleum Congress and Exhibition of Turkey*, Ankara, 197-203.

Geist, E.L., Childs, J.R. & Scholl, D.W. (1987). Evolution and petroleum geology of Amlia and Amukta intra-arc summit basins, Aleutian Ridge. *Marine and Petroleum Geology*, 4, 334-352.

Goossens, H., Duren, C., De Leeuw, J. W. & Schenck, P.A. (1989). Lipids and their mode of occurrence in bacteria and sediments-2. Lipids in the sediment of a stratified, freshwater lake. *Organic Geochemistry*, 14, 27-41.

Göktunalı, K. (1963). Report on Geological Survey of Beypazarı Lignites. *Mineral Research and Exploration (MTA)*, Report No. 3391 (in Turkish).

Griffin, W.R. (1949). Residual gravity in theory and practice. *Geophysics*, 14, 39-58.

Gülbay, R., Korkmaz, S. (2005). Organic geochemical characteristics and depositional environments of oil shales in Northwest Anatolia, Turkey. *Geological Bulletin of Turkey*, 2, 21-41 (in Turkish with English abstract).

Gülbay, K.R., Korkmaz, S. (2008). Organic geochemistry, depositional environment and hydrocarbon potential of the Tertiary oil shale deposits in NW Anatolia, Turkey. *Oil Shale*, 25, 444-464.

Gülbay, R. (2004). Organic geochemistry characteristics, depositional environments and hydrocarbons potential of bituminous shales in northwest anatolia (MSc. thesis). Karadeniz

Technical University, Trabzon, Turkey (in Turkish).

Hakimi, M.H., Al-Matary, A.M. & Ahmed, A. (2018). Bulk geochemical characteristics and carbon isotope composition of oils from the Sayhut sub-basin in the Gulf of Aden with emphasis on organic matter input, age and maturity. *Egyptian Journal of Petroleum*, 27(3), 361-370.

Hartkopf-Fröder, C., Kloppisch, M., Mann, U., Neumann-Mahlkau, P., Schaefer, R.G. & Wilkes, H. (2007). The end-Frasnian mass extinction in the Eifel Mountains, Germany: new insights from organic matter composition and preservation. Geological Society, London, Special Publications 278, London, UK.

Helvacı, C. (2018). Geology of the Beypazarı trona field, Ankara, Turkey. Post-Congress Trip to Beypazarı Trona Field, Ankara, Turkey. *71th Geological Congress of Turkey*, April 28, 33.

Hunt, J.M. (1995). Petroleum Geochemistry and Geology. W.H. Freeman and Company, New York, US.

Ivakhnenko, O.P, Abirov, R. & Logvinenko, A. (2015). New method for characterisation of petroleum reservoir fluid-mineral deposits using magnetic analysis. *Energy Procedia*, 76, 454-462.

İnci, U. (1991). Miocene alluvial fan-alkaline playa lignite-trona bearing deposits from an inverted basin in Anatolia: Sedimentology and tectonic controls on deposition. *Sedimentary Geology*, 71, 73-97.

Karatas, A., Ozdemir, A. & Sahinoglu, A. (2019). Investigation of Oil and Gas Potential of Karaburun Peninsula and Seferihisar Uplift (Western Anatolia) by Iodine Hydrogeochemistry and Total Petroleum Hydrocarbon (TPH) in Water Analysis. Marmara University, Project No (9505): SOS-A-100719-0267.

Kavuşan, G. (1993). Importance of tectonic during the bedding of lignite in Beypazarı-Çayırhan Coal Field. *Turkish Journal of Earth Sciences*, 2, 135-145 (in Turkish with English abstract).

Kreuzer, R.L., Darrah, T.H., Grove, B.S., Moore, M.T., Warner, N.R., Eymold, W.K. & Poreda, R.J. (2018). Structural and hydrogeological controls on hydrocarbon and brine migration into drinking water aquifers in Southern New York. *Groundwater*, 56(2), 225-244.

Kroon, J. (2011). Biomarkers in the lower huron shale (upper devonian) as indicators of organic matter source, depositional environment, and thermal maturity (MSc. thesis). Clemson University, South Carolina, US.

Larasati, D., Suprayogi, K. & Akbar, A. (2016). Crude oil characterization of Tarakan basin: Application of biomarkers. *The 9th International Conference on Petroleum Geochemistry in the Africa - Asia Region Bandung*, Indonesia, 15 -17.

Liu, S., Qi, S., Luo, Z., Liu, F., Ding, Y., Huang, H., Chen, Z., & Cheng, S. (2018). The origin of high hydrocarbon groundwater in shallow Triassic aquifer in Northwest Guizhou, China. *Environmental Geochemistry and Health*, 40(1), 415-433.

Lyatsky, H.V., Thurston, J.B., Brown, R.J. & Lyatsky, V.B. (1992). Hydrocarbon exploration applications of potential field horizontal gradient vector maps. *Bulletin of Canadian Society of Exploration Geophysicists Recorder*, 17(9), 10-15.

Meyers, P.A., Ishiwatari, R. (1993). Lacustrine organic geochemistry-an overview of indicators of organic matter sources and diagenesis in lake sediments. *Organic Geochemistry*, 20, 867-900.

Mille, G., Asia, L., Guiliano, M., Malleret, L. & Doumenq, P. (2007). Hydrocarbons in coastal sediments from the Mediterranean Sea (Gulf of Fos area, France). *Marine Pollution Bulletin*, 54, 566-575.

Ministry of Agriculture and Forestry of Turkey, (2004a). Surface Water Quality Regulation of Turkey (in Turkish). Retrieved 02 June 2020 from http://www.resmigazete.gov.tr/eskiler/2016/08/20160810-9.htm

Ministry of Agriculture and Forestry of Turkey, (2004b). Water Pollution Control Regulation of Turkey (in Turkish). Retrieved 02 June 2020 from https://www.mevzuat.gov.tr/mevzuat?MevzuatNo=7221&MevzuatTur=7&MevzuatTertip=5

Nettleton, L.L. (1976). Gravity and Magnetics in Oil Prospecting. McGraw-Hill, New York, US.

Ogden, D.E., Sleep, N.H. (2011). Explosive eruption of coal and basalt and the end-Permian mass extinction. *Earth, Atmospheric, and Planetary Sciences*, 109(1), 59-62.

Onojake, M.C., Osuji, L.C. & Oforka, N.C. (2013). Preliminary hydrocarbon analysis of crude oils from Umutu/Bomu fields, south west Niger Delta, Nigeria. *Egyptian Journal of Petroleum*, 22, 217-224.

Ozdemir, A. (2018). Usage of the Total Petroleum Hydrocarbons (TPH) in water analysis for oil and gas exploration: First important results from Turkey. *Journal of Engineering Sciences and Design of Suleyman Demirel University*, 6(4), 615-635 (English version).

Ozdemir, A. (2019a). Organic hydrogeochemical evidence of Hasanoğlan (Ankara) petroleum system. *Pamukkale University Journal of Engineering Sciences*, 25(6), 748-763 (English version).

Ozdemir, A. (2019b). Mature hydrocarbons-rich waters as geochemical evidence of working petroleum system of Mamak (Ankara) and potential trap area in the region. *European Journal of Science and Technology*, 17, 244-260 (English version).

Ozdemir, A. (2019c). Organic hydrogeochemical evidence of pre-Neogene petroleum system of the Buyuk Menderes graben and potential traps (Western Turkey). *European Journal of Science and Technology*, 16, 325-354 (English version).

Ozdemir A., Palabiyik, Y. (2019a). A review of Paleozoic - Miocene petroleum source rocks of Turkey by paleogeographic and paleotectonic data: New interpretations and major outcomes. *7th International Symposium on Academic Studies in Science, Engineering and Architecture Sciences*, November 15-17, Ankara, Turkey, 689-725.

Ozdemir A., Palabiyik, Y. (2019b). A new approach to petroleum source rock occurrence: The relationships between petroleum source rock, ophiolites, mantle plume and mass extinction. *IV. International Congress of Scientific and Professional Studies - Engineering (BILMES EN)*, November 07 - 10, Ankara, Turkey, 28-39.

Ozdemir, A., Karataş, A., Palabiyik, Y., Yaşar, E., & Sahinoglu, A. (2020). Oil and gas exploration in Seferihisar Uplift (Western Turkey) containing an operable-size gold deposit: Geochemical evidence for the presence of a working petroleum system. *Geomechanics and Geophysics for Geo-Energy and Geo-Resources*, 6(1), 1-22.

Özçelik, O. (2002). Organic geochemical characteristics of Miocene bituminous units, North of Beypazarı (Ankara). *Geological Bulletin of Turkey*, 45(1), 1-17 (in Turkish with English abstract).

Özçelik, O., Altunsoy, M. (2005). Organic geochemical characteristics of Miocene bituminous units in the Beypazari Basin, Central Anatolia, Turkey. *Arabian Journal for Science and Engineering*, 30, 181-194.

Özpeker, I., Çoban, F., Eseni, F., & Eren R.H. (1991). Mineralogical features of dolomite in the Hırka Formation (Beypazarı-Ankara). *Geological Bulletin of Turkey*, 34, 23-26 (in Turkish with English abstract).

Palabiyik, Y., Ozdemir, A. & Sahinoglu, A. (2019). Investigation of Oil and Gas Potential of Uludag Massif (Northwestern Anatolia) by Iodine Hydrogeochemistry and Total Petroleum Hydrocarbon (TPH) in water analysis, Istanbul Technical University, Scientific Research Project, Project No: MAB-2019-42217, 76. (in Turkish).

Palabiyik, Y., Ozdemir, A., Karataş, A. & Özyağcı, M. (2020). Identification of Oil and Gas Potential of Kastamonu and Sinop and their Surroundings (Central Pontides) by Using Total Petroleum Hydrocarbons (TPH) in water analysis, Istanbul Technical University, Scientific Research Project, Project No: MGA-2020-42587 (continue).

Palabiyik, Y., Ozdemir, A. (2020). Use of TPH (Total Petroleum Hydrocarbons) in water analysis for oil and gas exploration in Turkey: The case studies from Western, Northwestern and Central Anatolia regions and major outcomes. *Turkey IV. Scientific and Technical Petroleum Congress, October 26-28*, Ankara, Turkey (in Turkish) (in press).

Pašteka, R. (2000). 2D semi-automated interpretation methods in gravimetry and magnetometry. *Acta Geologica Universitatis Comeniana*, 55, 5-50.

Pehlivanlı, B.Y. (2011). Inorganic element depositions of hırka formation (Beypezarı, Ankara) bituminous shales and genetic relationships between organic and inorganic elements (PhD thesis). Ankara University, Ankara, Turkey (in Turkish).

Peters, K.E, Walters, C.C. & Moldowan, J.M. (2005). The Biomarker Guide: Biomarkers and Isotopes in Petroleum Exploration and Earth History. Second Ed, Vol 2. Cambridge University Press, UK.

Peters, K.E., Fraser, T.H., Amris, W., Rustanto, B. & Hermanto, E. (1999). Geochemistry of crude oils from eastern Indonesia. *AAPG Bulletin*, 83, 1927-1942.

Peters, K.E., Moldowan, J.M. (1993). The Biomarker Guide, Interpreting Molecular Fossils in Petroleum and Ancient Sediments. Englewood Cliffs, Jersey, Prentice Hall, US.

Piskarev, A.L., Tchernyshev, M.Y. (1997). Magnetic and gravity anomaly patterns related to hydrocarbon fields in northern West Siberia. *Geophysics*, 62(3), 831-841.

Satyana, A.H. (2015). Subvolcanic hydrocarbon prospectivity of Java: Opportunities and challenges. *Proceedings, Indonesian Petroleum Association, Thirty-Ninth Annual Convention & Exhibition*, May 2015. IPA15-G-105.

Senger, K., Millett, J., Planke, S., Ogata, K., Eide, C.H., Festøy, M., Galland, O. & Jerram, D.A. (2017). Effects of igneous intrusions on the petroleum system: A review. *First Break*, 35, 1-10.

Seyitoğlu, G., Esat, K., & Kaypak, B. (2017). One of the main neotectonic structures in the NW central Anatolia: Beypazarı Blind Thrust Zone and related fault-propagation folds. *Bulletin of the Mineral Research and Exploration*, 154, 1-14.

Siyako, F. (1983). Geology of Beypazarı Neogene Basin (Ankara) Containing Coal. *Mineral Research and Exploration (MTA)*, Report No. 7431 (in Turkish).

Sönmez, Ö.U. (2016). Mineralogical and geochemical ınvestigation of the sedimentary units around Beypazarı-Çayırhan, Ankara, Turkey (MSc. Thesis). Hacettepe University, Ankara, Turkey (in Turkish).

Stephen, O.I., Iduma, U. (2018). Hydrocarbon potential of Nigeria's Inland Basin: Case study of Afikpo basin. *Journal of Applied Geology and Geophysics*, 6(4), 1-24.

Stchhepirsky, V. (1941). Geology and Mineral Richness of Beypazarı-Nallıhan-Bolu Region. *Mineral Research and Exploration (MTA)*, Report No. 1332 (in Turkish).

Svancara, J. (1983). Approximate method for direct interpretation of gravity anomalies caused by surface three-dimensional geologic structures. *Geophysics*, 48(3), 361-366.

Svensen, H., Fristad, K.E., Polozov, A.G. & Planke, S. (2015). Volatile generation and release from continental large igneous provinces. In: Schmidt, A., Fristad, K.E., and Elkins-Tanton, L.T., (Eds.), Volcanism and Global Environmental Change, Cambridge University Press, UK.

Syaifudin, M., Eddy, A., Subroto, E.A., Noeradi, D. & Kesumajana, A.H.P. (2015). Characterization and correlation study of source rocks and oils in Kuang area, South Sumatra basin: The potential of Lemat formation as hydrocarbon source rocks. *Proceedings of Indonesian Petroleum Association, Thirty-Ninth Annual Convention & Exhibition*, May 2015, IPA15-G-034.

Şener, M. (2007). Depositional conditions of the coal-bearing Hırka Formation beneath Late Miocene explosive volcanic products in NW central Anatolia, Turkey. *Journal of Earth System Science*, 116, 125-135.

Şener, M., Şengüler, İ. (1991). Geology and Economic Usage Areas of Beypazarı Bituminous Marls. *Mineral Research and Exploration (MTA)*, Report No: 9202 (in Turkish).

Şener, M. Şengüler, İ. & Kök, M.V. (1995). Geological considerations for the economic evaluation of oil shale deposits in Turkey. *Fuel*, 74, 999-1003.

Tarvirdi, M. (2013). Investigation of variations of mineralogical, petrographical and elemental contents within the two working coal seams, Çayırhan-Beypazarı, Ankara (MSc. thesis). Hacettepe University, Ankara, Turkey (in Turkish).

Tissot, B.P., Welte, D.H. (1984). Petroleum Formation and Occurrence: A New Approach to Oil and Gas Exploration. Springer-Verlag, Berlin Heidelberg, Germany.

Toprak, S. (2010). Geology and coal prospecting of Haydarlar-Kabalar area (N of Beypazarı) (MSc. thesis). Çukurova University, Adana, Turkey (in Turkish).

Töpfer, K.D. (1977). Improved technique for rapid interpretation of gravity anomalies caused by two-dimensional sedimentary basins. Journal of Geophysics, 43, 645-654 (in Švancara, J., 1983. Approximate method for direct interpretation of gravity anomalies caused by surface three-dimensional geologic structures. *Geophysics*, 48(3), 361-366.

Tran, K.L., Philippe, B. (1993). Oil and rock extract analysis. In: Bordenave, M.L. (ed.), *Applied Petroleum Geochemistry, Editions Technip,* 373-394.

Vardaloğlu, H. (2016). The organic geochemical characteristics of the marine, lacustrine source rocks and coals, and the n-alkane systematics: applicatıon on selected areas (MSc thesis). Karadeniz Technical University, Trabzon, Turkey (in Turkish).

Volkman, J.K., Maxwell, J.R. (1986). Acyclic isoprenoids as biological markers. In: Johns, R.B., (ed.), Biological Markers in the Sedimentary Record, 1-42, Elsevier, New York.

Waples, D.W. (1985). Geochemistry in Petroleum Exploration. International Human Resources Development Corp., Boston, USA.

Yağmurlu, F., Helvacı, C. & Inci, U. (1988a). Geological setting and geometric features of the Beypazarı lignite deposits, Central Anatolia. *The Sixth Coal Congress of Turkey*, 529-545.

Yağmurlu, F., Helvacı, C. & Inci, U. (1988b). Depositional setting and geometric structure of the Beypazarl lignite deposits, Central Anatolia, Turkey. *International Journal of Coal Geology*, 10, 337-360.

Yağmurlu, F., Helvacı, C., Inci, U. & Önal, M. (1988c). Tectonic features to structural of the Beypazarı and Nallıhan Central Anatolia. *METU Journal of Pure and Applied Sciences*, 21, 127-143.

Zemo, D.A., Foote, G.R. (2003). The technical case eliminating the use of the TPH analysis in assessing and regulating dissolved petroleum hydrocarbons in groundwater. *Groundwater Monitoring & Remediation*, 23(3), 95-104.

Zheng, Y., Zhou, W., Meyers, P.A. & Xie, S. (2007). Lipid biomarkers in the Zoigê- Hongyuan peat deposit: Indicators of Holocene climate changes in West China. *Organic Geochemistry*, 38, 1927-1940.

Zieglar, J. (1939). Bituminous Shales Around Hırka (Beypazarı) and Karaköy (Nallıhan). *Mineral Research and Exploration (MTA)*, Report No. 984 (in Turkish).

TURKGEO
TURKISH JOURNAL OF GEOSCIENCES

ISSN: *2717-7696*
Research Article
Vol; 1, Issue; 2, pp. 53-62, 2020
DOI:
Journal homepage:
https://dergipark.org.tr/en/pub/turkgeo

Integration of Different Methods for Architectural Survey of Historical and Cultural Heritages

Sevgi Böge [*1], **Hakan Karabörk** [2]

[1] *Selcuk University, Kadinhani Faik Icil Vocational School, Map and Cadastre Programme, Konya, Turkey*
[2] *Konya Technical University, Faculty of Engineering and Natural Sciences, Department of Geomatics Engineering, Konya, Turkey*

Keywords
UAV
Laser Scanning
Architectural
Photogrammetry
Three-Dimensional Model
Statical Survey

ABSTRACT

Protection and documentation of cultural heritages which have historical significance for the sake of continuity of culture are inevitable events. In the light of this thought, using new techniques, in comparison to classic methods arising of new techniques in parallel with technology in order to achieve the most reliable results in works such as restoration, reconstruction, building survey and documentation of cultural entities are inevitable. In this study, Sille Aya-i Eleni Church, which has historical and cultural significance that can be evaluated in terms of architecture and allows the application of different techniques, was chosen. Different purchasing methods and drawing operations were carried out in accordance with the features of the selected object. The exterior drawings of the object, which will be created in a three dimensional model, are made with the photogrammetric method, while roof surveys that have risk are made thanks to the photographs taken with UAV. The surveying and drawing of the interior of the same object was also performed with a laser scanner. As a result, it is recommended to use the methods together in documentation studies of objects with different properties.

1. INTRODUCTION

Accurate and precise recording of cultural heritage is of vital importance because the current-state documents are the basis for conservation studies such as art history research, architectural and structural analyses, materials and deterioration analyses, determination of intervention strategies and application projects (Altay and Sağıroğlu, 2019). It is of great importance that the speed and accuracy of the work increases and also the cost decreases. Alternatives to traditional methods have increased with developing technology. Many types of research have been conducted on alternative methods for documentation purposes. As a result of these studies, the advantages and disadvantages of approaches have been listed. It is claimed that each method produces safer, more accurate and faster data than other methods (Uzun and Spor, 2019; Varlık et al., 2016).

In the statical survey and documentation studies of architects, the transition from classical methods to modern techniques is seen as an advantage. Advanced techniques do not only the traditional methods but also offer different solution alternatives in the process steps that have difficulty in analysing (Güleç, 2007). Also, it provides new solutions to facade survey of narrow spaces that do not allow measurement or roof survey and modelling them and making them ready for the project (Themistocleous et al., 2015; Themistocleous et al., 2016).

In addition to the terrestrial photogrammetry technique, the use of kinematic Global Navigation Satellite System (GNSS) survey method in making layout plan in statical survey is essential for speeding up the process.

Today, the rapid development of Unmanned Aerial Vehicles (UAV) with the developing technology has expanded the range of use of these vehicles and has taken its place in many different occupational disciplines (Vacanas et al., 2015; Yakar and Mırdan, 2017; Xue et al., 2019).

Historical sites to be modelled in 3D and inaccessible points of cultural heritage such as roofs should also be photographed and surveyed. At this

* **Corresponding Author**

*(sboge@selcuk.edu.tr) ORCID ID 0000-0001-6159-9721
(hkarabork@ktun.edu.tr); ORCID ID 0000-0001-7387-7004

Cite this article

Böge, S., Karabörk, H. (2020). Integration of Different Methods for Architectural Survey of Historical and Cultural Heritages. Turkish Journal of Geosciences, 1(2), 53-62.

Received: 29/05/2020; Accepted: 01/07/2020

point, terrestrial photogrammetry is insufficient (Böge, 2013). Furthermore, terrestrial photogrammetry can be challenging to work indoors (Yakar and Mırdan, 2017).

It is observed that when examining existing legislation in Turkey regarding the statical survey, multiple detailed works needs to be done in the statical survey operations and has many advantages in a particular purpose, of all the methods used in the studies. However, it is difficult to state that no technique can be used to cover all of the mentioned statical survey steps.

The exterior modelling and drawings of the Aya-i Eleni Church, which is the largest church of Sille, have been realized by both photogrammetric method and laser scanning technology and its drawing from the top has been missing. Besides, its interior has been scanned with laser scanning technologies, and no sectional drawings have been made (Yıldız et al., 1999; Göktepe et al., 2009). This research aims to reveal whether different methods of a statical survey of historical and cultural assets will be used together. The benefit expected from this research is to guide the people who survey statical to determine the historical and cultural assets in different locations and conditions to determine the statical survey. Within the scope of this study, 3D modelling of the exterior of Aya-i Eleni Church in Konya Sille was made. GNSS technology and terrestrial photogrammetry technique have been used in the survey of the surfaces. Roof survey is created and modelled with UAV technology and combined with exterior drawings in the computer environment. The indoor is scanned with laser scanning technology for the interior. Sections and drawings of the interior are created.

2. MATERIALS AND METHODS

2.1. Studying Area

Within the scope of this study, Konya Sille Aya-i Eleni Church was chosen as the study area (Figure 1). Sille Aya-i Eleni Church is located on the 3rd map section, the 3635th parcel in the urban protected area to the left of Tatkoy turnout, Selcuklu district of Konya province. Being the biggest church of Sille, Aya-i Eleni Church started to be built in 327 during sacred pilgrimages (Koyuncu, 2013).

Figure 1. Sille Aya-i Eleni Church

2.2. Hirobo Shuttle ZX Model Helicopter Unmanned Aerial Vehicle

UAV, high resolution images with low flight altitude can be produced at a lower cost than images obtained from aerial photogrammetry (Esposito et al., 2014). It also provides easy purchasing in hard-to-reach areas with less risk.

For the aerial photographs of the study, the Hirobo Shuttle ZX model helicopter was preferred. Futaba 7C brand remote control was used with equipment such as receiver, servo, battery that completed the flight of the helicopter (Figure 2).

Figure 2. Hirobo Shuttle ZX model helicopter

This model provides an efficient and balanced flight without loss of power thanks to its superior design compared to other models. This fueled model is a model with stable flight due to its large size (Böge, 2013). In order to minimize the cost of the study, this type of simpler structured helicopter has been preferred. Although the stabilization feature is better than other models, the tracking of the propellers has been made to minimize the motor vibration.

2.3. Canon Sx 150 IS Camera

The Canon Sx150 IS, which is preferred for use during flight, is slightly larger than the portable cameras, but not as equipped. However, it is an ideal choice considering the price/performance evaluation and weight. It is preferred because it is a camera that supports vibration prevention and autofocus system. In this way, the photo has improved quality. Besides, the camera is mounted with the help of a unique apparatus that will tolerate vibration during the flight (Figure 3).

Figure 3. Mounting the camera

2.4. Nikon D80 Digital Camera

During the terrestrial photogrammetry application stage, 24mm lens was used with Nikon D80 digital camera to take photographs.

2.5. ILRIS 3D Optech Terrestrial Laser Scanner

ILRIS-3D terrestrial scanner has been preferred in the scanning stages of the study due to its high resolution, having a distance measurement from 3 meters to 1 kilometer, using class one laser and not requiring levelling. ILRIS-3D terrestrial scanner is a portable package integrated with digital cameras and advanced software tools prepared for commercial surveys, engineering, mining and industry applications (Karabörk et al., 2007).

2.6. Topcon GPT 3007 Total Station

Considering the size of the object to be measured, the Topcon GPT 3007 total station was preferred to be able to read the details using the laser at heights that cannot be affixed.

2.7. Photomodeler Software

Photomodeler is a software which has the capability of camera calibration, photogrammetric evaluation and vector drawing. It can also envelop pictures on the drawings. It was used in the drawing works of the church after the survey by the terrestrial method. The camera calibration process, which is expressed as the finding of the parameters that best represent the camera system, was also carried out by software.

2.8. Parser, Polyworks and Z-Map Softwares

Parser software converts the .hdr file, which is obtained as a result of the survey made in the field with a laser scanner, into various formats that can be processed in Polyworks software. Polyworks software is software that processes point clouds. In IMAlign module, it is possible to combine point clouds and georeferencing. IMInspect module, on the other hand, is a tool for surveying and calculating on surfaces. Within the scope of this study, these two modules were used.

Z-Map software, which is capable of creating a digital elevation model (DEM) on point clouds, georeferencing pictures with the help of a point cloud, drawing, orthophoto and mosaic can be used.

2.9. Photogrammetry Survey

Photogrammetry is a technology and science where information about objects and the environment is obtained at the end of the recording, survey and interpretation of photographic images formed by the rays reflected from the objects and their surroundings and the electromagnetic energy they emit. While photogrammetry is first used to obtain the topographic structure of the earth, it also includes new and different application areas today. Today, photogrammetry is used to survey and model the geometric and structural properties of objects.

Roof photographs, which are difficult to survey due to height of church, were obtained with the help of UAV in this study. Pictures taken from terrestrial photogrammetry were also acquired with the help of digital cameras.

2.10. Laser Scanning

With the developing laser scanning technology, the surveying system has started to be widely used in the documentation of cultural heritage. Laser scanning is a technology that can collect three-dimensional position data quickly, reliably and in detail for many different applications (Uzar et al., 2019). Thanks to its speed and precision, terrestrial laser scanning has gained more importance as a surveying tool in the field of architecture and cultural heritage (Korumaz et al., 2010). Thanks to advances in terrestrial laser scanner technology, the point cloud of large-scale structures can be obtained quickly (Chen et al., 2014). The laser scanning technology preferred in the documentation of architectural objects was used in the interior of the church in the study.

3. RESULTS

In this study, it is aimed to determine the most appropriate surveying and drawing method by considering the size, height and historical-cultural importance of Sille Aya-i Eleni Church. The terrestrial photogrammetry technique surveyed the exterior facade of the church, and its roof was surveyed with UAV. Both data modelled and combined in a computer environment. The interior of the church and the ceiling decorations were surveyed with laser scanning technology, and their sections were created.

3.1. Statical Survey of Sille Aya-i Eleni Church Exteriors by Photogrammetry

For the survey of details of the object, in the Selcuklu 22/a Cadastre Renewal study carried out by Land Registry and Cadastre General Directorate (TKGM) in 2009, starting from C1, C2, C3 and Turkish National Fundamental GPS Network (TUTGA) points, a static session was held for at least 20 minutes, and cadastre polygons, whose coordinates were obtained and registered by the Directorate of Cadastre, were started. When the tool is installed on the polygons we have installed on the ground, the marks that allow us to easily survey on the object are affixed to the object so that the tool can read (Figure 4).

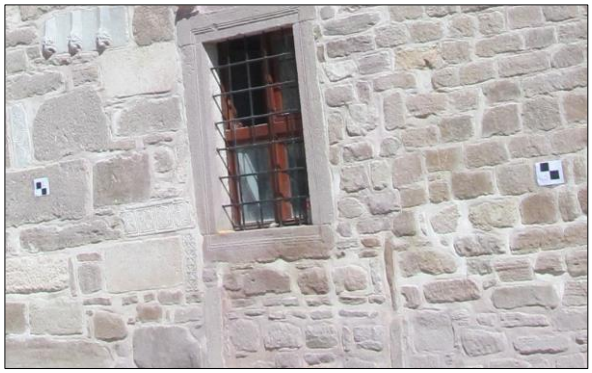

Figure 4. Facade marking of Aya-i Eleni Church

It was decided to print the images of the church before the field study and arrange it as a sketch, and the points whose coordinates were read were marked on the drawing. Also, unmarkable locations were targeted and read with the laser of the instrument (window edges, areas with different stones, sharp places). The points that were read numbered and their locations were indicated on sketches and markings were made to relevant areas at office stage. With the help of the Nikon D80 digital camera, of which we previously determined the calibration value, photographing of the church was started after the signs were applied. More photos were taken than needed, as some images may have poor lighting or poor focus settings.

A total of 128 photographs were taken locally around the church, and 16 of them were used during modelling. Besides, since the photos of the upper part of the North-East facade, which provide sufficient vision, could not be taken, four photographs taken by UAV. The total station surveyed the polygon points placed in the study area according to the local coordinate system. The data was collected by surveying the angle and distance (horizontal angle, vertical angle, oblique distance) data during the detailed survey of the points with the total station (by laser) to re-calculate when necessary.

Except for the roof of the object, a total of 69 points were surveyed homogeneously for all facades. While surveying facades, panels on the roof coordinated by reflector. Then the survey process was completed. In the office part of the study, the calculations of all the details collected in the field were made by connecting to the registered cadastre polygons, and the coordinates (y, x, h) of all surveyed points were calculated before modelling. Twenty images that can be used for facade drawings were transferred to the program and adjusted. With the conclusion of the adjusting, drawing operations had been started on two photographs that were required by photogrammetric modelling.

3.1.1. South-East facade

For the south-east facade, which is the front entrance part of the church, a total of 32 photos were taken from different angles, in the horizontal and vertical positions of the camera. 4 of these photos were used during modelling. 19 detail points were surveyed from the south-east facade of the church, marking and then adjusting the surveyed detail points and drawing was completed in the photomodeller program (Figure 5).

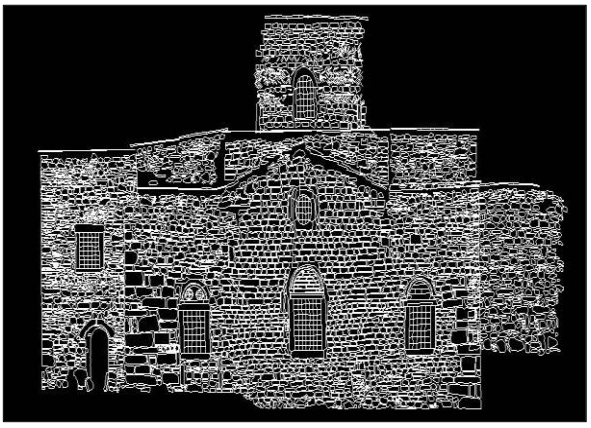

Figure 5. South-East facade drawings of the church

3.1.2. South-West facade

Starting from the front entrance of the church and turning clockwise, a total of 29 terrestrial photographs were taken from different angles for the other facade, the south-west facade. Among these photos, 4 of them facing the facade were chosen to be used. 14 detail points were surveyed from the south-west facade of the church, and the location of these points were defined on photographs and adjusted and drew (Figure 6).

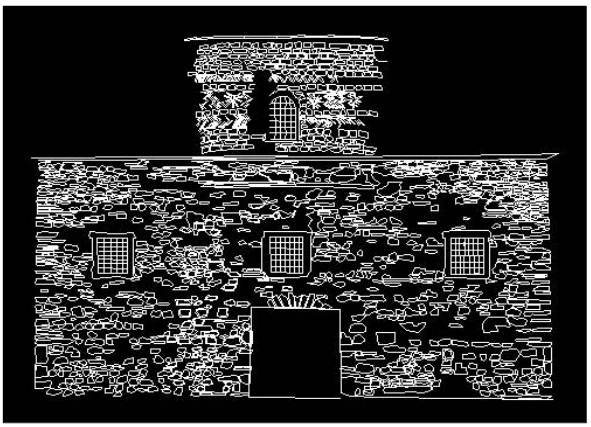

Figure 6. South-West facade drawings of the church

3.1.3. North-West facade

A total of 28 terrestrial photographs were taken from different angles and locations for the north-west facade, the rear entrance of the church. 4 of these photographs were selected to be used to meet the needs. During the field study from the north-west facade of the church, 16 detail points were surveyed, these points were marked in the relevant parts of the

photographs, adjusted and drawings were completed (Figure 7).

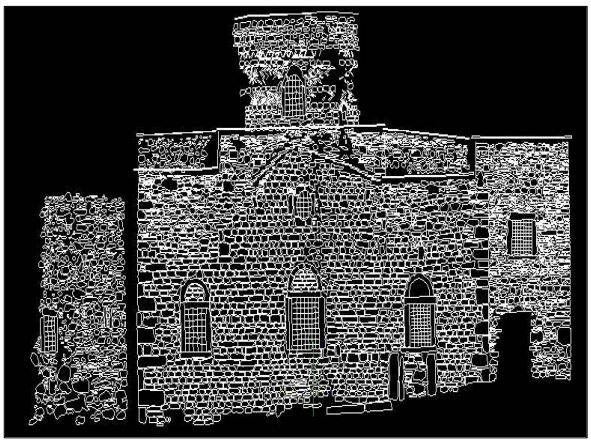

Figure 7. North-West facade drawings of the church

3.1.4. North-East facade

A total of 39 terrestrial photographs were taken for the north-east facade of the church, which we described as the last facade of the church during the study. 4 of these photos were selected to be used. In addition, 4 more photos taken by unmanned aerial vehicles for this facade were used in the drawings. A total of 20 detail points was surveyed from the north-east facade of the church, the photos and the points were matched, adjusted and their drawings were completed in the program (Figure 8).

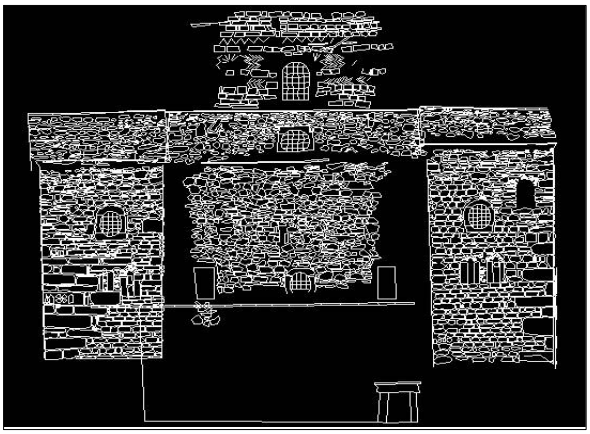

Figure 8. North-East facade drawings of the church

3.2. Roof Statical Survey with Unmanned Aerial Vehicle

UAV and photogrammetry explain the photogrammetric measurement platforms, the activities of a pilot and UAV sitting on the platform without the need for photogrammetric processing, or remote, semi-independent or independent activities. It includes balloons, kites, gliders, rotating and fixed-wing UAVs with its wide definition, photogrammetric data collection, semi-automatic and automatic flight mode. In this part of the study, UAV was prepared to show how they can be used for photogrammetric data collection and processing. For the surveying and modelling of the upper part of the church, the commanded Hirobo Shuttle ZX helicopter to be used in images was used. In the stages of preparing the unmanned aircraft for flight, it is aimed to minimize the vibration of the engine and to take good photographs. To adjust the required propellers, the camera is fixed with a piece of specialised equipment (Figure 3). Also, since the camera used is a camera with anti-vibration and autofocus system, the image acquisition may be at the desired quality.

A total of 20 plates were placed, only 9 of them were adjusted for reasons such as solar flare and coordinate shift, modelling was made. For the measurement of the upper part of the church, photographs were taken from different angles on the days and hours when the weather was favourable since it was not required to leave a shadow in the photo and the plates should not shine from the sun. On take-off from the north facade and once from the south facade, flew twice in total and took photos. The first take-off, reaching the desired height and acquiring images and landing took 10-15 minutes. It was decided to fly from the facade in the other direction to make the adjusting and modelling healthier. The photoshoot was completed within the same period considering the size of the object. Take-off and landing were done twice with the 300g camera and was left in the air for about 25 minutes with 300 ml of fuel. First, the flight was done, and then the phases of coordinating the plates with the total station were followed. Placing the plates, making the flight and giving the coordinates were all done in about 60 minutes. A total of 134 photographs were taken, including take-off and landing. Ninety-five images are available with the exact view of the object. Three images that saw the church not from piecemeal, but from the top and as a whole, were selected of the 95 images. Then marked with the coordinates given to the plates, adjusted and roof modelling was performed (Figure 9).

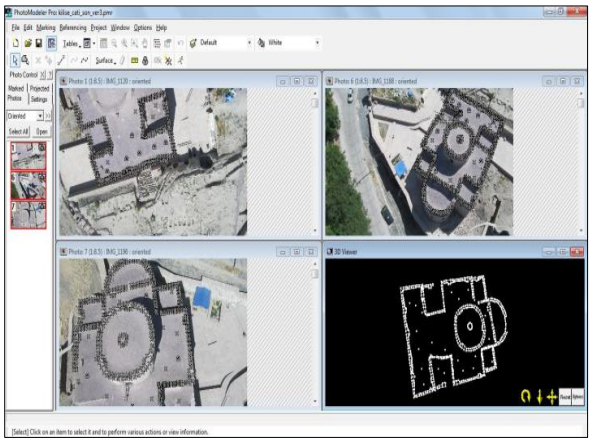

Figure 9. Roof drawings of Aya-i Eleni Church

The 3D model of the church was completed by combining the drawings of the facades and the roof of the church (Figure 10).

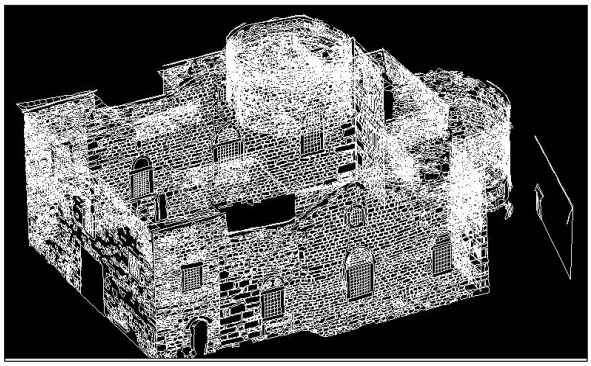

Figure 10. 3D version of Aya-i Eleni Church in AutoCAD environment

3.3. Survey of the Interior of Sille Aya-i Eleni Church with Terrestrial Laser Scanner

Scanning operations were carried out from different station points of the interior of Sille Aya-i Eleni Church (Göktepe et al., 2009). Processing and merging of point clouds belonging to the interior of the church was carried out. Sections of the model obtained in AA', BB', CC', DD' directions (Figure 11) were taken and their appearance was obtained (Figure 12, 13, 14, 15) (Böge, 2013).

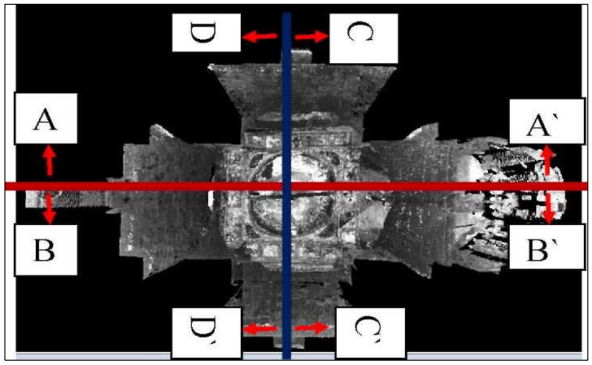

Figure 11. Sections taken inside the Aya-i Eleni Church

Figure 12. AA' section of the interior of Aya-i Eleni Church

Figure 13. BB' section of the interior of Aya-i Eleni Church

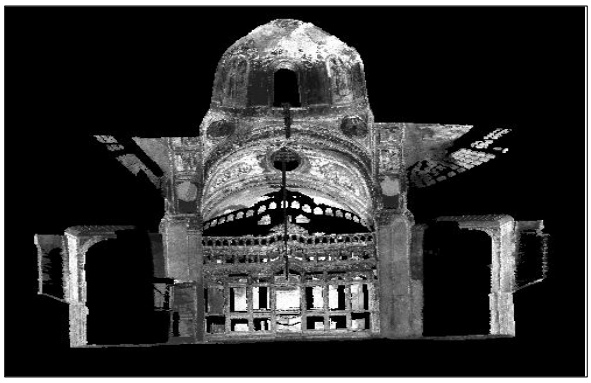

Figure 14. CC' section of the interior of Aya-i Eleni Church

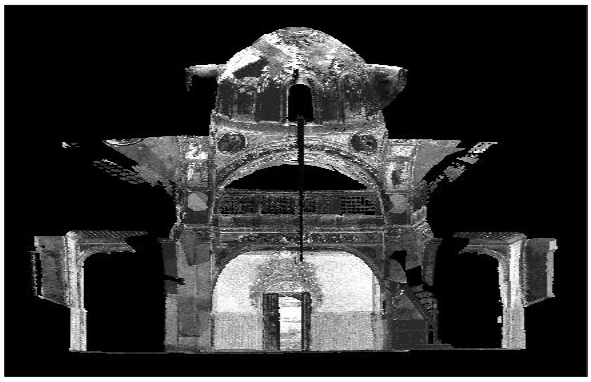

Figure 15. DD' section of the interior of Aya-i Eleni Church

3.4. DEM, Orthophoto and Drawing of Some Views of Sille Aya-i Eleni Church Interior

DEM, orthophoto and drawings of some sections of AA', BB', CC' and DD' sections specified in Figure 11 were realized in Z-Map software. Point clouds previously combined in the IMAlign module of Polyworks software have been imported into the IMInspect module. Other points in the IMInspect module have been deleted, except for point clouds from the entry part (DD'). After this process, the part of the point cloud to be transferred to the Z-Map software was selected and transferred to the .txt file

with the densities of the points. This file was opened in Z-Map software and also pictures taken with the previously calibrated Nikon D80 digital camera are included in the project. In the point clouds transferred to Z-Map software, a surface is passed through at least 4 points on the same surface. Now the defined coordinate system is the system of this surface. 3D coordinate transformation was realized by making picture matching with the point clouds included in the project (Table 1). Later, Digital Elevation Model (DEM) was created from point clouds. After DEM, orthophoto image with a pixel size of 3 mm was obtained. Thus, image shifts consisting of image skew and height difference were eliminated and a scaled image was obtained (Figure 16).

Table 1. Standard deviations resulting from the conversion between the point cloud and the picture of AA', BB', CC', DD' sections

Section Name	Image Number	σx (mm)	σy (mm)
AA'	190	15	3
AA'	192	7	2
BB'	165	12	5
BB'	166	9	2
CC'	161	13	8
DD'	202	14	11
DD'	201	11	12

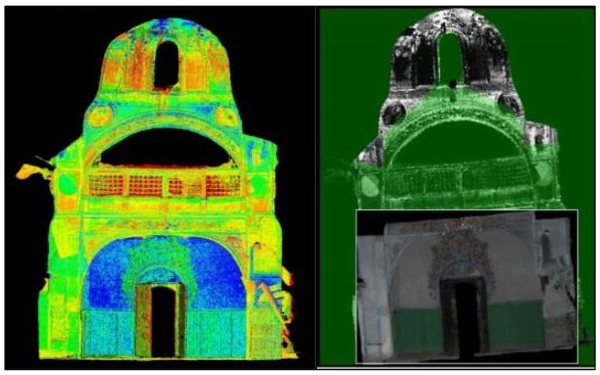

Figure 16. DEM and orthophoto obtained from point clouds of the entrance part (DD' section)

Processes of some parts of AA', BB', CC' sections are the repetition of the processes made for the input section (DD'). The conversion results obtained in the matching of the point clouds and the pictures are given in Table 1. As a result, DEM, orthophotos (pixel sizes 3mm) and drawings of each section were obtained (Figure 17, 18, 19, 20, 21).

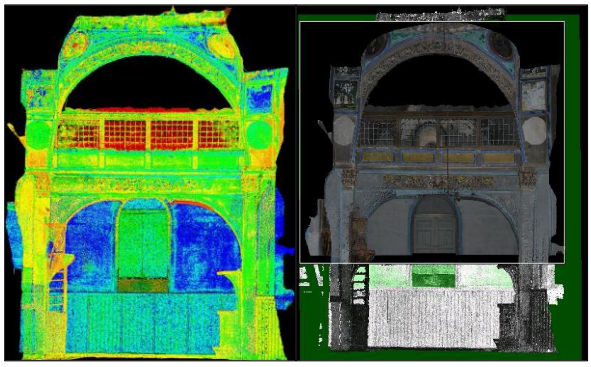

Figure 17. DEM and orthophoto (overlaid on point cloud) obtained from point clouds of AA' section

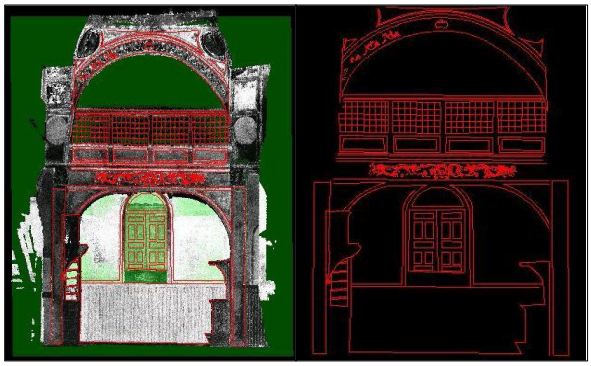

Figure 18. Drawing from point clouds of section AA'

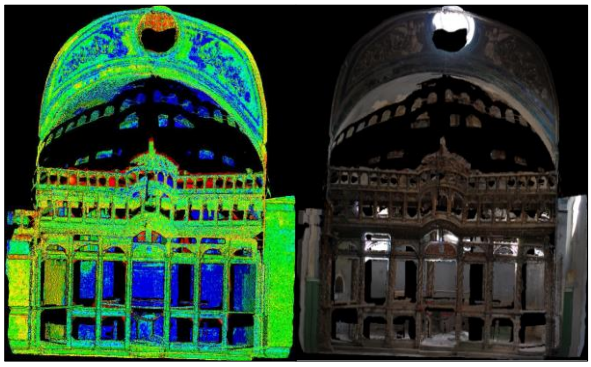

Figure 19. DEM and orthophoto obtained from point clouds of the CC' section

Figure 20. Drawing from point clouds of CC' section

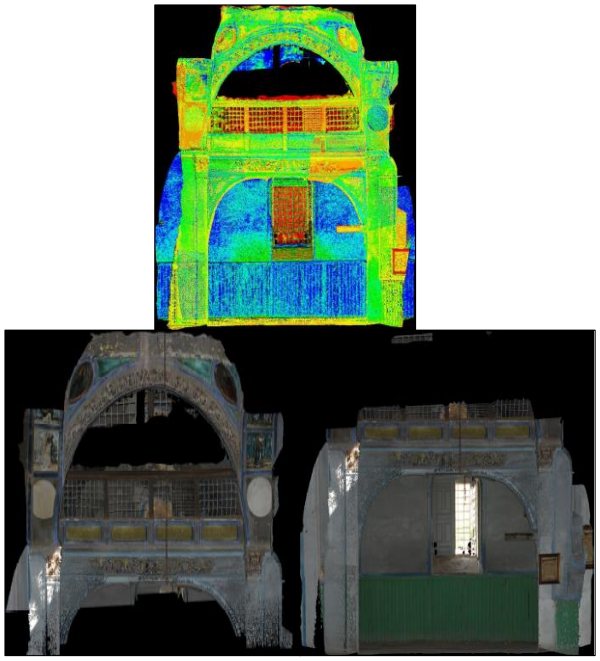

Figure 21. DEM and orthophoto obtained from point clouds of section BB'

Orthophoto mosaic processes were carried out to obtain the orthophotos of the BB' section in one piece. Two orthophoto images are combined in Z-Map software (Figure 22).

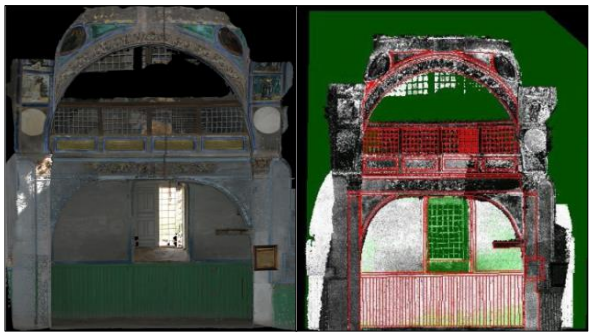

Figure 22. Drawing from mosaic and point clouds of section BB'

In addition to these sections, DEM, orthophoto image (pixel size 1cm) and drawing were obtained with the help of point clouds of an ornament on the ceiling, which is very difficult to reach (Figure 23, 24).

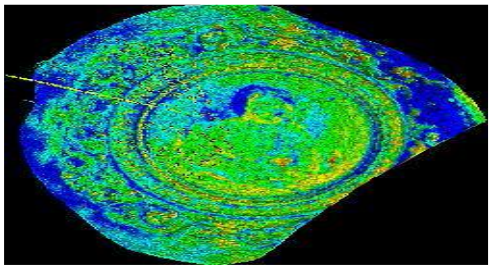

Figure 23. DEM obtained from the point clouds of the ceiling

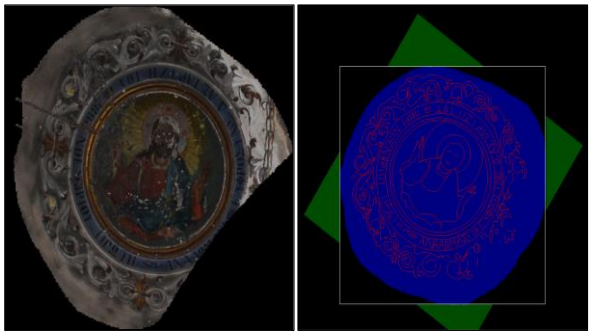

Figure 24. Orthophoto and drawing of the ceiling ornament from point clouds

4. DISCUSSION AND CONCLUSION

Exterior drawings of Sille Aya-i Eleni Church were made separately by the photogrammetric method and combined in the computer environment. The roof pictures of the church were taken with UAV, drawn by the photogrammetric way and combined with other exterior drawings; the 3D model of the object was created. Also, the interior of the church was scanned with a laser scanner, and some sections of its interior were drawn with the help of point clouds and pictures taken from the church.

In restoration projects, approximately 30% of the work consists of statical surveys. The statical survey consists of layout plan, plans, architectural details, exterior sections. In statical surveying studies, narrow street, high roofs, old writings and unsymmetrical detail surveys have difficulty in working. Scanning the interior of the object with the laser scanner made within the scope of the study allows both section drawings and archiving the purpose with its real dimensions. It is perhaps more critical than obtaining a 3D model of the object with its actual dimensions and the most exceptional detail than contributing to the section and exterior drawings. Currently, if there are different thoughts about the object, which is thought to be depicted with specific parts, in the following years, 3D point clouds in the archive can be used easily. We can say that it is not necessary to use laser data in the drawing of exterior facades that are open and without depth, and these drawings can be made efficiently and sufficiently with the photogrammetric method. Drawing with UAV on high and dangerous roofs is an efficient solution. Although it may be possible to bring roofs with lidar data later, it is not recommended now because it is costly in this method. Besides, images that can be taken from UAV can be used in obtaining sections of objects that have difficulties in taking photographs for various reasons (The upper part of the North-East facade in this study).

Both laser scanner data and photogrammetric methods provide an effective solution for studying more specific objects. With these methods, both drawings and orthophotos can be made. Orthophotos also offers an effective solution for

documenting. While studying the object with many details, it should be worked with the expert of the feature and the necessary corrections should be done in the detail drawing. Although effective solutions are offered with both methods, it can be said that drawing is more practical with point clouds when the ease of drawing is taken into consideration. Because to create a 3D coordinate in the photogrammetric method, the same detail point must be overlaid in at least two images (overlay of homologous rays). This process takes time and sometimes causes difficulty in marking the same detail point. However, the drawing of points in the same plane can be easily made in a plane passed through the points whose 3D coordinates known. This process is not recommended as an effective solution for uneven objects. In general, the images of the laser-scanned object are superimposed with hundreds of thousands of 3D point clouds, drawing and orthophoto are obtained. It is possible to say that these products are more accurate than the products obtained as a result of overlaying (made in practice) of a few 3-dimensional points taken with the total station.

Documentation of cultural and historical buildings is of great importance in terms of transferring the content of buildings between societies from generation to generation. For this reason, documenting cultural heritage is equally important. Architectural documentation is a complex process and contains much more information than other disciplines. From this point of view, it is thought that it is not right to document the cultural heritage only with laser scanning technology. Laser scanning is especially suitable for complex surfaces, surface analysis and visualization. However, instead of dealing with the dense point cloud, more straightforward terrestrial photogrammetry technique is recommended on uncomplicated surfaces. In addition to laser scanning technology, it is possible to say that according to the condition of historical buildings, to behave cost and time, UAV can be used on hard-to-reach surfaces, terrestrial photogrammetry technique on surfaces where detail drawing can be easy.

ACKNOWLEDGEMENT

This article was produced from Sevgi BÖGE's master thesis.

REFERENCES

Altay, G., Sağıroğlu, Ö. (2019). Heritage recording with 3D laser technology: The case of Lord' s Bath (Bey Hamami) In Muğla, Milas. *Gazi University Journal of Science Part B: Art Humanities Design and Planning,* 7(4), 489-496.

Böge, S. (2013). Tarihi ve kültürel varlıkların rölöve alımı için farklı yöntemlerin birlikte kullanılması (MSc thesis). Selcuk University, Konya, Turkey.

Chen, D., Zhang, L., Mathiopoulos, P.T., & Huamg, X. (2014). A methodology for automated segmentation and reconstruction of urban 3-D buildings from ALS point clouds. *IEEE Journal of Selected Topics in Applied Earth Observations and Remote Sensing,* 7(10), 4199-4217.

Esposito S., Fallavollita P., Wahbeh W., Nardinocchi C., & Balsi M. (2014). Performance evaluation of UAV photogrammetric 3D reconstruction. *IEEE Geoscience and Remote Sensing Symposium,* 4788–4791.

Göktepe, A., Karabork, H., Yakar, M., Yildiz, F., & Baygul, E. (2009). 3D modeling of Sille Aya-i Eleni Church with laser technology. *In 22nd CIPA Symposium – Digital Documentation, Interpretation & Presentation of Cultural Heritage,* Kyoto.

Güleç, A. (2007). Yersel fotogrametri yöntemi ile rölöve alım tekniğinin taç kapılarda uygulanışı Konya örnekleri (MSc thesis). Selcuk University, Konya, Turkey.

Karabork, H., Yildiz, F., Yakar, M., Altuntas, C., & Karasaka L. (2007). Modeling and visualization using laser scanner in documentation of Cultural Heritage. *XXI International CIPA Symposium, 01-06 October,* Athens, Greece.

Korumaz, A.G., Korumaz, M., Dulgerler, O.N., Karasaka, L., Yıldız, F., & Yakar, M. (2010). Evaluation of laser scanner performance in documentation of historical and architectural ruins, A case study in Konya. *International Archives of Photogrammetry, Remote Sensing and Spatial Information Sciences*, 38 (5), 361-366.

Koyuncu, A. (2013). Sille'deki değişimin sosyolojik analizi. 1. Ulusal Sille Sempozyumu, 26-28 Eylül, Konya.

Themistocleous K., Ioannides M., Agapiou A., & Hadjimitsis D.G. (2015). A new approach for documenting architectural cultural heritage: the case study of Asinou Church in Cyprus. *Proceedings of the International Conference on Sustainability in Architecture and Cultural Heritage*, 11-12 December, Limassol, Cyprus.

Themistocleous, K., Agapiou, A., & Hadjimitsis, D. (2016). 3D documentation and Bim modeling of cultural heritage structures using UAVs: the case of the Foinikaria Church. *The International Archives of the Photogrammetry, Remote Sensing and Spatial Information Sciences*, 42, 45-49.

Uzar, M., Tunalıoğlu, N., Arıcan, D., & Arda, T. (2019). Yersel lazer tarama verisi ile elde edilen 3B modellerde filtreleme etkisinin araştırılması. *Journal of the Faculty of Engineering and Architecture of Gazi University* 34(4),1765-1775.

Uzun, T., Spor, Y. (2019). Yersel lazer (Nokta bulut) tarama yöntemi ile rölöve-restitüsyon-restorasyon projesi hazırlama süreci ve bir örnek: Elazığ Harput Kale Hamamı. *Tasarım Kuram*, 15(28), 1-26.

Vacanas, Y., Themistocleous, K., Agapiou, A., & Hadjimitsis, D. (2015). Building Information Modelling (BIM) and Unmanned Aerial Vehicle (UAV) technologies in infrastructure construction project management and delay and disruption analysis. *Third International Conference on Remote Sensing and Geoinformation of the Environment*, 9535, 95350C.

Varlık, A., Uray, F., & Metin, A. (2016). Sokak sağlıklaştırma projelerinde yersel lazer tarayıcı ile mimari rölöve alımı: Afyonkarahisar kentsel sit alanı örneği. *Harita Teknolojileri Elektronik Dergisi,* 8(2), 141-150.

Xue, J., Fan, Y., Su, B., & Fuentes, S. (2019). Assessment of Canopy Vigor Information from Kiwifruit plants based on a Digital Surface Model from Unmanned Aerial Vehicle imagery. *International Journal of Agricultural and Biological Engineering*, 12(1), 165–171.

Yakar, M., Mırdan, Ö. (2017). Tarihi eserlerin İnsansız Hava Aracı ile modellenmesinde karşılaşılan sorunlar. *Geomatik Dergisi (Journal of Geomatics),* 2(3), 118-125.

Yildiz, F., Corumluoglu, O., Yakar, M., Karabork H. & Yilmaz, H.M. (1999). A photogrammetric investigation study on Ayai-Eleni Church (Sille-Konya). *Third Turkish-German Joint Geodetics Days,* 1, 265-274, 1-4 June, Istanbul.

TURKGEO
TURKISH JOURNAL OF GEOSCIENCES

ISSN: *2717-7696*
Research Article
Vol; 1, Issue; 2, pp. 63-71 2020
DOI:
Journal homepage:
https://dergipark.org.tr/en/pub/turkgeo

Comparison of Troposphere Models Used in Commercial GPS Softwares

İbrahim Özuğur*[1], Kemal Yurt [2]

[1]*Botas Tanap Land Acquisition Directorate, Ankara, Turkey*
[2]*Aksaray University, Faculty of Engineering, Department of Geomatics Engineering, Aksaray, Turkey*

Keywords
Tropospheric models
Atmospheric models
Atmospheric parameters
GPS

ABSTRACT

The Global Navigation Satellite System (GNSS) is one of the most important inventions in the history of the survey. GPS in 1974 and GLONASS in 1976 were established and used for military purposes, and they were opened to civil use since 1980 and 1982 respectively and started to be used in daily life. The GNSS system has developed very rapidly in line with technological studies and these rapid developments have directed scientists to develop new methods that can meet the needs of users and get the most accurate results. One of the best studies to minimize the effect on GNSS signals in the atmosphere is the use of dual-frequency GNSS receivers. These receivers can eliminate errors on GNSS signals in the ionosphere layer. However, they cannot eliminate the errors occurring in the troposphere layer. To eliminate these errors, the tropospheric effect can be minimized by measuring the humidity, temperature and pressure values at each point of the survey and using these values in calculations. But since this process will take a lot of time and is very costly, tropospheric models have been made by scientists. By using these models in GNSS software, the effect of the troposphere layer on the signals can be minimized. In this study, four different survey campaigns were conducted to observe the effect of Troposphere models under different atmospheric conditions. Topcon Tools ver.7 and Leica Geo Office 7.0 software were used to evaluate these campaigns. The effects of troposphere models on these calculations have been observed. The atmospheric values measured at the time of the session and the atmospheric values are taken from the General Directorate of Meteorology were included in the calculations and the results were compared.

1. INTRODUCTION

Global Navigation Satellite System (GNSS) is one of the navigation systems widely used in many civil and military fields. The number of people using Global Positioning Systems, which is developing each passing day, is increasing day by day (Koca and Ceylan, 2018). Today, the system, whose generic name is GNSS, has many satellite systems (GPS, GLONASS, GALILEO, BEIDOU / COMPASS, QZSS, IRNSS) (Ateş, 2011). The vast majority of existing error sources in this system is between the moment of the signal out from the satellite and the moment the GNSS receivers are received. When the signals broadcasted from GNSS satellites enter the atmosphere, they pass through the ionosphere and troposphere, respectively, reaching the GNSS receptors and diverging when passing through the atmosphere. This divergence is divided into two as signal path curvature and diffusion delay. The most important effect is the diffusion delay, which can be divided into ionospheric and tropospheric. The effect of the neutral (non-ionized) atmosphere on electromagnetic waves emitted in radio frequencies is called the tropospheric delay effect (or tropospheric refraction). This effect causes the electromagnetic wave to slow down and bend (Kahveci, 2011).

The signal propagation delay in the troposphere layer accounts for 80% of the total delay, and this delay is called the tropospheric delay (Hopfield, 1971). When talking about the troposphere, it is

* **Corresponding Author**

*(iozugur@hotmail.com) ORCID ID 0000–0002–5300–6057
(kemalyurt@aksaray.edu.tr) ORCID ID 0000–0002–1029–4052

Cite this article

Özuğur. İ., Yurt, K. (2020). Comparıson Of Tropospher Models Used In Commercıal GPS Softwares. Turkish Journal of Geosciences, 1(2), 63-71.

Received: 28/07/2020; Accepted: 24/08/2020

generally meant the lower part of the earth's atmosphere. Tropospheric delay is divided into dry delay and wet delay. The dry component can be determined with high accuracy with many tropospheric delay models prepared by surface meteorological measurements, and this part can be easily modelled with the law of ideal gases since it is in hydrostatic equilibrium. The wet part is difficult to calculate (estimate) due to the uneven distribution of liquid water and water vapour in the troposphere. The neutral atmosphere consists of dry air and water vapour. There is no significant change in the composition of dry air depending on latitude and altitude (Smith and Weintraub, 1953). The troposphere consists of two ideal gas mixtures, dry air and water vapour. Dry air is dependent on the gas density in the atmosphere, changes in the gas distribution, causing 90% of the total atmospheric delay. The pressure measured at the measurement point can be modelled with 2% error in the direction of temperature and humidity and zenith. It is much more difficult to model the existing water vapour component between the receiver and the satellite along the signal path, as the water vapour changes rapidly concerning for to the ground and time. Due to the water vapour component, the delay is 5–30 cm in medium latitudes and can be determined with a sensitivity of 2–5 cm. Troposphere errors can be reduced by using 92% suitable troposphere model (Saastamonien and Hoppfield) (Kınık, 1999). The effects of errors on the measurements can be minimized by using GNSS receivers and calculation and modelling methods in evaluation programs. In the tropospheric delay calculation, Saastamoinen and Hopfield models are widely used in the evaluation of GPS observations, together with atmospheric parameters independent of time and actual meteorological conditions (Özuğur, 2019). In meteorological applications, it is very difficult to represent the spatial and temporal distribution of water vapour in the atmosphere precisely. The numerical estimation quality of Precipitable Water (PW), which can be converted into precipitation, depends on the correct determination of the distribution of atmospheric moisture information (Glowacki et al., 2006).

Yılmaz (2013), reported in his study that the calculations made using meteorological data yielded 5mm better results than standard troposphere models.

Erkan (2008), also tested the PW values calculated with the global pressure and temperature model used in cases where meteorological parameters are not available at GPS stations. As a result of the test, it was observed that the differences between the actual meteorological values present in the GPS station and the use of these values from the model are compatible with approximately 1 mm standard deviation. However, if meteorological data are measured at GNSS stations, or if these values can be obtained from a numerical weather forecast model, the need to include these data in the assessment has been proven by many scientific articles.

Erdönmez (2008) came to the conclusion that the determining factor of the total delay is a wet delay, which varies according to the water vapour pressure and relative humidity, and the main factor affecting the delay is water vapour, which is an important factor due to the temperature.

In this study, three different GNSS sessions were held in order to identify the best results by comparing the troposphere models in the GNSS software used to minimize the errors caused by the broadcast delay.

The evaluations are also for GPS signal data as the GNSS receivers used only use data from GPS satellites. Therefore, in the next steps, GPS expression will be used instead of GNSS expression.

2. MATERIALS AND METHODS

2.1. Studying Area

In order to evaluate the effects of troposphere models in GPS software on GPS evaluation results, 3 different applications were made.

Application 1 with the long-edge (150 km * 250 km) GPS network, the point named NIGD established as part of the TUSAGA-Aktif project is taken as TUSAGA reference, and TUSAGA points named AKSR, FEEK, HALP, KAPN, KAYS, NEVS, NGDE, POZA, TUFA are connected to the GPS network in a suitable distribution. It was aimed to observe the effects of different troposphere models, at the long-distance measured bases between these points, which are between 7 km and 147 km with reference, at different atmospheric conditions and different satellite elevation angles. Selected observation points are located in settlements (Figure 1).

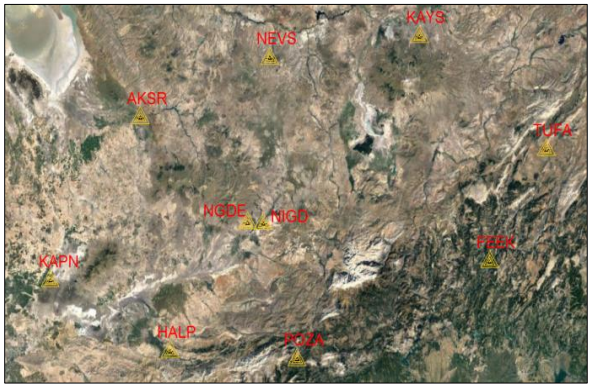

Figure 1. Application 1 project area and locations of points

Application 2 TUTGA points at a distance of 19 to 55 km from each other named L28-G001, L29-G001, L29-G002, M28-G001 and M29-G001 in the centre of Konya and L2810012, C1 degree triangulation point included in mid-range (40 km * 55 km) network (Figure 2).

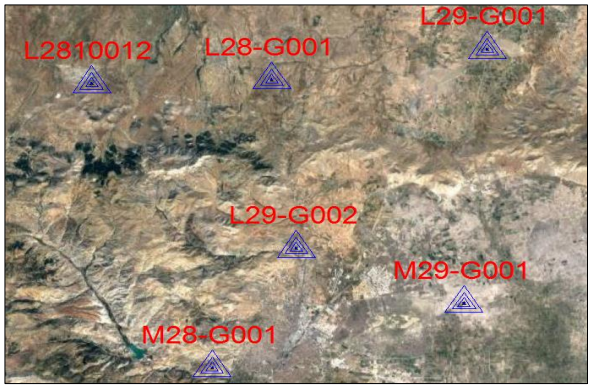

Figure 2. Application 2 project area and locations of points

Application 3 12 points have been identified and included in the network where the land changes character, started from Askarlihoyugu around Konya-Adana highway, along the Konya-Afyon highway in the direction of Istanbul road (north-south) to Calinbas Hill in the north of Karacaören Ciftligi (Figure 3).

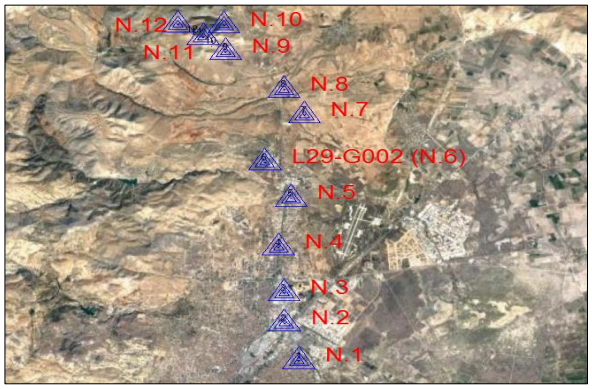

Figure 3. Application 3 project area and locations of points

2.2. Topcon Hiper Pro and Topcon Hiper Plus Receivers

Topcon Hiper Pro and Topcon Hiper Plus receiver, which is used in observations in application areas 2 and 3 and has wireless operation technology, can survey more than 14 hours and has 40 channeled receivers. It is waterproof and its sensitivity in static and fast static surveying methods is 3mm + 0.5ppm in positioning, 5mm + 0.5ppm in levelling. In Real Time Kinematics (RTK) application, precision is 10mm + 1.0ppm in positioning, 15mm + 1.0ppm in levelling.

2.3. Javad GNSS Receiver

The GPS branded Javad used in the Application 2 field, 2 SIM cards can be inserted and have the feature of bluetooth wireless technology. It has 216 channels and can work for 15 hours. In static and fast static surveying methods, the sensitivity is 0.3cm + 0.5ppm in positioning, 0.5cm + 0.5ppm in levelling. In Real Time Kinematics (RTK) application, precision is 1cm + 1.0ppm in positioning, 1.5cm + 1.5ppm in levelling.

2.4. Vaisala PTU 307 Meteorological Sensor

PTU307 is the sensor option developed for open and demanding meteorology applications of PTU300 series, which has the ability to measure three parameters at the same time, such as barometric pressure, humidity and temperature. PTU307 with the additional hot probe, total precision in barometric pressure measurement -40/+60°C, precision in relative humidity measurement +15/+25°C ±1.0 %RH, temperature measurement +20°C ±0.2 °C. With Vaisala PTU 307 meteorological sensor, pressure, humidity and temperature values were measured in the Application 2 area.

2.5. Ashtech Z Surveyor Receiver

Ashtech Z Surveyor receivers, which are used 2 in Application 3 field, are 12-channelled, dual-frequency GPS receivers. The sensitivity of the receiver, which can work up to 10 hours, in static and fast static surveying methods, is 5mm + 1ppm in positioning, 10mm + 1ppm in levelling.

2.6. Trimble 5700 Receiver

The Trimble 5700 receiver, a 24-channelled, dual-frequency GNSS receiver, can operate for up to 8 hours. The sensitivity of the receiver in static and fast static surveying methods is 5mm + 0.5ppm in positioning, 5mm + 1ppm in levelling. In Real Time Kinematics (RTK) application, precision is 10mm + 1ppm in positioning and 20mm + 1ppm in levelling.

2.7. Topcon Tools Ver.7 Software

Topcon Tools (TT) software, which is an adjustment software that can evaluate RTK observations and GPS static survey data, contains modules for different solutions. Free and based adjustment in application areas were made with Topcon Tools (TT) software.

2.8. Leica Geo Office 7.0 Software

Leica Geo Office (LGO) software, commercial software of Leica, was used in free and based adjustment steps in the application area. Troposphere models in the software are Hopfield, Simplified Hopfield, Saastamenion, Essen and Froome, No Troposphere and Computed models.

3. RESULTS

The calculation was made by entering the meteorological data of the locations close to the reference station in Table 1 requested for

Table 1. Requested meteorological data

T.C.
Ministry of Agriculture and Forestry
Turkish State Meteorological Service

Station Number	Station Name	Year	Month	Day	Average Temperature	Maximum Temperature	Minimum Temperature	Average Humidity	Total Precipitation	Average Air Pressure hPa	Calculated Average Air Pressure mbar	Average Cloud Amount	Average Wind Direction	Average Wind Speed	Maximum Wind Direction	Maximum Wind Speed	Maximum Wind Time
17192	AKSARAY	2012	1	15	2.8	5.6	0.1	82.2	0	899.8	996.8	4.5	241WSW	3.3	220SW	10.8	05:10
17193	NEVŞEHİR	2012	1	15	1.8	4.9	-1.1	75.8	0	868.0	994	3.7	209SSW	3.1	170S	11.3	01:23
17248	EREĞLİ	2012	1	15	7.4	11.6	2	52.3	0	890.8	995.4	4	208SSW	3.6	210SSW	14.4	11:00
17250	NİĞDE	2012	1	15	4.2	7.4	1.2	68.2	0	873.5	994.6	3.3	227SW	3.8	240WSW	11.3	18:44
17902	KARAPINAR	2012	1	15	3.8	7.4	1.1	79.7	0.5	896.1	995.7	0	138SE	2.9	207SSW	9.4	07:14
17934	POZANTI	2012	1	15	4.3	8	-7.2	79.8	0	889.6	997.6	0	271W	1.6	203SSW	7.2	13:03
17192	AKSARAY	2012	6	15	26.9	34.2	18.1	30.9	0	904.8	1001.8	1.9	354N	1.7	70ENE	10.3	23:23
17193	NEVŞEHİR	2012	6	15	25.6	32.8	17.5	27.5	0.2	875.5	1001.5	4	23NNE	1.8	50NE	7.7	17:39
17248	EREĞLİ	2012	6	15	25.3	34.5	15.9	42	3.6	896.2	1000.8	1.3	78ENE	1.2	170S	4.1	17:30
17250	NİĞDE	2012	6	15	25.5	34.2	15.3	30.8	0	879.6	1000.7	2.4	40NE	1.8	30NNE	6.2	19:40
17902	KARAPINAR	2012	6	15	26.7	35.3	15.8	32.1	0	901.2	1000.8	0	352N	1.9	308NW	6.3	11:39
17934	POZANTI	2012	6	15	26.4	35	17.3	30.2	0	892.6	1000.6	0	284WNW	2.1	283WNW	10.5	14:33

NOTES: 1 – Time Given is UTC (Coordinated Universal Time). Turkey to translate the winter time 2 hours, according to the daylight saving time is added 3 hours. 3 hours in 2016 and after are added. The information up to the last 35 days has not passed the quality control, values may change at a later date. The system and data have been edited, there may be occasional differences with the previous data. 2 – The air temperature is measured in the shade at a height of 2 meters in degrees Celsius (° C). 3 – The days when the Daily Minimum Temperature drops below 0 ° C are expressed as Frost Day. 4 – In the Wind Table; Calm (C): 0.0-0.2 m / s (0 Bofor), Breeze: 0.3-1.5 m / s (1 Bofor), Light Wind: 1.6-3.3 m / s (2 Bofor), Sweet Wind: 3.4-5.4 m / s (3 Bofor), Medium Wind: 5.5-7.9 m / s (4 Bofor), Strong Wind: 8.0-10.7 m / s (5 Bofor), Strong Wind: 10.8-13.8 m / s (6 Bofor), Storm Wind: 13.9-17.1 m / s (7 Bofor), Storm: 17.2-20.7 m / s (8 Bofor), Strong Storm: 20.8-

Application 1 into the Topcon Tools program. NIGD TUSAGA station was taken as reference, and other models were compared according to Hopfield troposphere model. Although there are also changes in Y and X coordinates in model comparison, comparisons have been made for the point heights most affected by tropospheric models. Based on the 15° elevation angle in January and the solution in the Hopfield layer shown in Table 2, monthly changes compared to the same parameters in other months were seen. As a result of the application, the height change in the points varies between -450mm and +450mm depending on the model used. Since the troposphere effect cannot be corrected by using GPS or any other method, the model that can give the best effect and the most accurate result should be selected according to the model survey area and weather.

As a result of the application, Hopfield and Saastamoinen models in the LGO program and Goad & Goodman models in the TT program were observed to give the best results compared to other models. In Table 2, the results obtained by meteorological methods and program data were compared on the Goad & Goadman model. After all; the height differences calculated were very small due to the fact that there are close values with the standard atmosphere model and the distance between the stations is large, it allows the entry of meteorological data belonging to only one point in the program and the points in the assessment are in different geographical regions but in similar weather conditions.

L2910012, L28-G001, L29-G001, M28-G001 and M29-G001 points calculated by using the free adjustment method by using the troposphere models in Leica Geo Office (LGO) and Topcon Tools (TT) program by taking reference the point numbered L29-G002 in the Application 2 area. Points numbered L28-G001, L29-G001 and M29-G001 were also calculated by taking the based balancing methods.

In addition to the based adjustment(s) made with the troposphere models in LGO and TT programs, there are small differences between the standard meteorological values in the TT program and the free and based adjustment(s) made by entering the meteorological data in the valuation of the days in 10.03.2012 and 11.03.2012 according to the meteorological data measured in the field in Table 3. In the evaluation of the days of 11.06.2013 and 12.06.2013, between the standard models in the TT program and the based adjustment(s) made by entering meteorological data, it has been shown to affect up to 10 mm. With the meteorological data entered in the Niell and UNBabc models in the TT program, +/-20 cm was seen that it made errors in calculations.

In the project site where the elevation range is between 1008 m and 1731 m as a result of GPS measurements made in the north-south direction of the Application 3 Area, which is given free adjustment results in Table 4; it was observed that the change in satellite cutting angles seen in Table 4 affected the heights between 1 and 5 mm. In the comparison of the troposphere models, it was observed that the models failed according to the height of the measured points.

4. DISCUSSION AND CONCLUSION

As a result of the calculations, when the results obtained from the troposphere models are compared among themselves based on the best model, it has been observed that it affects only the vertical position and the effect of the horizontal position is very small. Although the LGO program does not allow meteorological data to be entered, Hopfield model and Saastamoinen models selected automatically by the program have been shown to give the best results even in different weather conditions, on long-distance and short-distance bases, and even in flat or unevenness of the surveyed terrain. The sensitivity of the model disappears as the height difference between the reference point where the Simplified Hopfield model gives good results on the rough terrain and the point where GPS observation changes. As can be seen from the results of the application, in the comparison made with the 15° Hopfield model for the point height lower than the reference point, it gives a negative error and for the point height higher than reference point, it gives the positive error. Essen Froome model is a model suitable for use on relatively flat terrain and as seen in Application 3, it gives an error in the range of +6 cm and -6 cm even in less uneven terrain. Like the Simplified Hopfield model, the Essen Froome model also gives a negative error for the point height lower than the reference point and a positive error for the point heights above the reference point. Calculations made with the No Troposfer option will most likely give accurate results when calculating GPS signals with the same tropospheric effect in the same region and for points with the same altitude. We are very unlikely to encounter such an event in the project sites where we practice. Unlike the Simplified Hopfield and Essen Froome models, in the calculations that do not apply the troposphere model, it gives a negative error for the heights above the reference point and a positive error for the low heights. Computed model is a model with different tropospheric conditions and where the height difference between the points is high, it will be more suitable to use in the long-based calculations if Hopfield and Saastamoinen models cannot be used in long-based calculations.

The TT program allows the use of measured meteorological values, thanks to its menu that allows adding meteorological data. Goad & Goodman, Niell and UNBabc models used in the program give very close results in comparison of the program itself. Meteorological data fixed in the TT program; pressure is 1013.2 mbar, the temperature is 20 °C, humidity is 50%. While

Table 2. Adjustment results of other stations compared to NGDE reference station

Survey Days	Points			LEICA GEO OFFİCE							TOPCON TOOLS						METEOROLOGICAL DATA		
											PROGRAM DATA						Data of NIGD station		
	Station	Height (Ellipsoidal)	Distance to Reference M.	HOPFIELD 15°	HOPFIELD 15°	SIMPLIFIED HOPFİElD 15°	SAASTAMOINE N 15°	ESSEN FROOME 15°	NO TROPOSPHERE 15°	COMPUTED 15°	GOAD& GOODMAN 15°	NEILL 15°	UNBABC 15°	GOAD& GOODMAN 15°	NEILL 15°	UNBABC 15°	Average Temperature	Average Humidity	Average Pressure
15.01.2012	AKSR	1005.803	75194.356	0	0	27	0	174	-159	2	16	-2	26	-186	-186	-186	2.8°	82	996.80
	FEEK	600.315	109635.274	0	0	73	0	459	-427	38	-39	-37	-48	-535	-535	-535	4.3°	80	997.60
	HALP	1252.456	71877.256	0	0	0	0	0	7	-50	0	-4	-1	-1	-1	-1	7.4°	52	995.40
	KAYS	1138.758	111294.034	0	0	13	0	75	-89	-11	-8	5	15	0	-90	-90	1.8°	93	994.00
	NEVS	1292.459	73059.724	0	0	-4	0	-26	81	5	-4	-12	-3	-4	24	23	1.8°	93	994.00
	NGDE	1410.622	7641.969	0	0	-17	0	-102	110	-14	7	7	9	6	128	128	4.2°	68	994.60
	NIGD	1252.326	0	0	0	0	0	0	0	0	0	0	0	0	0	0	4.2°	68	994.60
	POZA	826.403	61941.176	0	0	48	0	283	0	-10	-18	-6	-5	-21	-332	-332	4.3°	80	997.60
	TUFA	1459.39	139300.83	0	0	-23	0	-147	135	5	-1	2	-1	5	142	142	4.3°	80	997.60
15.06.2012	AKSR	1005.803	75194.356	1	0	28	0	161	-152	24	-9	5	4	-6	-190	-190	27.9°	9	1001.80
	FEEK	600.315	109635.274	-6	0	76	0	457	-440	-3	1	1	-26	-1	-483	-483	26.4°	0	1000.60
	HALP	1252.456	71877.256	-3	0	0	0	0	44	32	25	3	22	20	20	21	26.2°	2	1000.80
	KAYS	1138.758	111294.034	0	0	12	0	74	-95	56	-8	2	-3	-2	-72	-73	25.6°	8	1001.50
	NEVS	1292.459	73059.724	1	0	-4	0	-26	29	40	4	6	0	4	30	30	25.6°	8	1001.50
	NGDE	1410622	7641.969	-8	0	-17	0	-102	109	11	-6	6	6	8	127	127	25.5°	1	1000.70
	NIGD	1252.326	0	0	0	0	0	0	0	0	0	0	0	0	0	0	25.5°	1	1000.70
	POZA	826.403	61941.176	-7	0	42	0	283	-290	14	14	4	-1	7	-314	-312	26.4°	0	1000.60
	TUFA	1459.39	139300.83	-7	0	-21	0	-130	85	13	7	2	13	20	144	144	26.4°	0	1000.60

Table 3. Adjustment results based on Application 2 site

Survey Days	Station Name	LEICA GEO OFFİCE						TOPCON TOOLS						
		HOPFIELD	SIMPLIFIED HOPFIELD	SAASTOMONİEN	ESSEN AND FROME	NO TROPOSFER	COMPUTED	GOAD& GOODMAN 15°	NİELL 15°	UNBABC 15°	GOAD& GOODMAN 15°	NİELL 15°	UNBABC 15°	GOAD& GOODMAN 10°	GOAD& GOODMAN 5°	GOAD& GOODMAN 1°
10.03.2012		Program Data; Pressure 1013.2 Mb Temperature: 20°C Humidity: 50						Avg. Pressure:1014.42			Temp:12			Humidity:%47		
	L2810012	0	-11	0	-31	33	-16	0	-1	-1	1	26	26	-1	-3	-3
	L29-G001	0	14	0	56	-80	-15	0	1	1	-2	162	162	-3	-5	-5
	M28-G001	0	-26	0	-136	198	-3	0	-2	-3	3	-148	-148	-1	-8	-8
11.03.2012		Program Data; Pressure 1013.2 Mb Temperature: 20°C Humidity: 50						Avg. Pressure::1015.56			Temp:6			Humidity:%48		
	L2810012	0	-9	0	-47	46	-50	4	8	1	4	23	23	7	7	8
	L29-G001	0	14	0	55	-92	1	22	24	25	21	189	189	20	20	19
	M28-G001	0	-28	0	-144	176	-4	-10	-10	-14	-9	-174	-174	-2	-2	-6
12.03.2012		Program Data; Pressure 1013.2 Mb Temperature: 20°C Humidity: 50						Avg. Pressure::1014.00			Temp:12			Humidity:%47		
	L2810012	0	-9	0	-44	43	-35	9	-18	-18	-34	7	31	14	15	15
	L29-G001	0	15	0	74	-94	1	21	-7	-7	-40	160	189	25	36	32
	M28-G001	0	-28	0	-145	167	-23	1	-7	-8	-7	-158	-149	-3	-8	-9
10.06.2013		Program Data; Pressure 1013.2 Mb Temperature: 20°C Humidity: 50						Avg. Pressure::1003.49			Temp:24			Humidity:%35		
	L2810012	0	-5	0	-28	36	17	-15	-18	-19	-15	6	6	-27	-29	-29
	L29-G001	0	20	0	117	-132	44	-4	-8	-10	-6	144	144	-8	-10	-9
	M28-G001	0	-22	0	-135	151	30	-30	-33	-38	-30	-184	-184	-43	-46	-46
11.06.2013		Program Data; Pressure 1013.2 Mb Temperature: 20°C Humidity: 50						Avg. Pressure::1003.126			Temp:31			Humidity:%20		
	L2810012	0	-5	0	-26	37	5	-18	-29	-22	-14	61	61	-25	-26	-26
	L29-G001	0	18	-2	107	-128	-2	-14	-12	-12	-5	174	174	-6	-4	-3
	M28-G001	0	-21	0	-134	148	21	-28	-35	-37	-36	-114	-114	-43	-44	-44
12.06.2013		Program Data; Pressure 1013.2 Mb Temperature: 20°C Humidity: 50						Avg. Pressure:1004.299			Temp:28			Humidity:%20		
	L2810012	0	-5	0	-28	39	11	-17	-13	-19	-15	8	4	-15	-16	-16
	L29-G001	0	20	0	112	-128	14	-1	-3	-10	6	146	146	4	10	10
	M28-G001	0	-22	0	-133	151	20	-29	-31	-28	-32	-164	-164	-36	-35	-35

Table 4. Application 3 site free adjustment results

NETWORK ADJUSTMENT RESULT																	
		Orthometric Height															
		Ellipsoidal Height															
		Distance to Reference m.															
	TOPCON TOOLS	NİELL															
		GOOD & GOODMAN															
		UNBABC															
	LEİCA GEO OFFİCE	COMPUTED															
		NO TROPOSFER															
		ESSEN FROOME															
		SAASTAMOINEN															
		SIMPLIFIED HOPFIELD															
		0° HOPFIELD															
		5° HOPFIELD															
		10° HOPFIELD															
		15° HOPFIELD															
		Station Name	N.1	N.2	N.3	N.4	N.5	N.6	N.7	N.8	N.9	N.10	N.11	N.12
			1012.50	1008.17	1025.46	1031.22	1094.87	1168.27	1135.16	1192.39	1413.19	1525.42	1732.45	1731.16
			1048.26	1043.94	1061.21	1067.02	1130.69	1204.22	1171.09	1228.39	1449.41	1561.68	1768.76	1767.50
			13835.06	11163.68	9082.26	5908.12	2872.37	0.00	3925.38	5149.34	7949.32	8577.51	9487.22	9698.85
			-22	-25	-19	-3	-13		-12	-7	-14	-12	9	8
			-11	-10	-8	-1	-8		-6	4	-8	-12	8	7
			-22	-24	-19	-3	-13		-12	-7	-14	-12	9	8
			29	38	27	37	28		42	1	29	29	35	30
			116	115	104	99	54		24	-18	-173	-229	-362	-324
			-106	-104	-95	-92	-50		-23	16	162	223	359	348
			0	0	0	0	0		0	0	0	0	-1	-1
			-18	-17	-16	-15	-8		-4	3	26	36	58	56
			-4	-5	-5	-3	-4		-1	3	3	3	3	4
			-3	-5	-4	-2	-3		-1	2	2	2	2	2
			-2	-3	-3	-1	-2		-1	1	1	1	1	1
			0	0	0	0	0		0	0	0	0	0	0

entering the measured or provided meteorological data into the program, the Goad&Goodman model gives similar results according to its closeness to the fixed parameters, while the Niell and UNBabc model gives very distant results by entering the meteorological data. Niell and UNBabc models should not be used while calculating with meteorological data in Topcon Tools program.

It is not a problem to calculate the troposphere models used in local calculations or in programs for less uneven terrain with models suitable for the application area and location. Since the moisture, temperature and pressure values in different regions will be different in calculations to be made as a result of broad-based GPS observations (such as TUSAGA application), the use of a standard troposphere model may give erroneous results according to the application area. Therefore, it will be appropriate to measure meteorological data in high-presentation measurements and to make calculations in the programs in which these data can be loaded.

In an academic study to be done to get a more effective result from the comparison of Troposphere models with the measurement of atmospheric data; measuring the atmospheric data of the points at the seaside and the points in the inner parts that have different height and pressure values will be more useful at the point of comparing the troposphere models.

ACKNOWLEDGEMENT

This article was produced from İbrahim ÖZUĞUR's master thesis.

REFERENCES

Ateş, H.B. (2011). TUSAGA-Aktif GPS ağ verileri ile bölgesel iyonosferik modelin oluşturulması (MSc thesis). Gebze Institute of Technology, Kocaeli, Turkey.

Erdönmez, O. (2008). Troposferik gecikmelerin GPS ölçülerine olan etkisinin araştırılması (MSc thesis). Yildiz Technical University, Istanbul, Turkey.

Erkan, Y. (2008). Troposferik gecikme modellerinin GPS nokta konumlarına etkisi (MSc thesis). Zonguldak Karaelmas University, Kocaeli, Turkey.

Glowacki, T.J., Penna, N.T., Bourke, W.P. (2006). Validation of GPS-based estimates of integrated water vapour for the Australian region and identification of diurnal variability. *Australian Meteorological Magazine*, 55(2), 131–148.

Hopfield, H. (1971). Tropospheric effect on electromagnetically measured range: prediction from surface weather data. *Radio Science*, 6(3), 357–367.

Kahveci, M. (1997). Investigation of the effects of propagation errors on GPS observations in Turkey region (PhD thesis). Istanbul Technical University, Istanbul, Turkey.

Kınık, İ. (1999). GPS ölçme ve değerlendirmelerinde hata kaynakları üzerine bir inceleme (PhD thesis). Yildiz Technical University, Istanbul, Turkey.

Koca, B., Ceylan, A. (2018). Uydu konum belirleme sistemlerindeki (GNSS) güncel durum ve son gelişmeler. *Journal of Geomatics*, 3(1), 63-73.

Özuğur, İ. (2019). Ticari GPS yazılımlarında kullanılan troposfer modellerinin karşılaştırılması (MSc thesis). Aksaray University, Aksaray, Turkey.

Smith, E.K., Weintraub, S. (1953). The constants in the equation for atmospheric refractive index at radio frequencies. *Proceedings of the IRE*, 41(8), 1035-1037.

Yılmaz, S. (2013). GNSS verilerinden hesaplanan elipsoid yüksekliklerinin atmosferik verilerle iyileştirilmesi (PhD thesis). Selcuk University, Konya, Turkey.

TURKGEO
TURKISH JOURNAL OF GEOSCIENCES

ISSN: *2717-7696*
Research Article
Vol; 1, Issue; 2, pp. 72-77, 2020
DOI:
Journal homepage:
https://dergipark.org.tr/en/pub/turkgeo

Burn Area Detection and Burn Severity Assessment Using Sentinel 2 MSI Data: The Case of Karabağlar District, İzmir/Turkey

Suhrabuddin Nasery [*1], **Kaan Kalkan** [2]

[1]*Eskişehir Technical University, Earth and Space Sciences Institute, Eskişehir, Turkey*
[2]*TÜBITAK Space Technologies Research Institute, Ankara, Turkey*

Keywords
Forest fire
Burn severity
NBR
dNBR
SAVI
Sentinel 2

ABSTRACT

Forest fires are serious environmental problems for ecosystem which destroys huge amount of forests every year across the world. Detecting burned areas is not the only important task, it is also very important to distinguish severity degrees of soil suffered for post-fire land management and vegetation regeneration. Remote sensing presents accurate and efficient methods for mapping burned areas and assessing burn severity levels. In this study we detected forest burn areas and assessed burn severity levels using Remote Sensing techniques and Sentinel 2 satellite data products in Karabağlar, Menderes and Seferihisar districts of İzmir, Turkey. A recent big forest fire occurred on 18 August 2019 is assessed in this study, which burned down about 500 hectares of the forest. Burned areas are detected using Normalized Burn Ratio (NBR) and Soil Adjusted Vegetation Index (SAVI) indices and burn area severity analysis is performed using Differenced Normalized Burn Ratio (dNBR) and Differenced Soil Adjusted Vegetation Index (dSAVI) indices. The results of dNBR index show that a total of 6909.708-hectare area is burned during forest fire while 11184.502-hectare is unburned. Areas with different levels of burn severity were detected: 9.3 % Low, 11.1% Moderate-low, 8.5% Moderate-high and 9.3% High. Furthermore, based on the results of dSAVI analysis, 6699.554-hectare area is burned and 11394.656-hectare is unburned; the following different levels of burn severity were detected in the area: 9.4 % Low, 6.4% Moderate-low, 8.7% Moderate-high and 12.5% High.

1. INTRODUCTION

Fire emissions have very strong influence on composition of the atmosphere which directly affect the global climate, as well as human health and security (Pereira et al., 2018). Forest fires disturb the ecological functioning of various ecosystems as they partially or completely burn vegetation layers and affect post-fire soil and vegetation processes, for example soil erosion, debris flow, flooding and vegetation recovery (Nasi et al., 2002).

Forest fires can change the physical and chemical form of the earth organic substances. These changes are sometimes very serious which can destroy the organic material in the soil thus vegetations will not be able to regrowth in the soil (Sazayya et al., 2020). Forest typically regrow after forest fires; but some areas which are seriously damaged, will not regrow naturally in short time so it is needed to detect those areas and enrich the soil for growing forest and vegetations (Keeley, 2009; Sazayya et al., 2020).

It is very crucial to have accurate knowledge about the fire distribution pattern, particularly burn severity degree, to plan and execute post-fire land management and vegetation restoration activities (Quintano et al., 2017; Pereira et al., 2018). Burn severity assessment, specifically the term burn severity, is widely used to represent the loss of organic matter on the soil surface caused by a fire (Pereira et al., 2018; Sazayya et al., 2020).

Generally, field observations are very difficult and time consuming for detection of burned area severity degrees, fortunately remote sensing has the capability of detecting burned areas and its severity which is very effective, time and money saving

* **Corresponding Author**

*(suhrabuddin_nasery@yahoo.com) ORCID ID 0000-0001-5846-2476
(kalkaan@gmail.com) ORCID ID 0000-0002-2732-5425

Cite this article

Nasery, S., Kaan K. (2020). Burn Area Detection and Burn Severity Assessment Using Sentinel 2 MSI Data: The Case of Karabağlar District, İzmir/Turkey. Turkish Journal of Geosciences, 1(2), 72-77.

Received: 17/07/2020; Accepted: 07/09/2020

method. Remote sensing methods for estimating burn severity can be categorized into physical and empirical groups. Physical methods work based on the interactions between radiations and burned canopies (Chuvieco et al., 2019; Veraverbeke et al., 2011).

Empirical methods benefit from statistical regression or machine learning to measure burn severity and are relatively easy to implement and interpret (De Santis and Chuvieco, 2009; Veraverbeke et al., 2011), for example spectral bands combinations and indexes, such as NBR, dNBR, relative differenced Normalized Burn Ratio RdNBR, Burn Area Index (BAI), Normalized Burn Ratio – Thermal (NBRT), SAVI and Burned Area Index for Sentinel-2 (BAIS2), NBR, dNBR and SAVI are widely used in the literatures for wildfires detection and measuring burn severity.

The primary aim of this study is mapping burned areas and burn severity assessment of a forest fire which was started in 18 august 2019 from Karabağlar district of İzmir and extended to two neighbor districts of Menderes and Seferihisar during three days and burned down about 500 hectares area (Url-1,2,3), using remote sensing-based methods and Sentinel 2 satellite data. The study focuses on fire severity classification and burn area detection through using dNBR, NBR, SAVI and dSAVI indices.

Figure 1. Area burned by forest fire occurred on 18/08/2019, Izmir/Turkey (Url-1)

1.1. Study Area

The study area is located in Karabağlar Menderes and Seferihisar districts of İzmir province and has 180.94 km^2 (18094.2 hectares) area. In Izmir, which is in the Mediterranean climate zone, summers are hot and dry and winters are warm and rainy. The steep extension of the mountains to the sea and the insertion of the plains up to the threshold of the Inner west Anatolia allows the spread of the maritime influences to the inner parts. However, differences in Physical Geography, such as altitude and distance from the Coast, also lead to climate differences that can be considered important in terms of rainfall, temperature and sunbathing. The average annual temperature in the province varies between 14-18 °C in coastal areas. July (27.3 °C) and August (27.6 °C) are the hottest months, while January (8.6 °C) and February (9.6 °C) months are the coldest (Url-4). According to statistics from Turkey's general directorate of forestry, Izmir has 1018259-hectare of forests and 1496478-hectare area dedicated for forestation purposes. Izmir experience many forest fires during summer which destroys significant amount of forests every year. During 2007 and 2016, Izmir had the third highest number of forest fires in Turkey with 1394 cases (Url-5,6). This year (until 28 June 2020), 16 forest fires cases were occurred in Izmir province (Url-7).

Figure 2. Location map of the study area, Izmir (Karabağlar, Menderes and Seferihisar district), Turkey

2. MATERIALS AND METHODS

2.1. Materials

Satellite images the study area have been downloaded from Copernicus Open Access Hub portal (https://scihub.copernicus.eu) which are acquired by sentinel 2B (S2B) satellite. Pre-fire and post-fire images of the study area were selected as close to fire occurrence day as possible; the image tile numbers, capturing date and cloud percentage of the scenes are given in table 1.

Table 1. Details of Sentinel 2 satellite images used in this study

Satellite Image	Cloud Cover (%)	Capturing Date
S2B_MSIL2A_20190816T085559	0.468	16/08/2019
S2B_MSIL2A_20190826T085559	0.199	26/08/2019

In addition, these images are Sentinel level 2A products which are both geometrically and radiometrically corrected; furthermore, they are bottom of atmosphere (BOT) products which are also atmospherically corrected (ESA, 2020). All

Sentinel 2A and 2B products are radiometrically corrected by Sentinel-2 Ground Segment and are available for users, level 0, 1A and 1B products which are without radiometric correction, are not available for users (Url-8).

2.2. Method

NBR and SAVI indices were selected for burned area detection and dNBR and dSAVI indices for determining fire severity degrees. Data analysis is performed in SNAP software environment and ArcGIS Pro is used for area calculation and plotting purposes.

The NBR is particularly sensitive to changes in living vegetation, moisture content and certain soil conditions in near infrared (NIR) and shortwave infrared (SWIR) bands that may occur after a fire (Miller and Thode, 2007), for this reason, NBR index is used for the detection of burnt green areas. NBR is expressed by mathematical formulas obtained using near infrared and shortwave infrared bands (Miller and Thode, 2007; Veraverbeke et al., 2011). The value range for NBR is in the interval between -1 to +1.

$$NBR = \frac{(NIR-SWIR)}{(NIR+SWIR)} \quad (1)$$

Burned area severity can be easily classified by dNBR index. The dNBR is obtained by subtracting pre-fire NBR and post-fire NBR indices (Miller and Thode, 2007).

$$\Delta NBR = NBR_{Pre-fire} - NBR_{Post-fire} \quad (2)$$

Hypothetically, the values for dNBR are between -2 and +2 where the values for burnt areas ranging from 0.10 to 1.35 and the unburned areas from -0.10 to +0.10 in most areas, but the minimum and maximum values can be different based on the study area (Key and Benson, 2006).

Table 2. Burn severity levels obtained calculating dNBR, proposed by USGS (Key and Benson, 2000; Lutes et al., 2006)

Severity Level	dNBR Range (not scaled)
Enhanced Regrowth, high (post-fire)	-0.500 to -0.251
Enhanced Regrowth, low (post-fire)	-0.250 to -0.101
Unburned	-0.100 to +0.99
Low Severity	+0.100 to +0.269
Moderate-low Severity	+0.270 to +0.439
Miderate-high Severity	+0.440 to +0.659
High Severity	+0.660 to +1.300

(These value ranges are flexible; scene-pair dependent; shifts in thresholds +0.100 points are possible. dNBR less than about -0.550, or greater than about +1.350 may occur, but usually are not considered burned. Rather, they likely are anomalies caused by miss-registration, clouds, or other factors not related to real land cover differences)

The SAVI index is identical to Normalized Difference Vegetation index (NDVI) and is used to correct NDVI for the influence of soil brightness or noise effects (soil color, soil moisture, soil variability across region, etc.) in areas with low vegetation cover (Xue and Su, 2017; Huete, 1988; EOS, 2019). This index was designed by Huete (1988) which can be expressed as follow:

$$SAVI = \frac{(NIR-R)}{(NIR+R+L)} * (1+L) \quad (3)$$

Where L is the soil adjustment factor.

The values for L factor vary based on the vegetation density of the land cover and is varied from 0 to 1; Huete suggests (L=0.25) for high vegetation density, (L=0.5) for intermediate vegetation density and (L=1) for low vegetation density (Huete, 1988).

Burned area severity assessment can be performed using the difference between pre fire and post fire SAVI index results, because the SAVI index is similar to NDVI. We can formulate the Differenced Soil Adjusted Vegetation index by subtracting pre fire and post fire SAVI for detecting burned areas and burn severity categories which can be expressed as follow:

$$dSAVI = SAVI_{Pre-fire} - SAVI_{Post-fire} \quad (4)$$

Based on the review performed, this index is not used in any literature before, this index works similar to Differenced Normalized Difference Vegetation Index (dNDVI) which is widely used in vegetation cover change detection and assessment.

3. RESULTS

Based on the results of the analysis, dNBR value range was derived between -1.508 to +1.378, the value range was then classified into 7 classes in accordance with burn severity value range defined by USGS (Table 2); the resulted burn severity map is shown in figure 4. The results indicate that 9.3% of the study area is highly burned, also 8.5%, 11.1% and 9.3% of the area is covered by Moderate-high severity, Moderate-low severity and Low severity classes respectively (Figure 3).

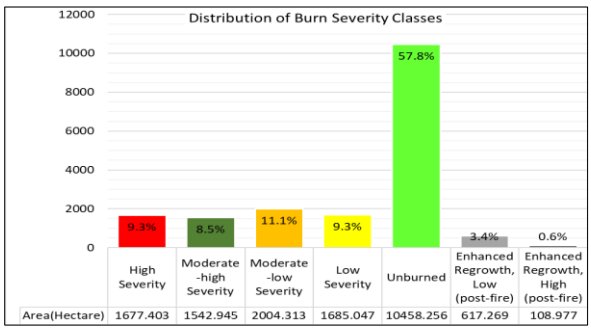

Figure 3. Distribution of burn severity classes derived from dNBR index

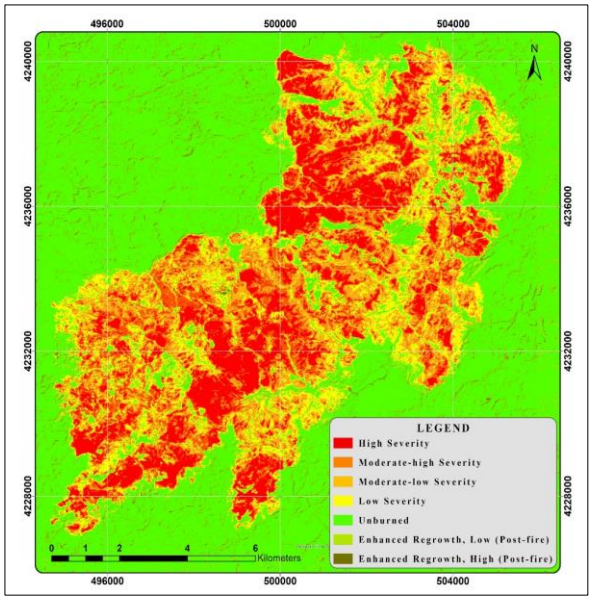

Figure 4. dNBR resulted burn severity map, showing the distribution of severity classes across the study area

The dSAVI data range was derived between -0.523 to +0.747 and the results were thresholded into 5 classes considering its histogram and burn severity classes, the resulted burn severity map is shown in figure 5.

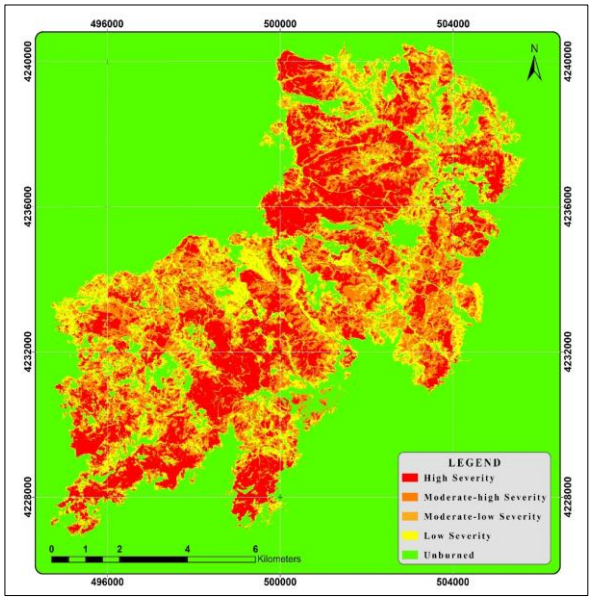

Figure 5. dSAVI resulted burn severity map, showing the distribution of severity classes across the study area

Based on the results of dSAVI, 12.5% of the study area is highly burned, 8.7%, 6.4%, 9.4% and 63.0% of the area is covered by Moderate-high severity, Moderate-low severity, Low severity and Unburned classes respectively (Figure 6).

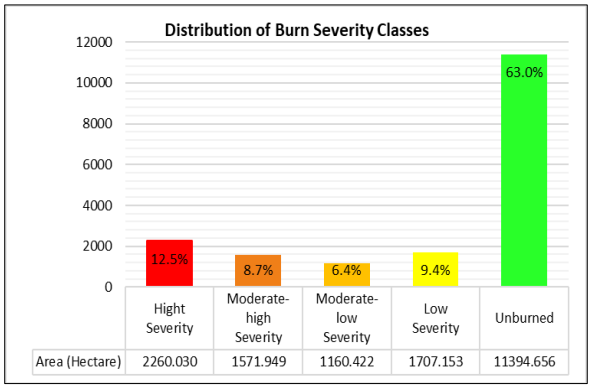

Figure 6. Distribution of burn severity classes derived from dSAVI index

4. DISCUSSION AND CONCLUSION

Wildfires change the physical and chemical properties of soil and vegetation. Significant changes in spectral reflections can be observed as a result of reduced moisture in vegetation, covering the surface with ashes and a sudden increase in surface temperature (Lanorte et al., 2012). This study demonstrates that burned area detection and burn severity assessment can be successfully executed using remote sensing indices and sentinel 2 satellite imageries. The NBR, dNBR, SAVI and dSAVI indices used in this study had very good performance (Figure 5) which shows the suitability of the indices used.

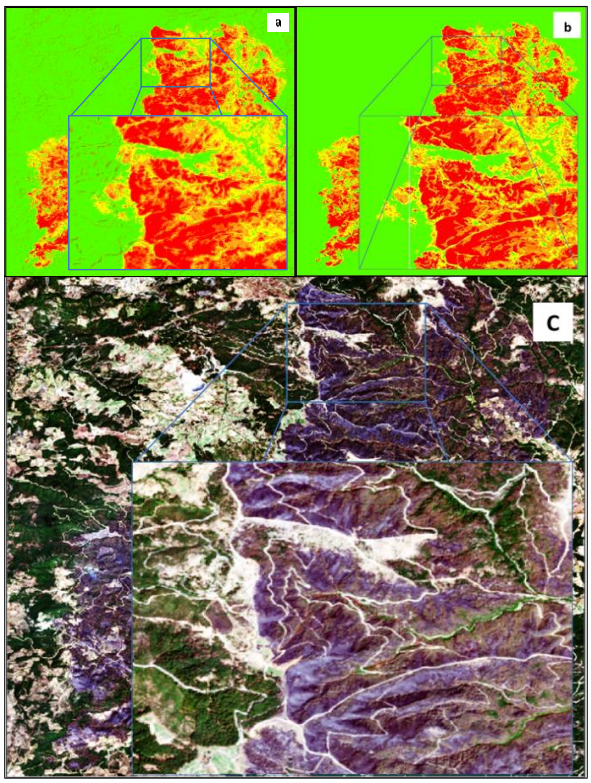

Figure 7. (a) burned areas detected by NBR and dNBR indices, (b) burned areas detected by SAVI and dSAVI indices, (c)RGB composite of the burned area

The NBR and dNBR indices had very good performance in detection of burned areas and burns severity analysis in many studies (Veraverbeke et al., 2011; Key and Benson, 2006; Miller and Thode, 2007). Recently, Roy et al. (2006) have questioned the efficiency of the NBR index assessing forest fires in South Africa, Australia, Russia and South America; they have used Landsat and MODIS satellite data in their study.

The results obtained in this study are the opposite of the results obtained by Roy et al. (2006), the fires they have assessed are likely to be understory surface fires which were not visible due to very dense canopy. In addition, the optimality analysis performed by them would have included burned and unburned pixels in their calculations. The results of the analysis show that NBR index is more sensitive to pre and post fire spectral changes in the scene than SAVI index. The dNBR index had better performance in discriminating between different severity levels than dSAVI, especially in high severity class.

The study revealed that from the total 18094.21 hectares of the study areas, 6909.708-6699.554 hectare is burned. According to the statistics announced by authorities and news agencies, the burned area is repeatedly reported 500 hectares after the fire was extinguished (Url-1,2,6), which have an extreme difference with the results obtained in this study. The results indicate that only High severity class detected by dNBR and dSAVI covers 1677.403-hectare and 2260.030-hectare area respectively, which is about three to four times bigger than it was reported in media.

REFERENCES

Chuvieco, E., Mouillot, F., Van Der Werf, G.R., San Miguel, J., Tanasse, M., Koutsias, N., García, M., Yebra, M., Padilla, M., Gitas, I., Heil, A., Hawbaker, T. J., & Giglio, L. (2019). Historical background and current developments for mapping burned area from satellite Earth observation. *Remote Sensing of Environment*, 225, 45-64.

De Santis, A., Chuvieco, E. (2009). GeoCBI: A modified version of the Composite Burn Index for the initial assessment of the short-term burn severity from remotely sensed data. *Remote Sensing of Environment*, 113(3), 554–562.

EOS (2019, February). 6 Spectral indexes to make vegetation analysis complete. Retrieved from https://eos.com/blog/6-spectral-indexes-on-top-of-ndvi-to-make-your-vegetation-analysis-complete/

ESA (2020, July). European Space Agency. Retrieved from https://earth.esa.int/web/sentinel/user-guides/sentinel-2-msi/overview

Huete, A. (1988). A Soil-Adjusted Vegetation Index (SAVI). *Remote Sensing of Environment*, 295-309.

Keeley, J.E. (2009). Fire intensity, fire severity and burn severity: A brief review and suggested usage. *International Journal of Wildland Fire*, 18(1), 116–126.

Key, C.H., Benson, N.C. (2000). Measuring and remote sensing of burn severity. *Joint Fire Science Conference and Workshop Proceedings*, 284–285.

Key, C.H, Benson, N.C. (2006). Landscape assessment: Remote sensing of severity, the Normalized Burn Ratio. FIREMON: Fire Effects Monitoring and Inventory System. *General Technical Report*, RMRS-GTR-164-CD, 305–325.

Lanorte, A., Danese, M., Lasaponara, R., & Murgante, B. (2012). Multiscale mapping of burn area and severity using multisensor satellite data and spatial autocorrelation analysis. *International Journal of Applied Earth Observation and Geoinformation*, 20(1), 42–51.

Lutes, D., Keane, R., Caratti, J., Key, C., Benson, N., Sutherland, S., & Gangi, L. (2006). FIREMON: Fire Effects Monitoring and Inventory System. General Technical Report, United States Department of Agriculture. Retrieved from https://www.fs.fed.us/rm/pubs/rmrs_gtr164.pdf

Miller, J. D., Thode, A.E. (2007). Quantifying burn severity in a heterogeneous landscape with a relative version of the delta Normalized Burn Ratio (dNBR). *Remote Sensing of Environment*, 109(1), 66–80.

Nasi, R., Dennis, R., Meijaard, E., Applegate, G., & Moore, P. (2002). Forest fire and biological diversity. *Unasylva*, 53(209), 36–40.

Pereira, P., Francos, M., Brevik, E.C., Ubeda, X., & Bogunovic, I. (2018). Post-fire soil management. *Current Opinion in Environmental Science and Health*, 5, 26–32.

Quintano, C., Fernandez-Manso, A., & Roberts, D. A. (2017). Burn severity mapping from Landsat MESMA fraction images and Land Surface Temperature. *Remote Sensing of Environment*, 190, 83–95.

Roy, D., Boschetti, L., & Trigg, S. (2006). Remote Sensing of Fire Severity: Assessing the Normalized Burn Ratio. *IEEE Geoscience and Remote Sensing Letters*, 3(1), 112-120.

Sazayya, K., Sugano, T., & Kuramitz, H. (2020). High-heat effects on the physical and chemical properties of soil organic matter and its water-soluble components in Japan's forests: A comprehensive approach using multiple analytical methods. *Analytical Sciences*, 36(5), 601–609.

Veraverbeke, S., Lhermitte, S., Verstraeten, W.W., & Goossens, R. (2011). Evaluation of pre/post-fire differenced spectral indices for assessing burn severity in a Mediterranean environment with Landsat thematic mapper. *International Journal of Remote Sensing*, 32(12), 3521–3537.

Xue, J., Su, B. (2017). Significant Remote Sensing Vegetation Indices: A Review of Developments and Applications. *Journal of Sensors*, 2017, 1-18.

Url-1: https://www.aa.com.tr/tr/turkiye/izmirde-yanan-ormanlik-alanlar-havadan-goruntulendi/1559816 (last accessed 1 July 2020)

Url-2: https://www.haberturk.com/son-dakika-izmir-deki-orman-yangini-45-saattir-devam-ediyor-2514596 (last accessed 5 May 2020)

Url-3: https://www.hurriyet.com.tr/gundem/izmirde-bu-yilin-en-buyuk-yangini-41306741 (last accessed 10 July 2020)

Url-4: https://www.izmir.bel.tr/tr/IzmirinCografyasi/220/255 (last accessed 12 May 2020)

Url-5: https://www.yenisafak.com/gundem/turkiyede-orman-yangininin-en-cok-yasandigi-3-il-2759389 (last accessed 5 July 2020)

Url-6: https://www.aa.com.tr/tr/turkiye/10-yilda-24-bin-264-orman-yangini-cikti/865449 (last accessed 3 July 2020)

Url-7: https://www.ogm.gov.tr/Sayfalar/OrmanYanginlari.aspx (last accessed 7 June 2020)

Url-8: https://www.sentinel-hub.com/eoproducts/ndvi-normalized-difference-vegetation-index (last accessed 20 June 2020)

TURKGEO
TURKISH JOURNAL OF GEOSCIENCES

ISSN:2717-7696
ResearchArticle
Vol; 1, Issue; 2, pp. 78-84, 2020
DOI:
Journalhomepage:
https://dergipark.org.tr/en/pub/turkgeo

The Effects of Urban Regeneration on the City: The Case of Zagnos Valley of Trabzon Province

Yaşar Selçuk ERBAŞ *[1]

[1]*Gümüşhane University, Faculty of Engineering and Nature Sciences, Department of Geomatics Engineering, Gümüşhane, Türkiye*

Keywords
Urban Regeneration
City
Trabzon
Zagnos Valley

ABSTRACT

In recent years, urban regeneration has become a topic discussed in almost all countries worldwide. Cities exposed to constant change can be compared to evolving living organisms. However, rapid population growth, migration, natural disasters and unplanned construction in cities require external intervention. The process of urban regeneration is in theory one of these needed interventions and should be put into practice in Turkey. Urban regeneration is an approach which seeks to ensure the reconstruction of cities in line with modern urban planning and principles. Urban renewal applications are increasing rapidly in almost every province in Turkey. Each urban regeneration project can have a large or small effect on the city. Trabzon has attracted attention as a city where urban regeneration has been applied intensively in recent years and selected as the pilot subject of this study. In this study, the urban regeneration projects of Zagnos Valley (28 ha), Tabakhane (17.2 ha), Ortahisar (19 ha), Narlıbahce (22 ha), Ayasofya (2.13 ha) and Comlekci- 1st and 2nd Phases (2.26 ha) cover a total area of 90.59 ha was evaluated. Within the scope of the project, the urban regeneration of Zagnos Valley was examined. According to the findings, the urban regeneration projects in Trabzon revealed that spatial components are important for urban identity and it was determined that urban regeneration projects within the city should continue.

1. INTRODUCTION

Recently, urban regeneration practices have been realized in many cities in Turkey, on different scales and varying in quality. Rapid population increase, inadequate supply of affordable land for residential purposes, and economic reality of low-income residents have been the most important reasons behind the squatter settlements all over the world (Uzun and Celik, 2015). It is possible to classify urbanization in Turkey as a driving force that attracts people from the village to the city and as a compelling power that appeals to people in cities. The most important driving force in the migration of the villagers to the city was the replacement of human labor by machines with the emergence of agricultural technology in the 1950s. The rapid increase in the urban population reached a noticeable level as the villagers took their families with them or brought them there shortly afterward when they migrated to the city (Celik, 2017). Urban regeneration in Turkey is commonly seen together with the problems of urbanization and is implemented as an inevitable "solution". However, in some cases, urban regenerations bring about problems and debates. The positive and negative effects of urban regeneration practices on the city and city dwellers are under discussion and remain a current issue. The fact is that urban regeneration is a popular issue in Turkey and the debates on this issue necessitate a multidimensional examination of urban regeneration projects in our country and their effects. Thus, the general concept of urban regeneration, different examples in our country, and in many instances, the effects of urban regeneration have little by little begun to be investigated by a number of researchers.

* **Corresponding Author**

*(yselcukerbas@hotmail.com) ORCID ID 0000-0001-8991-0964

Cite this article

Erbaş, Y.S. (2020). The Effects of Urban Regeneration on the City: The Case of Zagnos Valley of Trabzon Province. Turkish Journal of Geosciences, 1(2), 78-84.

Received: 30/07/2020; Accepted: 09/09/2020

When urban regeneration in Trabzon Municipal Province over recent years is taken into consideration, Trabzon attracts attention as a city where urban regeneration projects have been applied extensively, making it worth examining as one of the most important examples of urban regeneration in Turkey. Consequently, some urban regeneration projects in Trabzon and their effects have been examined by several researchers. On the other hand, the urban regeneration projects in Trabzon are interrelated and as such should be considered as a whole and in this respect, seen as a total sum of the applications. The effects of urban regeneration on the city must be considered, and in the case of Trabzon, the urban regeneration projects are ongoing, but their results and effects have only begun to emerge. In this respect, although an examination of the effects of urban regeneration in Trabzon provides a forward-looking idea, the process must be completed and a certain period of time must pass in order to examine these effects in reality and in all dimensions. Therefore, in this study, the effects of the urban regeneration of Zagnos Valley in the city of Trabzon were examined based on previous studies and the data available on the current situation.

The most distinctive feature of the city is that it has a differentiated and specialized non-agricultural work order and a differentiated and stratified population working in these occupations (Tolanlar, 2007). When moving back to the origin of the city, this feature is clearly seen in the leap from village culture to urban culture. According to Mumford (2007), in the new plane that emerged, the old elements of the village moved into the new urban unit and became part of it, but as a more complex and changing model than in the village. Under the influence of new elements, it was organized in a structure that was prone to other regenerations and developments. Within this new unit, the elements of the human group became equally complex. The hunter, the peasant and the shepherd, as well as other unsophisticated professionals entered the city and contributed to its existence. This new urban blend resulted in the tremendous development of human abilities in all directions.

According to another definition, the city is not only a collection of intense structures designed to provide goods and services to its anonymous inhabitants, but also an active human unity and a moral and socio-economic community in its most developed state (Bookchin, 1999).

Urbanization, like the city, is a concept with a wide variety of definitions from different perspectives. Urbanization in the narrow sense refers to the increase in the number of cities and the population living in urban areas. However, urbanization should be considered and understood as a much wider concept than this because urbanization is not just a demographic phenomenon, but an expression of a multi-dimensional economic, social, political and cultural process. Urbanization is the economic, social, political and cultural regeneration of society. It is the process of regeneration of a rural society into an urban society as well as the process of change and evolution of urban space and social practices. Taking all these into consideration, it is possible to define urbanization as follows:

"a population accumulative process that, in parallel with industrial and economic development, leads to an increase in the number of cities and the growth of today's cities, increasing the structure of society, creating a division of labor and specialization, and bringing about changes in human behavior and relations" (Kaya et al., 2007).

Although the emergence and history of urbanization is very old, the process of urbanization has gained a new dimension and great speed with the rise and development of industrial societies. The appearance of urbanization as the dominant spatial form on the world scale has arisen with the production-based industrial relations of the modern age. The urbanization process has increased rapidly throughout the world, especially post World War II, and continues to grow. Statistics show that the differentiation between the urban and rural population is constantly turning in favour of the city and thus, they show that the cities, especially the big cities, will shape the destiny and future lifestyle of the people. Therefore, today's urbanization does not appear as an increase in the number of small-scale cities, but rather as an increase in the number of medium- and large-scale cities. For example, in 1975, there were only three cities in the world with a population of more than 10 million, while in 2007 their number had increased to 25. An increasing proportion of the world's urban population is amassing in these big or medium-sized cities (Kaygalak and Isık, 2007).

Urban regeneration is also referred to as "a comprehensive vision and action that seeks to find a lasting solution for economic, physical, social and environmental conditions and provides an answer to urban problems and regional changes" (Turok, 2004). Another definition of urban regeneration states: "In the course of time, urban areas which have lost their character become degraded from the physical and environmental aspects and are faced with social and economic exclusion. With certain social and economic programs, these areas within the city are renewed and transformed" (Yuksel, 2007). Thus, in order for urban regeneration projects to come into play and become a solution, first of all, a part of the city must be in a decrepit state from which it cannot recover and become productive by itself (Ceylan, 2007).

Cities are as old as the history of civilization and have been in constant change since the day they emerged. At the root of the city, there is the phenomenon of the settlement that arose as a result of the necessity of living together with the desire to solve and eliminate the difficulties, problems and

inconveniences that people encounter and cannot solve alone (Kaya et al., 2007).

2. MATERIALS AND METHODS

2.1. Evolution of Urban Regeneration in the World and in Turkey

The first applications of urban regeneration in the world emerged as the result of urban growth movements in Europe in the 19th century and the destruction and reconstruction of some areas (urban renewal). In this period, the urban regeneration processes were realized by the public sector leadership model and were based on two different foundations. In the UK, urban policy was issued with the 1851 Housing Act. In France development interventions were issued for the city of Paris in 1851 –1873 (Sisman and Kibaroğlu, 2009). From those years onward, urban regeneration began to spread all over the world (Acıkgoz, 2014). The urban regeneration that has evolved is shown in more detail together with the variables in Table 1.

Table 1. Evolution of urban regeneration (Demirkiran, 2008)

Period	1950s	1960s	1970s	1980s	1990s
Type of Policy	Reconstruction	Revival	Renovation	Redevelopment	Regeneration
Basic Strategy and Orientation	Reconstruction and expansion of suburban areas; usually based on a master plan	Continuing the understanding of the 1950s; the growth of the suburbs; the beginnings of urban sprawl	Renovation and concentration on neighbourhood projects	Many basic development and re-development projects; naval projects; out-of-town projects	A more comprehensive approach to policies and practices; greater emphasis on integrated education
Key Actors and Financing Owners	Central and local government, private sector developers and contractors	Aiming to balance the public and private sectors	The increasing role of the private sector and decentralization in local governments	Emphasis on private sector and expert units; increasing partnerships	The dominance of partnerships
Field of Action Size	Highlighting of local and regional levels	The emergence of regional levels in actions	Regional and local levels first, then local levels to the fore	Focusing on a local scale at the beginning of 1980	Development of strategic actions; re-presentation of regional actions
Economic Focus	Small private sector investment; public sector investments in general	The growing importance of the private sector in the late 1950s	Mandatory public resources and increases in private investments	Private sector dominance with selective public funds	Increasing balance between public, private sector and voluntary funds
Social Content	Improvement of housing and living standards	Improving social conditions and welfare	Community-based actions and increased powers	Selective government support and the community to see to their own business	Importance of the role of society
Physical state	Importance of internal regions and nearby environmental development	Improvement of 1950s areas and existing areas	Extensive renewal of aging urban areas	Preparation of basic projects for replacement and new development	More unobtrusive preservation/conservation than in the 1980s
Environmental Approach	Landscape and planting	Selective improvements	Environmental improvements with new inventions	Wider-perspective environmental approaches	Comprehensive presentation of the idea of sustainable environment

At first, in the 1980s, Turkey's foreign development was applied as an open export-oriented model. Migration from rural to urban areas began with the security concerns brought about by the political turmoil in the eastern provinces, bringing about an increase in the urban population ratio. The rapid population growth brought with it squatters and shantytowns. In the 1970s, a holistic regeneration

project was created with the idea that the slum areas should be redeveloped. This was actually the first urban regeneration movement; however, it could not be implemented due to lack of resources. In the 1980s, when competitive policies were implemented, with the re-emergence of the slum problem, large-scale mass housing construction projects were realized with the cooperation of the Turkey Real Estate Bank, cooperatives, private entrepreneurs, TOKI (Housing Development and Public Participation Administration) and local governments.

2.2. Urban Regeneration in the city of Trabzon

The Metropolitan Province of Trabzon, located in in the eastern Black Sea region of Turkey, covers an area of approximately 4685 km2 and has a population of approximately 800 thousand people. The provincial capital of Trabzon is one of the three most important cities of the region. Zagnos Valley in the Trabzon City Ortahisar District, at an altitude of 37 m above sea level, was selected as the pilot region within the scope of the study (Figure 1).

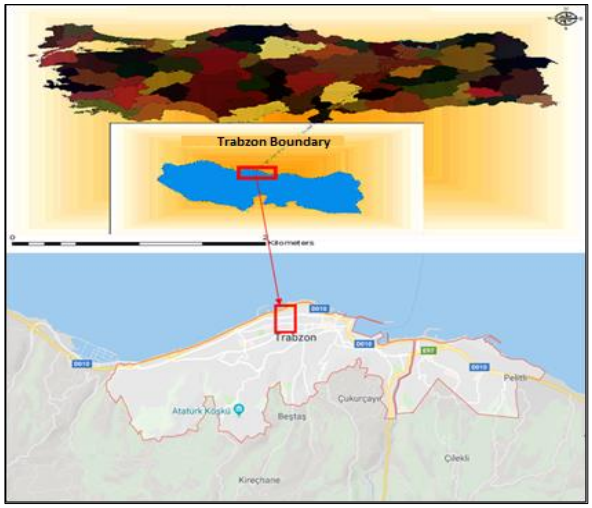

Figure 1. Zagnos Valley in the Ortahisar District of Trabzon

As time progressed, and with rapid population growth, a distorted, unhealthy, congested urban structure had emerged in Trabzon, as in many cities in Turkey, due to various reasons such as unsuitable practices and unplanned growth. As a result, the green valleys had disappeared, the city's airways had become congested and depressed areas devoid of aesthetic began to appear. In other words, urban regeneration had become an inevitable necessity for Trabzon. Therefore, in the last 10 years, various urban regeneration projects have been initiated, covering a large area of the city.

When we look at the urban regeneration projects in Trabzon as a whole, the great extent of the urban regeneration can be understood more clearly. In this respect, Trabzon is a living laboratory for studies on urban regeneration. When seen as a whole, the urban regeneration projects in Trabzon, including those of the Zagnos Valley (28 ha), Tabakhane (17,2 ha), Ortahisar (19 ha), Narlibahce (22 ha), Ayasofya (2.13 ha) and Comlekci Phases 1 and 2 (2.26 ha), cover a huge area totaling 90.59 ha. Trabzon is a large city, with the boundaries of Trabzon Municipality encompassing 3,980 ha, which means that 3% of the provincial capital of Trabzon Province is undergoing urban regeneration.

The Zagnos, Tabakhane, Ortahisar and Narlıbahce projects, which are located in the vicinity of the old city center of Trabzon, are linked to each other via their different phases and seem like parts of a whole as each project is completed (Figure 2).

It is impossible for all these projects not to have an impact on the city. Each urban regeneration project will make a positive contribution to the city. Within the scope of the study, the urban regeneration of Zagnos Valley was investigated in light of the data that was possible to access.

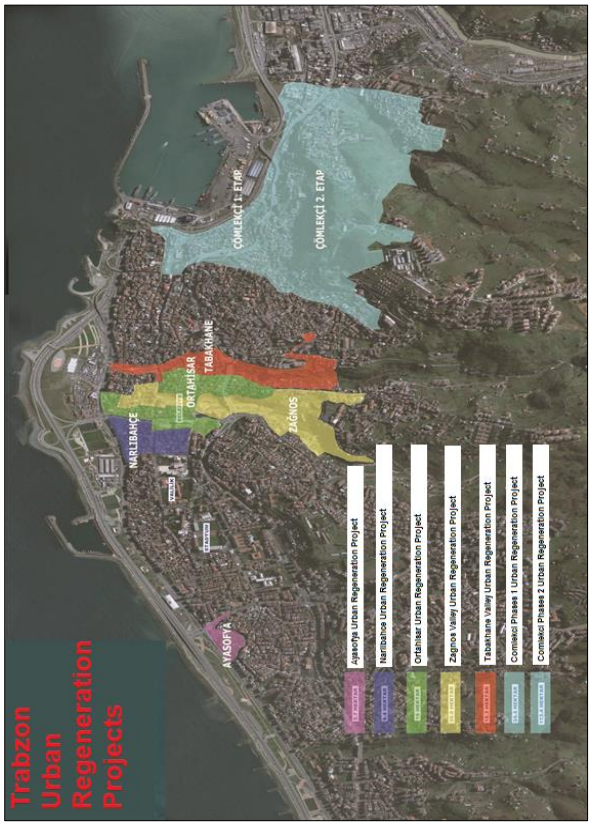

Figure 2. Boundaries of urban regeneration projects in Trabzon

2.3. Zagnos Valley Urban Regeneration Projects

Zagnos Valley is one of the valleys surrounding the ancient city of Trabzon. Zagnos Valley is located close to business centers and government offices. The 1st class historical site of the Ortahisar fortress and settlement is adjacent to Zagnos Valley, with the İmaret Creek to the West, and Tabakhane Valley

and Kuzgun Creek to the East. This valley, which is an important air corridor for the city and which is shown as a green area in the development plans, had become a texture containing negative examples of irregular and shoddy structures and distorted and unhealthy urban construction. Within the historical development process of the city, Zagnos Valley provided a ventilation and green space corridor and had fulfilled this function well until the 1960s (Oksuz, 2010). However, in more recent times, the rapid urbanization and unplanned development generally seen in other countries also appeared in Trabzon, and showed up in this valley. In order to learn more about when and how these developments occurred in the valley, the change in the valley's structure over time was analyzed using geographic information systems (Figure 3 and 4).

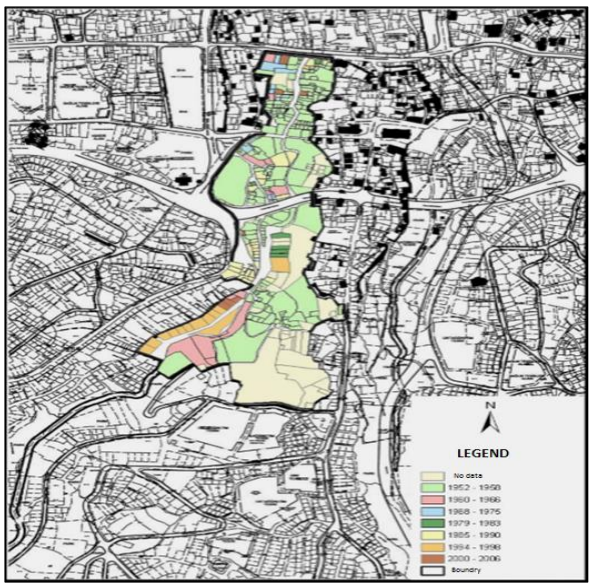

Figure 3. Distribution of parcels in the Zagnos Valley according to their first acquisition date

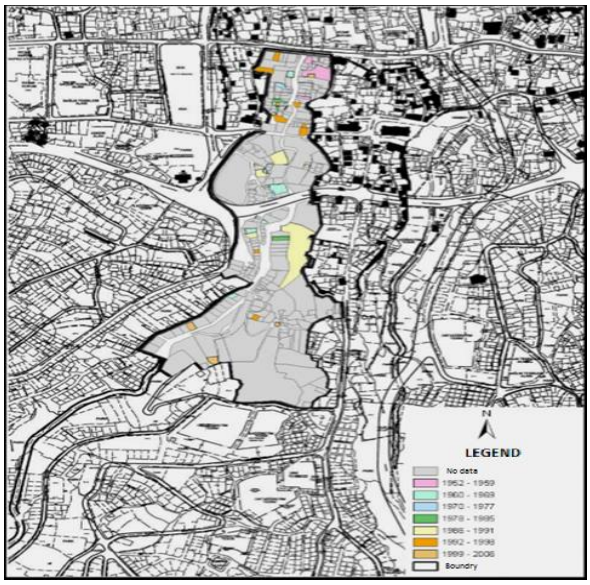

Figure 4. Distribution of the parcels in the Zagnos Valley according to the reasons for their acquisition

According to this data, the majority of the parcels in the area were obtained via a cadastral / allotment process, with intense activity observed during the early acquisition dates between 1952 and 1958. It was determined that some of the parcels in the regeneration area were licensed by taking advantage of the zoning amnesty in 1984 although most did not have a registered license or building permit. When the 1977, 1984 and existing (pre-demolition) construction statuses were compared, a high concentration of construction was observed in the valley in 1977, whereas there was no escalation in construction between 1977 and 1984. After the zoning amnesty in 1984, it was determined that the construction in the valley was gradually expanding and it had reached its final state before the demolition. The urban regeneration process for Zagnos Valley was completed between 2004 and 2014. In this process, a huge area of approximately 28 ha was expropriated (Fig. 5).

Figure 5. Buildings in Zagnos Valley before expropriation for urban regeneration

The total cost of the expropriation was 170,308,991.40 TL including additional protocol expenses. In total, 736 buildings were completely demolished under the additional protocol. A total of 580 flats were constructed in place of the demolished buildings, 354 in the first phase and 226 in the second phase. After the regeneration, the valley became wrapped in a breath of fresh air and was transformed into an area of urban organization (Figures 6, 7 and 8).

Figure 6. Zagnos Valley urban regeneration (Phase 1)

Figure 7. Zagnos Valley urban regeneration (Phase 2)

Figure 8. Zagnos Valley urban regeneration (Phase 3)

3. RESULTS

It is a fact that the urban regeneration practices completed and ongoing in Trabzon will have many effects on the city. These effects that begin to emerge are likely to be addressed in a multifaceted manner. The most evident finding from the urban regeneration example in the study was that the urban regeneration practices were a necessity arising from the urbanization problems in Trabzon. The city appears to have rid itself of distorted structures and image pollution and to display a more modern city image, but this was made possible only through urban regeneration. In addition, the urban regeneration project, which covered a large part of the historical area of the city, has helped to reveal the historical texture of Trabzon, made its historical identity more visible and increased its tourist attraction. This aspect of Trabzon is becoming more prominent, especially with the completion of the Zagnos regeneration project. Together with the Zagnos Valley urban regeneration another historical attraction of Trabzon, the city ramparts, has come to the fore. The green areas, which had been destroyed as a result of unhealthy and unplanned construction, have been reintegrated into the city. Increasing these green areas contributes to the creation of a new living space for people. Thus, there has been a significant environmental impact on the city. Zagnos Valley is in a strategic position and due to its location has a positive effect on the climate of the city with its open-green area and its influence on the city's microclimatic features.

One of the most important criticisms of many urban regeneration practices has concerned the reduction of public spaces. According to this view, as a result of urban regeneration, public spaces are shrinking with each passing day and access to existing ones is becoming increasingly limited. This criticism was taken into consideration for this project. With this regeneration, many commercial areas located in the city centre of Trabzon are very close to public buildings and residential areas and are easily accessible, and new and wide public spaces were gained, with areas for recreation and parking. In this way, the regeneration has made a significant contribution to the people in the city by enabling them to enjoy their free time and carry on their social life.

Apart from all these positive impacts, the most important problem of urban regeneration, that of displacement, has emerged here. The area that was evacuated with the Zagnos Valley urban regeneration project was projected as a recreation area available to the public, making it impossible for the rights holders living in the expropriated areas to be resettled in the same area. For this reason, urban regeneration in the Zagnos Valley was criticized because of the fact that it only dealt with the physical aspects of the process, whereas the social dimension was neglected.

4. DISCUSSIONS AND CONCLUSIONS

Urban regeneration is a spatial, economic, social and physical reproduction process brought about through conscious interventions in the city. In this respect, urban regeneration is undoubtedly versatile and directly or indirectly brings with it many effects. In the case of Trabzon, the urbanization of the city has been the main characteristic of urban development in recent years, and has defined its direction. In this respect, the effects of urban regeneration in Trabzon should be considered as a whole. Indeed, the parts of this urban regeneration, already mentioned as project phases that complement each other, are tightly bound to each other. However, some parts of the urban regeneration are on-going. Although the consequences and impacts of urban regeneration have partially begun to emerge and can provide an idea of what to expect, in order to examine these effects in all their economic, social and spatial dimensions, the urban regeneration process needs to be completed and a certain period of time needs to pass. On the other hand, when we look at the possible effects of the current urban regeneration in Trabzon, it can be seen that the positive effects outweigh the negative on the scales by a very big margin.

Urban regeneration in Trabzon has contributed to the economic and social development of the city, eliminated its polluted image, and increased the green areas and public spaces as a whole, in addition to improving the quality of life. Moreover, as a result of this study, the city's historical identity, its ramparts and its identity as a seaport have demonstrated that urban identity has a vital function and reveals very important spatial components. For this reason, the other urban regeneration projects in the city of Trabzon should be completed and additional ones should be designed and implemented. Local governments and decision-making bodies should set new goals.

REFERENCES

Acıkgoz, A. (2014). Kentsel dönüşümün ekonomik, mekânsal, sosyal etkileri ve kamunun rolü: Ankara Gültepe (Çinçin) örneği (MSc thesis). Gazi University, Ankara, Turkey.

Bookchin, M. (1999). Kentsiz Kentleşme. Istanbul: Ayrıntı Yayınları.

Celik, K. (2017). Kentsel dönüşüm alanlarının seçimi ve dönüştürülmesine yönelik örnek bir uygulama. *Gümüşhane Üniversitesi Fen Bilimleri Enstitüsü Dergisi*, 7(2), 221-235.

Demirkiran, S. (2008). Türkiye'de kentsel dönüşüm uygulamalarında yerel yönetimlerin rolü: Bursa büyükşehir belediyesi örneği (MSc thesis). Trakya University, Edirne, Turkey.

Ceylan, A. (2007). Yaşam kalitesinin arttırılmasında kentsel yeşil alanların önemi ve kentsel dönüşüm ile ilişkilendirilmesi (MSc thesis). Istanbul Technical University, Istanbul, Turkey.

Kaya, E., Şentürk, H., Danış, O., & Şimşek, S. (2007). Modern Kent Yönetimi. İstanbul: Okutan Yayıncılık.

Kaygalak, I., Isık, S. (2007). Kentleşmenin yeni ekonomik boyutları. *Ege Coğrafya Dergisi*, 16(1-2), 17-35.

Mumford, L. (2007). Tarih boyunca kent: kökenleri, geçirdiği dönüşümler ve geleceği. Istanbul: Ayrıntı Yayınları.

Oksuz, M. (2010). Trabzon'da dere ıslahına ilk örnek: Tabakhane ve Zağnos derelerinin yüzyıl önceki hikayesi. *Karadeniz İncelemeleri Dergisi*, 8(8), 91-100.

Sisman A., Kibaroğlu, D. (2009). Dünyada ve Türkiye'de kentsel dönüşüm uygulamaları. *TMMOB Harita ve Kadastro Mühendisleri Odası*, 12, 11-15.

Tolanlar, M. (2007). Kentsel dönüşüm projeleri ve toplumsal yansımaları (MSc thesis). Afyon Kocatepe University, Afyon, Turkey.

Turok, I. (2004). Kentsel dönüşümde yeni eğilimler ve yönetişim. *International Symposium on Urban Regeneration Applications*, İstanbul: Küçükçekmece Municipality Publication, 25-30.

Uzun, B., Celik, N. (2015). Upgrading of illegal settlements in Turkey; the case of North Ankara entrance urban regeneration project. *Habitat International*. 49, 157-164.

Yuksel, O. (2007). Kentsel dönüşümün fiziksel ve sosyal mekâna etkisi: kuzey Ankara girişi kentsel dönüşüm projesi (MSc thesis). Gazi University, Ankara, Turkey.